Synthesis, Structure Peculiarities and Acid−Basic Behaviour of Triazoleporphyrazines

Mikhail K. Islyaikin[a,@], Olga N. Trukhina[a], Yulia V. Romanenko[c], Elena A. Danilova[a], and Olga G. Khelevina[b]

[a]*Department of Fine Organic Synthesis, Ivanovo State University of Chemistry and Technology, Ivanovo, 153000, Russia*
[b]*Department of Organic Chemistry, Ivanovo State University of Chemistry and Technology, Ivanovo, 153000, Russia*
[c] *Department of Polymers, Ivanovo State University of Chemistry and Technology, Ivanovo, 153000, Russia*
[@]*Corresponding author E-mail: islyaikin@isuct.ru*

Recent advances in the chemistry of triazoleporphyrazines, structural analogues of porphyrazine containing one 1,2,4-triazole ring instead of one of pyrrole subunits, are reviewed. Experimental data of stepwise protonation equilibrium are discussed and basicity centers of macroheterocyclic compounds are revealed. Spacial configurations and electronic structure peculiarities of the tautomers of triazoleporphyrazine and its protonated forms are calculated using DFT method. Aromaticity of various conjugation contours is evaluated using HOMA and NICS criteria.

Introduction

Macroheterocyclic compounds (porphyrins, porphyrazines, phthalocyanines) having a high symmetry tetrapyrrole macrocycle as a basis of their structure are of an outstanding importance. Porphyrins,[1,2] porphyrazines[3] and phthalocyanines[4,5] are substances with numerous biological and practical applications. Many research efforts were focused also on noncentrosymmetric compounds.[6] The lack of a symmetry center in their molecules makes them good targets for development of materials with non-linear optical applications.[7] Amphiphilic structure of the molecules is especially appropriate for the Langmuir-Blodgett films formation. Besides, they can be used as constructional blocks for molecular ensembles of nanosized supramolecular architectures.[8,9]

There are two main approaches to reduce symmetry of these macrocycles. The first one is introduction of different substituents to the periphery of the macrocycle to form the noncenrosymmetric molecules.[10] The presence of substituents provokes perturbation of molecular orbitals and as consequence induces the permanent dipole moment. In this connection, significant attention has been paid to the synthesis of substituted phthalonitriles and their functional derivatives used as phthalocyanines precursors.[11-13] The second way to gain access to noncentrosymmetric macrocycles is a modification of a central core by formal substitution of one of pyrrole or isoindole rings by another cycle. Azoles seem to be the most attractive heterocycles for core modification since they are heteroanalogues of pyrrole. Using azoles as a heteroaromatic subunit, one can assemble ABBB-systems with 18 π-electrons containing inner cross similar to that of porphyrazines and phthalocyanines. Moreover, a possibility to influence deeply conjugation system *via* lone electron pairs of heteroatoms of azole subunits seems to be very attractive.

Following this strategy the noncentrosymmetric porphyrin[14] and phthalocyanine[6,15] analogues have been synthesized recently. The triazolephthalocyanines, structural analogues of phthalocyanine, have been extensively studied by the group of Prof. Torres.[16-19] In particular, it has been shown that these compounds have permanent dipole moments and, hence, ability to form well-ordered Langmuir-Blodgett monolayers[20] and to produce the second harmonic generation[21] as well.

Recently the first representatives of a new class of noncentrosymmetric tetrapyrrole macrocycles – triazoleporphyrazines, have been synthesized.[22] These compounds should be considered as analogues of porphyrazine in which one pyrrole subunit is replaced by 1,2,4-triazole.*

Synthesis of Substituted Triazoleporphyrazines

Hexa(4-*tert*-butylphenyl)triazoleporphyrazine (**1**) and its N-substituted analogue (**2**) was synthesized by condensation of 3,4-bis(4-*tert*-butylphenyl)-2,5-pyrrolinediimine and 3,5-diamino-1,2,4-triazole (guanazole) or 1-dodecyl-3,5-diamino-1,2,4-triazole in stoichiometric ratio (3:1), in anhydrous *n*-butanol at reflux (Scheme 1). High solubility of these products (**1**, **2**) in organic solvents allows to purify them by column chromatography on silica gel.

The metal complexes (**3-5**) were prepared[22] by treatment of metal free triazoleporphyrazine (**1**) with an appropriate metal acetate in DMF at 100 ºC in 78-90% yields (Scheme 2).

Alternatively, nickel (II) triazolephthalocyanine was synthesized by crossover macrocyclization of 3,4-bis(4-*tert*-butylphenyl)-2,5-pyrrolinediimine and guanazole in 2-ethoxyethanol at 135 ºC, in presence of a metal template. However, this method seems to be less efficient than the stepwise procedure. Thus, the complex **3** bearing one nickel (II) ion within its central binding core was obtained with 14% yield.

* Correspondingly they can be named more correctly as diazasubstituted porphyrazines, *i.e.* 2,3-diazaporphyrazines (Edr).

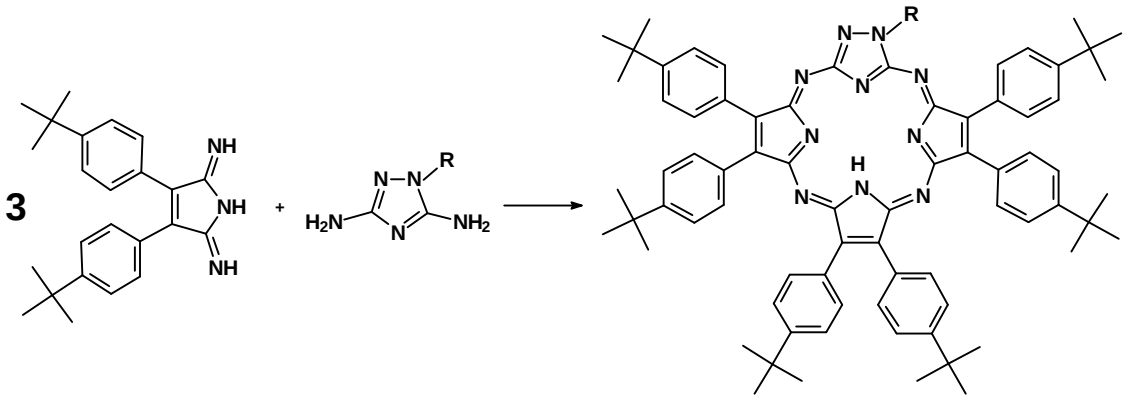

Scheme 1. Synthesis of substituted triazoleporphyrazines.

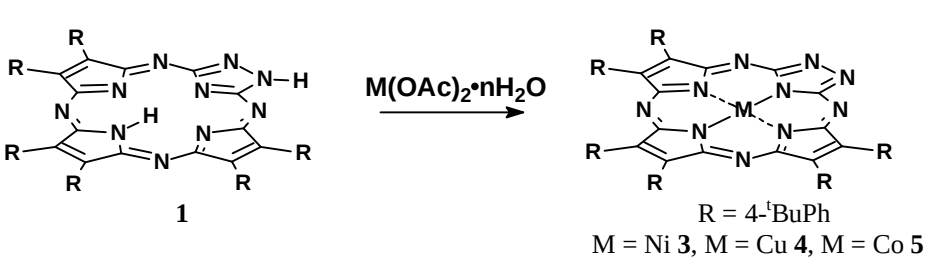

Scheme 2. Preparation of metal complexes of triazoleporphyrazine **1**.

Compounds (**1-5)** were characterized by elemental analysis, UV-vis, IR, NMR and MS data. The signals of the molecular ion [M] (*m/z* = 1108.6) and the monoprotonated form $[M+H]^+$ (*m/z* = 1109.5) were found in MALDI TOF spectra of **1**.

The absorption bands in the IR-region 3200–3500 cm^{-1} are of especial importance for determining the position of hydrogen atom in the triazole ring. One can see three bands at 3430, 3379, 3299 cm^{-1} in the spectrum of **1** (Figure 1a). The signal at 3299 cm^{-1} can be assigned to stretching vibrations of pyrrole N-H bond. Its position is low variable from the state of the compound on going from a solid state to a chloroform. Thus, the absorption band is slightly shifted up to 3302 cm^{-1} in the IR-spectrum of **1** in chloroform. Moreover, the band appears at 3299 cm^{-1} in the spectrum of **2** (Figure 1b) and disappears in the spectrum of the complex **3** (Figure 1c). The stretching vibrations of the triazole N-H bond result in the second band at 3379 cm^{-1} in the IR-spectrum of **1**. It is noted that this band is absent in spectra of the dodecyl-substituted compound **2** or the metal complexes (**3-5)**.

The proton absorption of *tert*-butyl-group is detected at 1.25 ppm in the ^{1}H NMR spectrum of **1** in $C_2D_2Cl_4$ solution. The low-pronounced multiplet at 7.26 ppm is assigned to protons of phenyl rings. The signal broadening at 15.24 ppm is a consequence of transannular protons absorption of the pyrrole N-atoms. The signal becomes well-pronounced and shifts to 15.14 ppm at 120 °C, whereas it becomes hardly observable at -30 °C. Absorption at low external magnetic field shows the absence of strong ring current within the core area of the macrocycle **1**. This provides evidence to weak conjugation in the molecules of **1.**

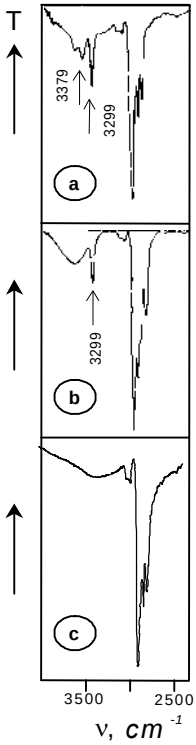

Figure1. IR spectra of triazoleporphyrazines a – **1**, b – **2**, c – **3**.

Structure Peculiarities

A molecule of triazoleporphyrazine **6** can be represented by three tautomers: **7a, 7b, 7c** (Scheme 3).

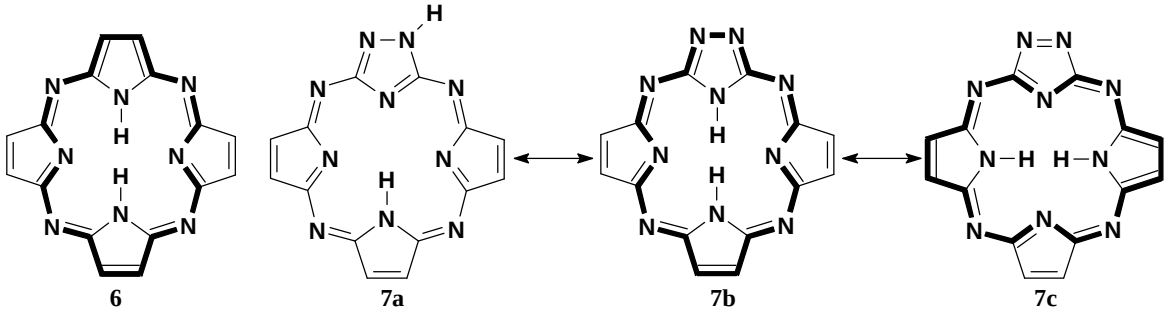

Scheme 3. Porphyrazine (**6**) and tautomerism of triazoleporphyrazines.

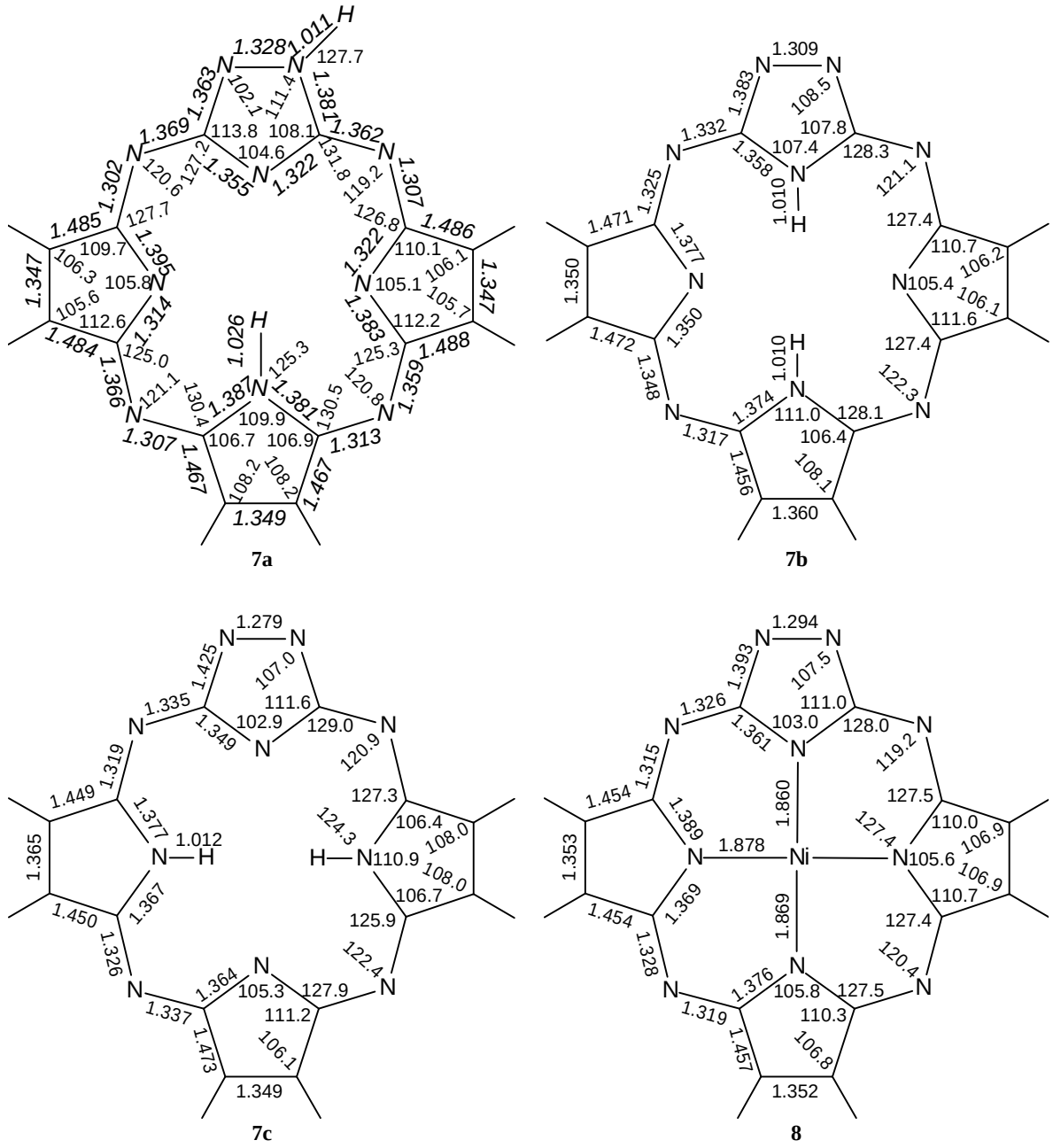

Figure 2. Bond lengths (Å) and bond angles (degrees) of **7a-c**, and **8** structures optimized at DFT B3LYP/6-31G (*d*, *p*) level.

Since the monocrystals appropriate for X-Ray study have not been available until now, the geometry and electron configuration of porphyrazine (**6**), the tautomers (**7a-c**) and the nickel complex (**8**) of triazoleporphyrazine were calculated using quantum chemistry methods. The full geometry optimization as well as the NBO and GIAO calculations were carried out at the DFT level. The functional employed was the Becke three parameter (B3LYP) hybrid functional at the 6-31G(*d*,*p*) basis set. The results are shown in Tables 1, 2 and Figures 2, 3.

Comparison of the calculated energies (Table 1) shows that **7c** is the most energy-advantageous compound among the tautomers **7a-c**. Besides, **7c** has the structure of the inner macrocycle most closely corresponding to that of porphyrazine.

Table 1. Total (*E*) and relative (ΔE) energies, ionization potentials (IP) and dipole moments (μ) of structures **6**, **7a-c** and **8** optimized at DFT B3LYP/6-31G(*d,p*) level.

Structure	*E*, a.u.	$\Delta E_{rel,}$ [a] kJ·mol^{-1}	IP, eV	μ, D
6	-1053.72663826	-	5.82	0.00
7a	-1085.75771329	52.50	6.45	2.66
7b	-1085.77012851	19.89	6.48	7.21
7c	-1085.77770003	0.00	6.36	6.13
8	-2592.8681607	-	6.41	6.67

[a]For the structures **7a-c**.

It should be noted that N-N bond length of triazole ring decreases in the order **7a>7b>7c** and approaches N=N double bond in the molecule **7c** (Figure 2), whereas the length of the N–C bond linking the N–N group with the inner macrocycle increases in the sequence **7a>7b>7c** reaching 1.425 Å for **7c**. This fact indicates that an interaction between N–N fragment and the rest of the system becomes weaker in this series. Thus, the structure **8** has the length of the N-N bond equal to 1.294 Å which is between those of **7b** and **7c** due to substitution of both inner hydrogen atoms of the macrocycle for the metal atom.

Molecule of triazoleporphyrazine (**7**) as well as molecule of porphyrazine (**6**) are systems with multicontour conjugation. It was attractive to estimate the effect of tautomerism on aromaticity. Thus, total aromaticity of the macrocycle molecules and local aromaticity of various conjugation contours were evaluated using Harmonic Oscillator Model of Aromaticity (HOMA)[23,24] and Nucleus Independent Chemical Shifts (NICS)[25] criteria.

HOMA and NICS criteria were obtained[26] on the basis of geometries shown in Figure 2. Table 2 displays the values calculated for HOMA and its components EN and GEO, and NICS indices of the compounds of interest. It is obvious that the aromaticity of triazoleporphyrazine is affected by tautomerism arising from the hydrogen atoms migration.

Following the HOMA criteria calculated for the whole molecules (Table 2), the aromaticity increases in the sequence **7a<7b<7c<8,** which is in a good agreement with equalization of the bonds lengths.

The increase of total aromaticity in the **7a<7b<7c** order along with the decrease of local triazole aromaticity is observed. This fact confirms the idea that the triazole ring which is involved into a macrocyclic conjugation system should lose a part of its aromaticity. Interaction of triazole ring with conjugation system of the inner macrocycle results in the N-N bond isolation and enlarged alternation of double/single bonds of the triazole ring. The GEO indices

Table 2. EN, GEO и HOMA indices for **7a-c** and **8** structures optimized at DFT B3LYP/6-31G (d, p) level[a].

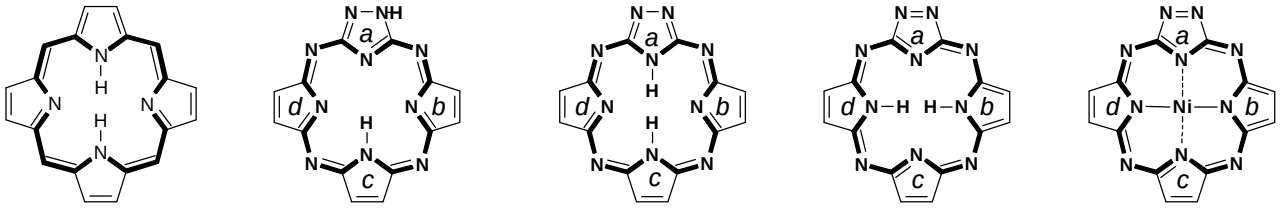

6 **7a** **7b** **7c** **8**

Structure	EN	GEO	HOMA
Porphyrazine **6**	0.115	0.322	0.562
internal cross	0.022	0.036	0.942
7a (whole system)	0.122	0.464	0.414
triazole ring *a*	0.044	0.034	0.922
internal cross	0.015	0.094	0.892
7b (whole system)	0.103	0.322	0.567
triazole ring *a*	0.081	0.032	0.887
internal cross	0.018	0.039	0.943
7c (whole system)	0.098	0.287	0.615
triazole ring *a*	0.118	0.225	0.657
internal cross	0.016	0.036	0.948
8 (whole system)	0.080	0.277	0.643
triazole ring *a*	0.090	0.074	0.835
internal cross	0.019	0.069	0.913

[a]The EN, GEO, HOMA indices calculated for the free base porphyrin are 0.107, 0.240 and 0.666 respectively.

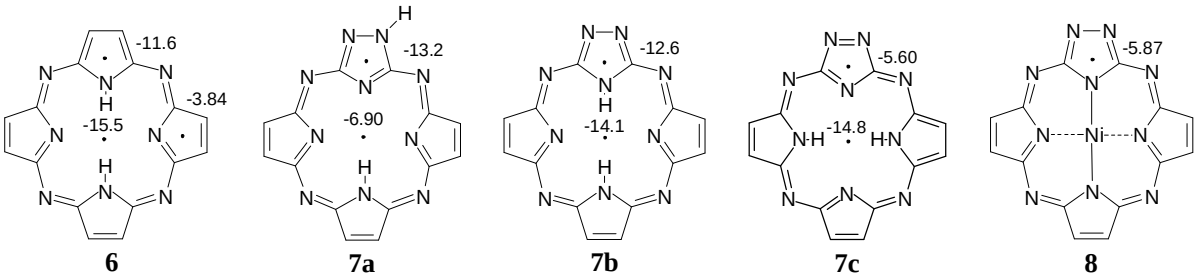

6 **7a** **7b** **7c** **8**

Figure 3. Calculated NICS values (ppm) of the studied compounds.

increase from 0.034 to 0.225 for **7a-c (**Table 2). The inner macrocycle aromaticity increases from **7a** (HOMA=0.892) to **7c** (HOMA=0.948).

The NICS magnetic criteria confirm the tendency of aromaticity changes revealed by the HOMA criterion in the consecution **6**, **7a-c**, **8** (Figure 3). They are based on the magnetic properties of π-electron systems and indicate that the compound **7a** has the lowest aromaticity (NICS=-6.90 ppm), whereas the compound **7c** is the most aromatic of tautomers (NICS=-14.80 ppm).

It was found that an internal cross ([16]heteroannulene contour) bearing 18 π electrons was the most aromatic part of the molecules.

UV-vis Characterisation

The UV-vis spectrum of the compound **1** (Figure 4) is formed of four strong absorption bands. The electron transfers within phenyl rings result in the strongest band at 244 nm. The band at 324 nm is the Soret band similar to the equivalent absorption of its porphyrazine counterpart.

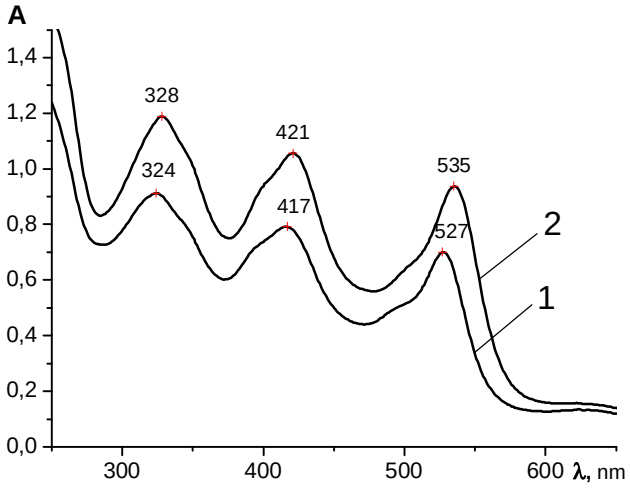

Figure 4. UV-vis spectra: 1 – **1**, $CHCl_3$, c=2.16·10^{-5} M; 2 – **2**, $CHCl_3$, c=1.71·10^{-5} M.

The strong band at 417 nm (or less intense band, red-shifted to 450 nm, in the spectrum of substituted porphyrazine) is a consequence of symmetry lowering due to the substitution of pyrrole fragment for triazole fragment in the molecular core.

The long-wave absorption band at 527 nm of substituted triazoleporphyrazine is hypsochromically shifted by 139 nm as compared with corresponding porphyrazine.[27] Thus, there is no effective conjugation in the macrocycle due to the presence of the triazole ring.

The peculiarities mentioned above are confirmed for the dodecyl-substituted compound **2**. Compounds **1** and **2** have the analogous spectral curves, that is a proof of similarity of their chromophoric systems. The presence of dodecyl substituent in **2** fixes the 1H form of the triazole ring. This fact shows the presence of hydrogen atom in position 1 within a triazole ring in triazoleporphyrazines **1** and **2**.[28] The absorption bands of **2** are slightly shifted hypsochromically due to weak +*I*-effect of dodecyl group.

The UV-vis spectra of the complexes **3-5** (Figure 5) have three regions: i) the long-wavelength absorption bands at 602-629 nm and the line broaderning at 570 nm (inflexion for **3** and **4**), ii) the broad band in the middle part of the spectrum at 472-518 nm, iii) two bands in UV region at 325-391 nm. The positions and intensities of the long-wave absorption bands argue for aromatic character of the metal complexes. Nature of the metal has an influence upon the position of the absorption bands. Bathochromic shift of the long-wavelength absorption band increases in the sequence Ni<Co<Cu.

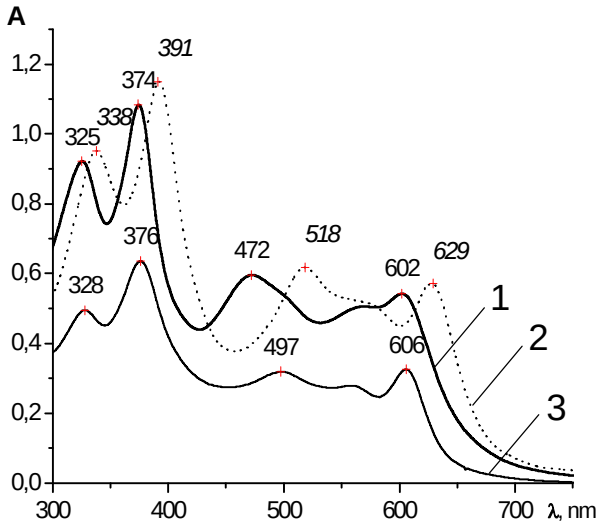

Figure 5. UV-vis spectra: 1 - M = Ni, 3, CH_2Cl_2,c=1.71·10^{-5} M; 2 - M = Cu, 4, $CHCl_3$, c=2.05·10^{-5} M; 3 - M = Co, 5, $CHCl_3$, c=1.03·10^{-5} M.

To clarify the nature of the absorption bands we carried out calculations of electron absorption spectra of the model molecules **7a-c** and **8** using ZINDOS method, their geometries were obtained using DFT B3LYP 6-31G(*d*,*p*) method. Essential results of our calculations are given in Table 3.

Table 3. Calculated values of energy of three high occupied molecular orbitals and three lower unoccupied molecular orbitals, energies of first singlet-singlet passages (Δ*E*) of **6, 7a-c, and 8** structures.

№	Energy of molecular orbital, eV						Δ*E*, eV
	LUMO+2	LUMO+1	**LUMO**	**HOMO**	HOMO-1	HOMO-2	
6	-0.33	-1.78	**-2.14**	**-6.22**	-8.63	-9.15	4.08
7a	-0.72	-1.29	**-2.40**	**-7.49**	-8.75	-9.32	5.09
7b	-0.85	-1.89	**-2.71**	**-6.91**	-9.13	-9.56	4.20
7c	-0.85	-2.28	**-2.42**	**-6.63**	-8.92	-9.70	4.21
8	-0.94	-2.11	**-2.64**	**-6.89**	-9.08	-9.14	4.25

It can be seen that substitution of one pyrrole subunit by 1,3,4-triazole moiety in porphyrazine core gives rise to stabilization of the highest occupied molecular orbitals (HOMO) and the lower unoccupied molecular orbitals (LUMO). However, occupied molecular orbitals are stabilized greater than virtual ones. This results in increasing of the energy gap between frontier orbitals of triazoleporphyrazine **7** in comparison with those of porphyrazine **6**. The difference between HOMO and LUMO positions becomes more pronounced in the sequence of the tautomers **7a-c**.

Acid–Base Behavior in Proton-Donating Media

In comparison with porphyrazine, triazole-porphyrazine has two extra nitrogen atoms (nitrogens of triazole ring), which could be considered as additional centers of protonation. Thus, sequential equilibria of protonation may be formulated as follows:

$MPz + H^+ \leftrightarrow MPzH^+$

$MPzH^+ + H^+ \leftrightarrow MPzH_2^{2+}$

and so on, where $MPzH^+$ and $MPzH_2^{2+}$ are the first and the second protonated forms of the MPz initial base, respectively.

The proton transfer from acid HA to base B is a complex process with the stages of the acid associate, H-associate, ion-ion associate and ionized protonated form. Formation of the first acid form of the compounds **1**, **2** and **4** is completed in media having acidities that are stronger than those of pure acetic acid, *i.e.* in H_2SO_4 – antipyrine – HOAc mixtures (H_0=3.95 for **1** and **2** and 4.60 for **4**). The *Q*-bands are shifted hypsochromically by 473, 376 and 755 cm^{-1}. The character of the spectral changes observed for **1** and **4** are shown in Figures 6 and 7**,** respectively. Taking into account that the shift of the *Q*-band maxima are observed in media with poor ionizing ability, it can be concluded that ion–ion associate is formed.

The $\log I_i$–H_0 dependences are linear for **1**, **2** and **4** in benzene–acetic acid media (Figure 8). The slopes of the $\log I_i$–H_0 lines are 0.97, 0.79 and 1.14 for **1**, **2** and **4**, respectively.

This result indicates that only one donor center is protonated by acid in all studied systems. Further increase of acidity leads to the rapid destruction of triazoleporphyrazines.

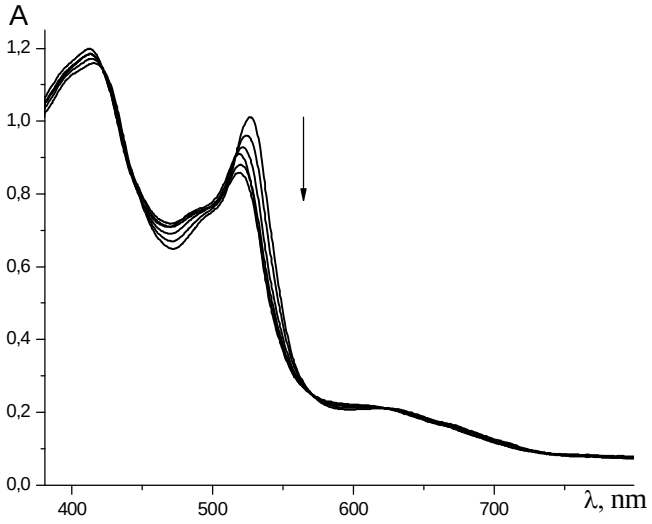

Figure 6. Changes of UV-vis spectrum of **1** in benzene-AcOH; H_0 decreases from 6.33 to 4.60.

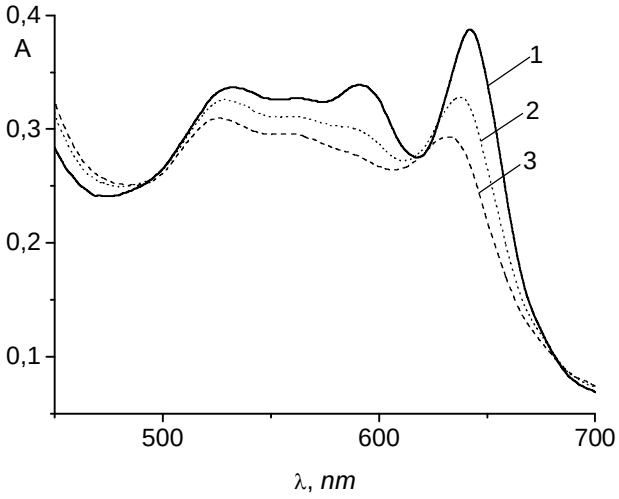

Figure 7. UV-vis spectra of solutions of **4** in (1) benzene, (2) benzene-HOAc (H_0=6.44), (3) benzene-HOAc (H_0=6.17).

To determine a position of protonation, the quantum chemistry calculations were carried out for modelling species: triazoleporphyrazine, 1-methyltriazoleporphyrazine, Zn-triazoleporphyrazine cores and their protonated forms.

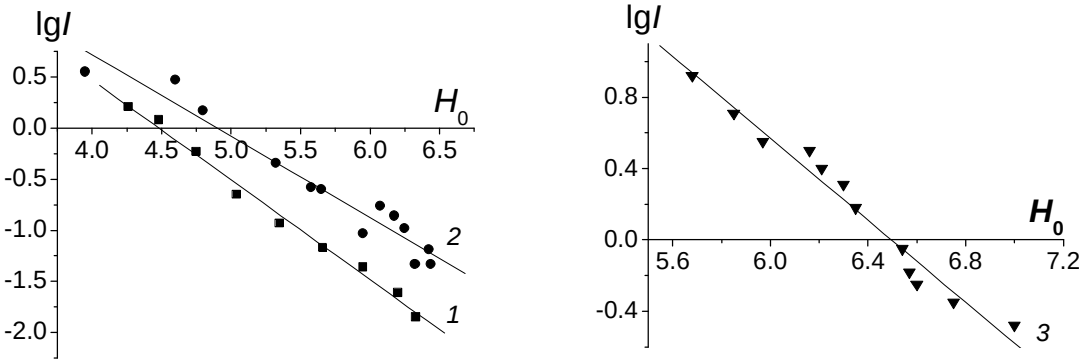

Figure 8. Relationships $\log I$-H_0 for the equilibrium of the ion-ion associate formation in the benzene-acetic acid system. Series *1, 2, 3* correspond to compounds **1, 2, 4.**

Table 4. Heats of formation (ΔH_f), relative energies ($\Delta\Delta H_f$), ionization potentials (IP), dipole moments (μ), nitrogen atoms charges, and first singlet-singlet transitions (λ_{max}) of triazoleporphyrazine **7a** and its monoprotonated forms.

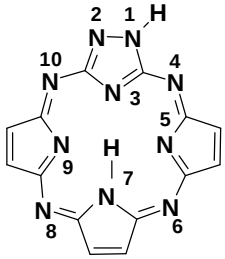

Proto-nated N-atom	ΔH_f, kcal mol^{-1}	$\Delta\Delta H_f$, kcal mol^{-1}	IP, e*V*	μ, *D*	charges on the nitrogen atoms, charge unit										λ_{max}* nm
					1	2	3	4	5	6	7	8	9	10	
-	350.01	-	9.11	3.07	-0.175	-0.025	-0.110	-0.086	-0.190	-0.146	-0.285	-0.100	-0.159	-0.012	478
1	522.42	33.69	12.65	4.46	-0.033	-0.136	-0.107	-0.168	-0.310	-0.172	-0.313	-0.130	-0.247	-0.094	279
2	506.79	18.06	12.64	4.38	-0.171	-0.151	-0.149	-0.141	-0.271	-0.153	-0.316	-0.154	-0.271	-0.142	273
3	488.73	0.00	12.89	2.37	-0.122	0.031	-0.212	-0.127	-0.361	-0.170	-0.321	-0.122	-0.307	-0.039	341
4	502.22	13.49	12.50	7.35	-0.194	0.028	-0.107	-0.184	-0.294	-0.144	-0.205	-0.017	-0.159	0.024	565
5	490.10	1.37	12.66	6.63	-0.136	0.026	-0.178	-0.037	-0.311	-0.216	-0.291	-0.027	-0.187	0.022	572
6	501.20	12.47	12.40	10.95	-0.150	0.020	-0.105	-0.014	-0.190	-0.189	-0.210	-0.014	-0.160	0.030	674
7	511.21	22.48	12.56	6.67	-0.135	0.038	-0.137	-0.015	-0.179	-0.018	-0.059	-0.010	-0.192	0.037	636

Found for the configurations optimized by AM1 method, UV-vis data calculated by ZINDOS, CI = 5*3.

Table 5. Heats of formation (ΔH_f), relative energies ($\Delta\Delta H_f$), ionization potentials (IP), dipole moments (μ), nitrogen atoms charges, and first singlet-singlet transitions (λ_{max}) of 1-methyltriazoleporphyrazine and its monoprotonated forms

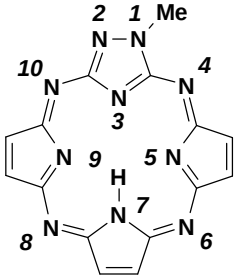

Proto-nated N-atom	ΔH_f, kcal mol^{-1}	$\Delta\Delta H_f$, kcal mol^{-1}	IP, e*V*	μ, *D*	charges on the nitrogen atoms, charge unit .										λ_{max}* nm
					1	2	3	4	5	6	7	8	9	10	
-	355.50	-	9.05	2.99	-0.131	-0.022	-0.110	-0.084	-0.186	-0.144	-0.284	-0.100	-0.158	-0.012	498
1	526.37	34.78	12.57	4.75	0.002	-0.130	-0.105	-0.164	-0.305	-0.171	-0.314	-0.129	-0.247	-0.089	276
2	508.83	17.24	12.52	5.19	-0.132	-0.147	-0.143	-0.139	-0.263	-0.151	-0.315	-0.151	-0.265	-0.135	276
3	491.59	0.00	12.79	2.71	-0.071	0.027	-0.209	-0.122	-0.353	-0.167	-0.321	-0.122	-0.304	-0.039	351
4	506.12	14.53	12.38	7.43	-0.149	0.029	-0.108	-0.180	-0.293	-0.146	-0.205	-0.018	-0.159	0.023	590
5	493.92	2.33	12.42	6.65	-0.086	0.024	-0.180	-0.036	-0.308	-0.218	-0.292	-0.029	-0.186	0.021	593
6	504.36	12.77	12.06	10.95	-0.103	0.019	-0.104	-0.014	-0.187	-0.188	-0.209	-0.014	-0.159	0.030	696
7	505.04	23.45	12.22	6.27	-0.075	0.043	-0.134	-0.009	-0.175	-0.017	-0.057	-0.010	-0.189	0.038	658

Found for the configurations optimized by AM1 method, UV-vis data calculated by ZINDOS, CI = 5*3.

Full geometry optimisation of these models was carried out by AM1 method. The optimized geometries were used to calculate the theoretical UV-vis spectra by ZINDOS method with configuration interactions. The results of the calculations are shown in the Tables 4-6.

Results of theoretical study show that most probably monoprotonation involves the internal nitrogen atom of the triazole ring of triazoleporphyrazines. The energy of long-wave singlet-singlet transitions increases in going from non-protonated to protonated forms, that corresponds to red shift of *Q*-bands. Theoretical studies agree with the experimental data for **1** and **2**. It's worthy to note that protonation of the isolated 1,2,4-triazole ring occurs on the nitrogen atom located at the position 4 of the ring.

Table 6. Heats of formation (ΔH_f), relative energies ($\Delta\Delta H_f$), ionization potentials (IP), dipole moments (μ), nitrogen atoms charges, and first singlet-singlet electron transitions (λ_{max}) of Zn-triazoleporphyrazine and its monoprotonated forms.

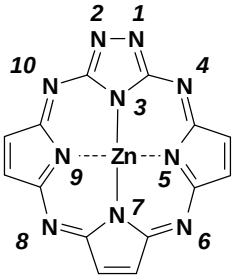

Proto-nated N-atom	ΔH_f, kcal mol^{-1}	$\Delta\Delta H_f$, kcal mol^{-1}	IP, e*V*	μ, D	charges on the nitrogen atoms, charge unit .										λ_{max}* nm
					1	2	3	4	5	6	7	8	9	10	
-	366.54	-	8.69	5.16	0.025	0.020	-0.306	-0.033	-0.324	-0.168	-0.318	-0.071	-0.308	-0.115	642
1	512.75	0.00	12.81	2.33	0.032	-0.119	-0.269	-0.022	-0.329	-0.160	-0.396	-0.185	-0.365	-0.097	374
3	529.03	16.28	12.81	4.40	0.082	0.082	-0.255	0.010	-0.330	-0.142	-0.402	-0.142	-0.330	0.010	629
4	514.19	1.44	12.37	4.62	0.019	0.081	-0.244	-0.137	-0.262	-0.047	-0.351	-0.157	-0.373	-0.029	665
5	524.97	12.22	12.73	5.38	0.078	0.060	-0.313	0.009	-0.236	-0.034	-0.323	-0.134	-0.400	-0.098	642
6	516.21	3.46	12.32	10.69	0.070	0.059	-0.355	-0.009	-0.261	-0.167	-0.265	-0.046	-0.347	-0.111	673
7	525.21	12.46	12.76	6.41	0.072	0.072	-0.399	-0.092	-0.318	-0.033	-0.234	-0.033	-0.319	-0.093	622

Found for the configurations optimized by AM1 method, UV-vis data calculated by ZINDOS, CI = 5*3.

In the metal complex, only *meso*-nitrogen atom can be protonated due to involvment of φ_n orbitals of the internal nitrogen atoms in the formation of donor-acceptor bonds with metal. The analysis of the heats of formation of the protonated forms shows that the structure with proton located at nitrogen atom N1 of triazole ring is more preferable.

The stability constants of the first acid forms pK_{s1} for **1**, **2** and **4** determined from Hammett's equation are 4.48 ± 0.18, 4.90 ± 0.32 and 6.50 ± 0.41, respectively.

The pK_{s1} values of **1** and **2** are of the same order of magnitude, suggesting that the protonation center is the same for both cases. Nevertheless, the basicity of **2** is significantly higher than that of **1**. To explain this fact one should consider the electron-donating (+I) effect of the alkyl substituent in the triazole ring containing the proton acceptor center. Introduction of the Cu^{2+} ion into the macrocycle (**4**) increases basicity by two orders of magnitude with respect to **1** and **2**.

This may indicate that the protonation center in the metal complex differs from that in **1** and **2**. In fact the protonation of the N atom located in position 4 of the triazole ring is impossible due to the presence of the metal cation at the center of the macrocycle cavity. Comparison of the pK_{s1} values obtained in this work for the triazoleporphyrazines (which ranged from 4.48 to 6.50) and those reported for the tetraazaporphyrins (1.00 and -1.33 for the octaphenyltetraazaporphyrin and its Cu complex, respectively) shows that the basicity increases when one pyrrole ring in the macrocycle is substituted by the triazole ring. It was shown previously that the first stage of the acid–base interaction in tetraazaporphyrins proceeds on one of the four *meso*-nitrogen atoms and leads to a bathochromic shift of the *Q*-band in the spectra.

To discover the possible effects of protonation on the molecular electronic structure of the triazoleporphyrazine at an adequate theoretical level with reasonably small computational effort, we selected three model protonated structures derived from the low-aromatic free-base triazoleporphyrazine **7a**. Two of these structures are protonated in the triazole ring, **9a** (position 4) and **9b** (position 3), and one is protonated in a *meso* N-atom, **9c** (Figure 9).

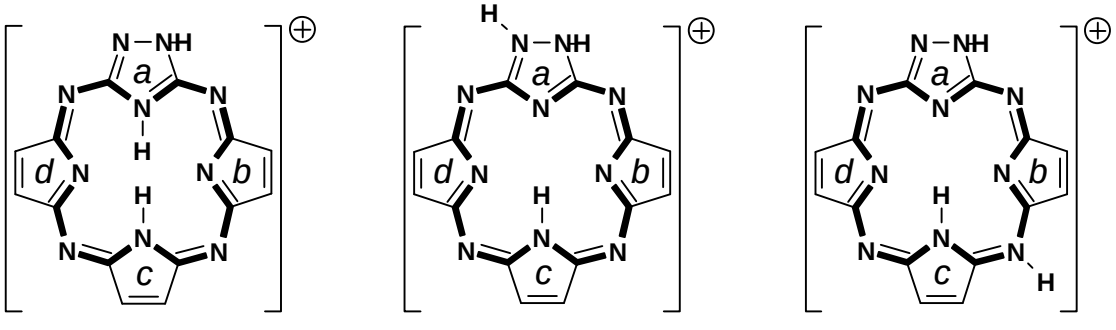

9a **9b** **9c**

Figure 9. Protonated (**9a–c**) structures of the unsubstituted free-base triazoleporphyrazine considered in this work. The internal cross of the structures is emphasized in bold.

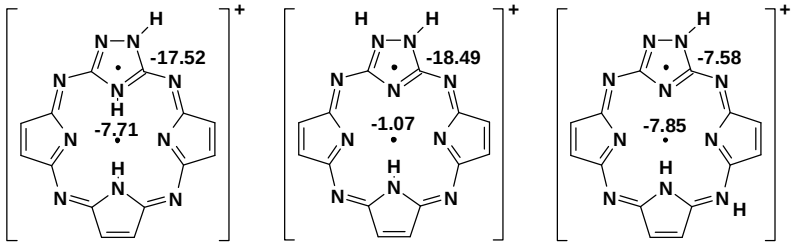

9a **9b** **9c**

Figure 10. Calculated NICS values (ppm) for the compounds **9a–c**.

The full geometry optimization performed at the DFT B3LYP/6–31(*d,p*) level yields plane configurations for the protonated forms **9a-c**. Upon protonation the planarity of the macrocycle is maintained, but its other geometric parameters are strongly changed. Considerable increases of the C–N (N–N) bond lengths are observed when the N atom captures a proton. For example, if a proton addition occurs to the nitrogen atom located at the position 4 of the triazole ring, the C–NH^+–C bonds elongate by more than 0.020Å. The magnitudes of total and relative electronic energies of the protonated forms **9a–c** are shown in Table 7.

Table 7. Total and relative energies of the protonated forms **9a-c**.

Structure	E_{tot}, au	ΔE_{rel}, au	ΔE_{rel}, kJ· mol^{-1}
9a	-1086.1604513	0.0000000	0
9b	-1086.1296643	0.0307870	80.75
9c	-1086.1359859	0.0244654	64.16

The cationic configuration **9a** bearing one proton at the position 4 of the triazole ring is found to be the most stable among the forms examined. Analysis of the charge distribution over all the molecule shows that in the cases of **9a** and **9b**, the positive charge is locally accumulated in the triazole ring, reaching values of +1.025 and +0.969, respectively. In contrast, the positive charge is more uniformly distributed over the whole molecule when the proton addition takes place along the exocyclic *meso* atom.

In order to estimate possible influence of the protonation on the aromatic properties, both geometry (EN, GEO and HOMA) and magnetic (NICS) based criteria of aromaticity were evaluated for the protonated forms of triazoleporphyrazine.

Table 8 gives the calculated values of geometry-based criteria of aromaticity for the systems under investigation.

In contrast to **9b**, proton addition to either the position 4 of the triazole ring (structure **9a**) or to the exocyclic-*meso*-N atom (structure **9c**) leads to equalization of the bond lengths in the cations. The GEO values decrease to 0.450 and 0.407 in **9a** and **9c**, respectively. The average bond lengths of these cations tend towards the optimal magnitude (EN criterion).

In **9a**, the formation of a porphyrazine-like internal cross explains the global increase in the HOMA, but simultaneously the local HOMA aromaticity index of triazole ring increases up to 0.956.

The description of the aromaticity based on geometry criteria is in a good agreement with that obtained by means of magnetic-based criteria (NICS).

Table 8. EN, GEO and HOMA indices for protonated forms **9a–c** optimized by B3LYP/6–31G(d,p).

Structure	EN	GEO	HOMA
9a (whole system)	**0.117**	**0.450**	**0.433**
Triazole ring (a)	0.028	0.016	0.956
Pyrrole ring (b)	0.346	0.767	-0.113
Pyrrole ring (c)	0.322	0.506	0.172
Pyrrole ring (d)	0.344	0.732	-0.076
Internal cross	0.019	0.077	*0.904*
9b(whole system)	**0.133**	**0.541**	**0.326**
Triazole ring (a)	0.057	0.037	0.906
Pyrrole ring (b)	0.371	0.959	-0.330
Pyrrole ring (c)	0.357	0.566	0.077
Pyrrole ring (d)	0.371	0.959	-0.330
Internal cross	*0.011*	*0.078*	*0.911*
9c (whole system)	**0.111**	**0.407**	**0.482**
Triazole ring (a)	0.040	0.053	0.907
Pyrrole ring (b)	0.264	0.715	0.021
Pyrrole ring (c)	0.256	0.391	0.353
Pyrrole ring (d)	0.402	0.666	-0.068
Internal cross	*0.018*	*0.124*	*0.858*

The value of the NICS index calculated for the center of the macrocycle **9a** (Figure 10) changes from -6.90 (neutral molecule) to -7.71 ppm, *i.e.* the aromaticity increases. Similar behavior was observed for the triazole ring of **9a**: the proton addition to the position 4 of the triazole ring (**9a**) produces an increase of the local aromaticity of this group. The NICS value of the center of the triazole ring changes from -13.20 (neutral molecule) to -17.52 (**9a**) ppm. This aromaticity increase for the structure **9a** can also serve as an explanation of the hypsochromic displacement of the absorbtion band.

Strong alternation of double and single bonds of the pyrrole rings *b* and *d* induces a considerable increase of the GEO values (Table 8) calculated for the structure **9b**. Therefore, global aromaticity of the ion decreases as the value obtained for the global HOMA (0.326) indicates.

The NICS value calculated for the center of the **9b** macrocycle cavity (-1.07 ppm) confirms very low aromatic character of this cation. The most aromatic part of this cation is the internal cross (depicted in Figure 9 in bold) as the HOMA index 0.911 obtained for this part of the molecule (Table 8) indicates. Accordingly, the single protonation of the triazoleporphyrazine throughout the position 4 of the triazole ring acts as an intramolecular switch for aromaticity.

In the case of exocyclic N atom (**9c**) protonation the HOMA increases up to 0.482. This increase is caused mostly by the HOMA contributions of pyrrole rings to the HOMA of the whole system. Since the N_{meso}-C bond lengths become elongated, the HOMA value of the internal cross decreases from 0.891 (neutral molecule) to 0.858 (**9c**). However, the N atom which is the acceptor of a proton is maintained as sufficiently good conductor of electron effects over molecule **9c**, as the NICS value of -7.85 ppm indicates.

Conclusion

Behaviour of hexakis(4-*tert*-butylphenyl)triazole-porphyrazine, its Cu complex and its 1-dodecyl derivative in proton-donating media was investigated. It was found that triazoleporphyrazines can be protonated in a proton-donating medium with poor ionizing ability (HOAc–benzene) forming ion–ion associates. Stability constants of the acid forms show that replacement of pyrrole moiety in porphyrazine by triazole ring increases basicity. Protonation of the triazoleporphyrazines results in a hypsochromic shift of the *Q*-bands in their UV–visible spectra.

Quantum chemical calculations show that the protonation of the triazoleporphyrazines strongly influences both their molecular electron structure and aromaticity. Investigations of the protonated forms confirm that the high basicity of triazoleporphyrazines is conditioned by protonation of the nitrogen atom located at the position 4 of the triazole ring, the corresponding protonated form has more aromatic character than the neutral structure. However, addition of one proton to the nitrogen atom at the position 4 of the triazole ring is responsible for the dramatic macrocycle aromaticity decrease. Hence one may consider the triazoleporphyrazines as an intramolecular switch for aromaticity.

References

1. Berezin B.D. *Koordinazionnye soedinenija porfirinow i ftalotcianinow.* [*Coordination compounds of porphyrines and phthalocyanines*] Moskwa, Nauka **1978**, 280. (in Russ.)
2. *The Porphyrin Handbook* Vols. 1-10 (Kadish K.M, Smith K.M, Guilard R., Eds) San Diego, Academic Press, **2000**.
3. Stuzhin P.A, Ercolani C. Porphyrazines with Annulated Heterocycles, in *The Porphyrin Handbook* (Kadish K.M., Smith K.M., Guilard R., Eds) Ch. 101, Amsterdam, Academic Press, **2003**, *15*, 263-364.
4. Leznoff C.C. In *Phthalocyanines: Properties and Applications* Vols. 1-4 (Leznoff C.C., Lever A.B.P., Eds), New York, VCH, **1989-1996**.
5. *The Porphyrin Handbook* Vols. 15–20 (Eds. Kadish K.M., Smith K.M., Guilard R.) Amsterdam, Academic Press, **2003**.
6. Rodríguez-Morgade M.S., De la Torre G., Torres T. Design and Synthesis of Low-Symmetry Phthalocyanines and Related Systems, in *The Porphyrin Handbook* Ch. 99 (Kadish K.M., Smith K.M., Guilard R., Eds), Amsterdam, Academic Press, **2003**, *15*, 125 – 160.
7. De la Torre G., Vazquez P., Agullo-Lopez F., Torres T.J. *Chem. Rev*. **2004**, *10*, 3723-3750.
8. De la Torre G., Blau W., Torres T.J. *Nanotechnology* **2003**, *14*, 765–771.
9. Guldi D.M., Gouloumis A., Vazquez P., Torres T., Georgakilas V., Prato M. *J. Am. Chem. Soc*. **2005**, *127*, 5811-5813.
10. Böhme R., Breitmaier E. J. *Synthesis* **1999**, *12*, 2096–2102.
11. Sharman W.M., Van Lier J.E. Synthesis of Phthalocyanine Precursors, in *The Porphyrin Handbook* (Kadish K.M., Smith K.M., Guilard R., Eds) Ch. 97, Amsterdam, Academic Press, **2003**, *15*, 1–60.
12. Leznoff C.C., Terekhov D.S., McArthur C.R., Vigh S., Li J. *Can. J. Chem.* **1995**, *73*, 435-443.
13. Wang J., Khanamiryan A.K., Leznoff C.C. *J. Porphyrins Phthalocyanines* **2004**, *8*, 1293-1299.
14. Latos-Grażyński L. Core-Modified Heteroanalogues of Porphyrins and Metalloporphyrins, in *The Porphyrin Handbook* (Kadish K.M., Smith K.M., Guilard R., Eds.) Ch. 14. Amsterdam, Academic Press, **2003**, *2*, 61-416.
15. Kudrik E.V., Islyaikin M.K., Smirnov R.P. *Zh. Org. Khim.* **1997**, *33*, 1107-1110. (Russ).
16. Fernández-Lázaro F., Sastre A., Torres T. *J. Chem. Soc., Chem. Com.* **1994**, 1525-1526.
17. Nicolau M., Cabezón B., Torres T. *J. Org. Chem.* **2001**, *66*, 89–93.
18. Esperanza S., Nicolau M., Torres T. *J. Org. Chem*. **2002**, *67*, 1392-1395.
19. Nicolau M., Cabezón B., Torres T. *Coord. Chem. Rev*. **1999**, *190-192***,** 231-243.
20. Armand F., Martínez-Díaz M.V., Cabezón B., Albouy P.-A., Ruaudel-Teixier A., Torres T. *J. Chem. Soc., Chem. Commun.* **1995**, 1673-1674.
21. Rojo G., Agulló-López F., Cabezón B., Torres T., Brasselet S., Ledoux I., Zyss J. *J. Phys. Chem., B* **2000**, *104*, 4295-4299.
22. Islyaikin M.K., Rodríguez-Morgade M.S., Torres T. *Eur. J. Org. Chem*. **2002**, *15*, 2460 – 2464.
23. Krygovski T.M., Cyrański M.K. *J. Chem. Rev*. **2001**, *101*, 1385–1419.
24. Scheyer Pv.R., Maerker C., Dransfeld A., Jiao H., Hommes N.J.Rv.E. *J. Am. Chem. Soc.* **1996**, *118*, 6317-6318.
25. Cyranski M.K., Krygovski T.M., Wiciorowski M., Hommes N.J.Rv.E., Shleyer Pv.R. *Angew. Chem. Int. Ed*. **1998**, *37*, 177-180.
26. Islyaikin M.K., Ferro V.R., García de la Vega J.M. *J. Chem. Soc., Perkin Trans.* 2. **2002**, *12*, 2104 – 2109.
27. Marinina L.E., Mikhalenko S.A., Lukyanets E.A. *Zh. Org. Khim.* **1973**, *43*, 2025-2029. (Russ).
28. Alonso J.M., Martin M.R., De Mendoza J., Torres T., Elguero J. *Heterocycles* **1987**, *26*, 989-1000.

Received 15.04.2008
Accepted 06.06.2008

Synthesis of Hemipyrazinoporphyrazines Bearing Peripheral Pyrrolic Substituents

M. Salomé Rodríguez-Morgade,[a] G. Dan Pantos,[b] Esmeralda Caballero,[a] Jonathan L. Sessler,[b,@] and Tomás Torres[a,@]

[a]*Departamento de Química Orgánica, Universidad Autónoma de Madrid, Cantoblanco,28049 Madrid, Spain*
[b]*Department of Chemistry and Biochemistry and Institute for Cellular and Molecular Biology 1 University Station - A5300, University of Texas at Austin, Austin, Texas 78712-0165, USA*
[@]*Corresponding authors E-mail: sessler@mail.utexas.edu, tomas.torres@uam.es*

Described in this report is the synthesis and optical spectroscopic characterization of two new dipyrrolylquinoxaline analogues. These new systems consist of novel hemipyrazinophyrazines that are functionalized on their respective peripheries with four pyrrole rings. The electronic features of these compounds are typical of those expected for hemiporphyrazines, although slight bathochromic shifts are observed for the absorption bands in the violet-blue region of the electromagnetic spectrum.

Introduction

Hemiporphyrazines (Figure 1) are members of the generalized class of porphyrin analogues known as azaporphyrins.[1-5] They can be considered as ABAB phthalocyanine analogues in which two isoindole subunits have been replaced by heterocycles other than pyrroles. As a consequence, hemiporphyrazines generally display D_{2h} symmetry, that is, they bear two opposite faced isoindole moieties. This feature has made them interesting building-blocks for the construction of linear arrays, such as ribbon- or ladder-type polymers. Hemiporphyrazines also offer the advantage of being easy to prepare. For instance, the first example of this nonaromatic, cross-conjugated compounds, the 28 π-electron macrocycle **1** (Figure 1) reported by Elvidge and Linstead[6] was obtained through condensation of 1,3-diiminoisoindoline with 2,6-diaminopyridine. This synthetic procedure, like the name originally proposed, has now been extended to the whole hemiporphyrazine class. In fact, the general procedure currently used to obtain any of a number of hemiporphyrazines is to condense a suitable 1,3-diimino-isoindoline derivative with the corresponding (hetero)-aromatic ring endowed with two primary amines. Here, the position of the two amino functions should be such that it permits the crossover [2+2] cyclotetramerization of the two components. Further, metallation with appropriate metal salts can be used to access the corresponding metallohemiporphyrazines.

The Madrid group has been involved in the modification of the tetraazaporphyrin structure in order to obtain other macrocycles structurally related to phthalocyanines and porphyrazines but exhibiting non conventional physicochemical features.[2,3,8] One of the modifications that we have carried out involves the incorporation of the 1,2,4-triazole or 1,3,4-thiadiazole heterocycles into the tetrazaporphyrin structure. Thus, we have described the synthesis, characterization and properties of *triazoleazaporphyrins* (**2**, Figure 1),[9,10] intrinsically unsymmetrical compounds that constitute aromatic azaporphyrin analogues in which one isoindole moiety has been formally replaced by a 1,2,4-triazole subunit. The introduction of this heterocycle into the phthalocyanine framework leads to a lower degree of electronic delocalization, which results in an hypsochromic shift of its *Q*-band in relation to the corresponding phthalocyanine absorption.[5,11] This property, coupled with the lack of symmetry center, has made these derivatives good targets for the development of materials with non-linear optical applications.[12,13,14] In addition, their amphiphilic structure, characterized by a polar 1,2,4-triazole head and an aromatic macrocycle, is especially appropriate for Langmuir-Blodgett film formation.[9]

The replacement of two isoindole subunits in a Pc by two 1,2,4-triazoles affords the so-called

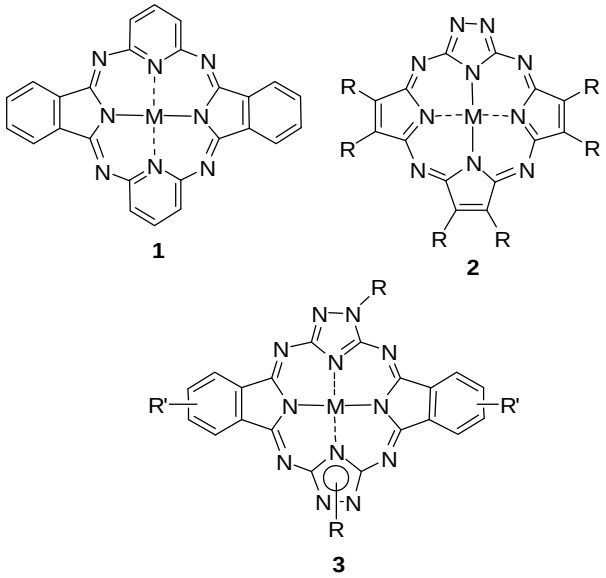

Figure 1. Chemical structures of hemiporphyrazine (**1**), triazoleazaporphyrin (**2**) and triazolehemiporphyrazine (**3**).

triazolehemiporphyrazines (**3**, Figure 1),[3] macrocycles that possess a 20 π-electron cross-conjugated system and therefore, nonaromatic character. We have functionalized these hemiporphyrazines to produce materials with special optical and liquid crystalline properties.[3,15] Furthermore, we have taken advantage of the hemiporphyrazine ABAB symmetry to prepare heterobinuclear and heterotrinuclear phthalocyanine-hemiporphyrazine hybrids with extended conjugation.[16] We have also extended the π system of the hemiporphyrazines by preparing the first examples of expanded triazolehemiporphyrazine[17] and thiadiazolehemiporphyrazine.[18] These expanded heteroannulenes display unusual coordination features, including an ability to bind two or three metal ions, respectively, within their central cavity.

Recently, the group in Austin has developed a variety of pyrrole-based anion receptors, including some based on calixpyrroles, sapphyrins, and dipyrrolylquinoxalines.[19,20] Several of the latter systems allow for the direct, so-called naked eye detection of several biologically relevant anions. Others have served to underscore the fact that small changes in the structure can produce receptors with very different anion binding properties. Thus, we had a two-fold motivation to combine the chemistry of pyrrolic macrocycles with that of the hemiporphyrazines: First, it would allow the effect of structure on pyrrole-based anion recognition to be further probed. Second, the reddish color of hemiporphyrazines could enable the use of these compounds as colorimetric anion sensors. With this medium-term purpose in mind, we decided to incorporate the dipyrrolylquinoxaline motif into the hemiporphyrazine structure. Thus, in this paper we wish to report briefly on a new class of dipyrrolylquinoxaline analogues consisting in triazolehemiporphyrazines further functionalized with peripheral pyrrole rings.

Experimental

UV-vis spectra were recorded with a Hewlett-Packard 8453 spectrophotometer. IR spectra were recorded with Bruker Vector 22 spectrophotometer. MALDI-TOF MS spectra were recorded with a Bruker Reflex III spectrometer. NMR spectra were recorded with a Bruker AC-300 instrument. Column chromatographies were carried out on silica gel Merck-60 (230-400 mesh, 60 Å) and TLC was performed on aluminium sheets precoated with silica gel 60 F_{254} (E. Merck). Chemicals were purchased from Aldrich Chemical Co. and used as received without further purification.

*General procedure for the synthesis of hemipyrazinoporphyrazines **8a,b:*** A mixture of pyrazinocarbonitrile **5** (1 mmol) and the corresponding diaminotriazole derivative **7a,b** (1 mmol) was dissolved in ethyleneglycol and the solution was heated at 100º C for 4 h. After this time a precipitate was observed. The temperature was raised to 160º C and the mixture was heated for other 20 h at this temperature. The suspension was cooled to r.t., the solid was filtered and washed with ethanol. The obtained solid was suspended in ethanol and triturated at reflux, filtered, washed with ethanol and dried at 10^{-1} mm Hg.

7,17(18)-Dihydrodi(5',6'-bis(1"H-pyrrol-2"-yl)pyrazino)[b,g]-5,7,8,10,15,17,18,20-octaazaporphyrin **8a:** (58%). *m/z* (MALDI-TOF) 685 (100) $[(M+H)^+]$. ν_{max} (KBr)/cm^{-1} 3283, 2966, 1722, 1641, 1547, 1425, 1398, 1358, 1263, 1182, 1047, 804. λ_{max} (DMF) 387, 432 nm.

7,17(18)-Didodecyl-7,17(18)-dihydrodi(5',6'-bis(1"H-pyrrol-2"-yl)pyrazino)[b,g]-5,7,8,10,15,17,18,20-octaazaporphyrin **8b:** (52%). *m/z* (MALDI-TOF, dithranol) 1021 (100) $[(M+H)^+]$. ν_{max} (KBr)/cm^{-1}, 3290, 2925, 2856, 1718, 1651, 1539, 1435, 1398, 1356, 1258, 1190. λ_{max} (DMF) 390, 435 nm.

Results and Discussions

Appropriate dinitrile precursors were prepared using synthetic procedures previously reported by the Austin group.[19] Specifically, condensation of 1,2-bis-(1*H*-pyrrol-2-yl)ethane-1,2-dione (**3**) with diaminomaleonitrile (DAMN, **4**) was found to afford the corresponding 5,6-bis(1*H*-pyrrol-2-yl)pyrazine-2,3-dicarbonitrile **5** in 55% yield (Scheme 1).

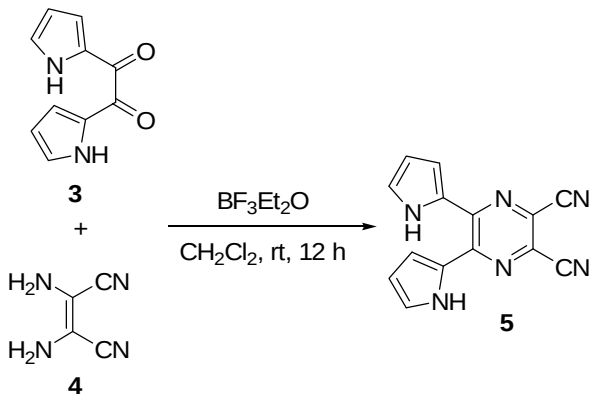

Scheme 1. The synthesis of the pyrazinedicarbonitrile **5**.

As mentioned above, the synthesis of hemiporphyrazines usually involves the condensation reaction of a diamine with a diiminoisoindoline derivative which in turn, is obtained by reaction of the corresponding phthalonitrile with ammonia in an alcoholic solvent and catalyzed by a sodium alkoxide. However, in some cases it is also possible to obtain a hemiporphyrazine directly from an appropriately chosen dinitrile precursor. In the latter case, harsher conditions are necessary to complete the cyclotetramerization reaction. This is thought to reflect the fact that diiminoisoindolines are reaction intermediates under these conditions. In fact, the condensation of a diamine with a phthalonitrile should begin with the nucleophilic attack of one of the amino moieties on one of the nitrile groups. Subsequently, a pyrrole ring is produced from the dicyano compound, to yield a two-unit intermediate of type **6**, which already contains the iminoisoindoline moiety (see Scheme 2). The further dimerization of this two-unit intermediate affords the hemiporphyrazine macrocycle.

Triazolehemiporphyrazines have also been obtained both from diiminoisoindoline, or directly from the condensation reaction of phthalonitrile precursors and 2,5-diamino-1,2,4-triazole derivatives.[21] In the latter case, treatment of the starting materials at high temperature (198º C at reflux in ethyleneglycol) proved to be the most convenient method in terms of reaction time and efficiency. The thermal instability of the dicyano derivative **5** precludes prolonged heating at high temperatures. Therefore, hemiporphyrazine **8a** was prepared *via* a cyclotetramerization reaction involving the pyrazinocarbonitrile **5** and guanazole (**7a**), which could be carried out at a temperature of 160 °C (Scheme 3). Under these conditions, an yield of 58% was obtained.

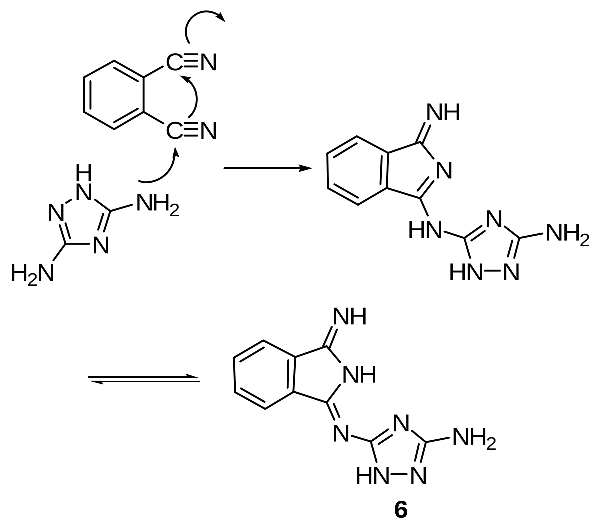

Scheme 2. The mechanism of the formation of a triazolehemiporphyrazine starting from a phthalonitrile precursor.

Macrocycle **8a** proved to be extremely insoluble in organic solvents. However, it was appreciated that functionalization of 1,2,4-triazole derivatives at the 1 position with dodecyl chains leads to enhanced solubility in organic solvents.[21] Accordingly, we have prepared the triazolehemiporphyrazine **8b**; it was produced following the same methodology but using 3,5-diamino-1-dodecyl-1,2,4-triazole (**7b**)[21] as the triazole precursor. Unfortunately, the solubility of this compound was not greatly improved relative to its non substituted congener.

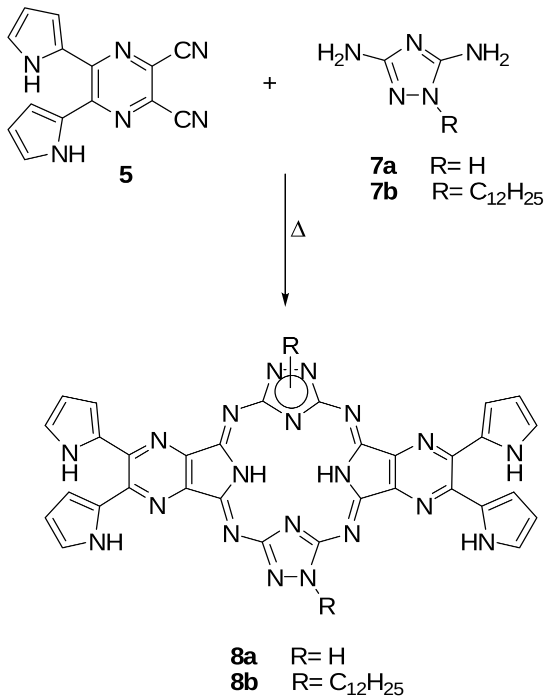

Scheme 3. Synthesis of hemipyrazinoporphyrazines **8a,b**

All new compounds were characterized using standard spectroscopic techniques. Compounds **8a,b** displayed a single peak at m/z = 685 and 1021, respectively corresponding to $[M+H]^+$ in the MS (MALDI-TOF). In addition, the UV-vis spectra of both hemipyrazinoporphyrazines **8a** and **8b** were found to be almost identical.

In Figure 2 the electronic spectra of a typical Ni^{II} triazolehemiporphyrazine, compound **8b**, and the associated pyrazinecarbonitrile precursor are shown.

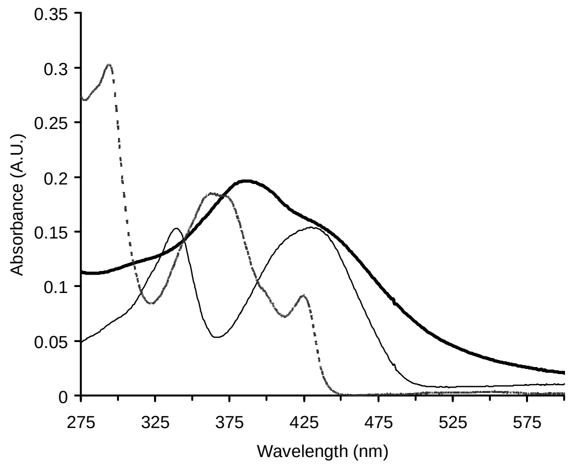

Figure 2. UV-vis spectra of hemipyrazinoporphyrazine **8b** (thick solid line), a typical triazolehemiporphyrazine (**3**, R = $C_{12}H_{25}$, R' = OC_8H_{17}, M = Ni, dotted line), and 5,6-bis(1*H*-pyrrol-2-yl)-pyrazine-2,3-dicarbonitrile (**5**) (thin solid line) in DMF.

The electronic properties of macrocycle **8b** are typical for a triazolehemiporphyrazine, in that two bands are seen at 390 and 435 nm, respectively. As expected, neither the fused pyrazino rings nor the peripheral pyrrole moieties produces any substantial alteration in the optical properties of the triazolehemiporphyrazine, apart from a slight bathochromic shift in the absorption bands of ca. 20 nm. While not yet fully established, this shift is likely due to the incorporation of the four pyrazino nitrogens within the hemiporphyrazine structure.

Conclusion

In summary, two new dipyrrolylquinoxaline analogues are described. They consist of novel hemipyrazinoporphyrazines that are functionalized on their respective peripheries with four pyrrole rings. The electronic properties of these compounds are typical of those expected for hemiporphyrazines, in that UV-vis absorption bands in the violet-blue region of the electromagnetic spectrum are displayed. However, slight bathochromic shifts are seen. Unfortunately, the poor solubility of these macrocycles in typical organic solvents precluded their testing as anion sensors. Further studies in order to obtain soluble compounds are currently underway and will be published in due course.

Acknowledgements. The work in Madrid was supported by the Spanish MEC (CTQ-2005-08933-BQU), the Comunidad de Madrid (S-0505/PPQ/000225), and the ESF-MEC (project SOHYD). M. S. R.-M. thanks the Spanish MEC for a R & C contract. The work in Austin was supported by the National Science Foundation (CHE 0515670 to J.L.S.).

References

1. Campbell J.B. *U.S. Patent* 2765308, **1956**; *Chem. Abstr.* **1956**, *51*, 8143f.
2. Fernández-Lázaro F., Torres T., Haushel B., Hanack M. *Chem. Rev*. **1998**, *98*, 563-575.
3. Rodríguez-Morgade M.S., de la Torre G., Torres T. Design and Synthesis of Low-Symmetry Phthalocyanines and Related Systems, in *The Porphyrin Handbook*, Vol. 15, Ch. 99 (Kadish K.M., Smith K.M., Guilard R., Eds) San Diego, Academic Press, **2003**, 125-159.
4. Rodriguez-Morgade M.S., Stuzhin P.A. *J. Porphyrins Phthalocyanines* **2004**, *8*, 1129-1165.
5. Rio Y., Rodríguez-Morgade M.S., Torres T. *Org. Biomol. Chem.* **2008**, *6*, 1877-1894.
6. Elvidge J.A., Linstead R.P. *J. Chem. Soc.* **1952**, 5008-5012.
7. de la Torre G., Nicolau M., Torres T. Phthalocyanines: Synthesis, Supramolecular Organization, and Physical Properties, in *Supramolecular Photosensitive and Electroactive Materials* (Ed. Nalwa H.R.) New York, Academic Press, **2001**, 1-111.
8. Claessens C.G., González-Rodríguez D., Torres T. *Chem. Rev*. **2002**, *102*, 835-853.
9. Nicolau M., Cabezón B., Torres T. *Coord. Chem. Rev.* **1999**, *190-192*, 231-243.
10. Islyaikin M.K., Rodríguez-Morgade M.S., Torres T. *Eur. J. Org. Chem.* **2002**, 2460-2464.
11. Cabezon B., Rodríguez-Morgade S., Torres T. *J. Org. Chem.* **1995**, *60*, 1872 -1874.
12. de la Torre G., Vázquez P., Agulló-López F., Torres T. *J. Mat. Chem.* **1998**, *8*, 1671-1683.
13. de la Torre G., Vazquez P., Agullo-Lopez F., Torres T. *Chem. Rev*. **2004**, *104*, 3723-3750.
14. Rojo G., Agulló-López F., Cabezón B., Torres T., Brasselet S., Ledoux I., Zyss J. *J. Phys. Chem. B* **2000**, *104*, 4295-4299.
15. Diaz-Garcia M.A., Ledoux I., Fernandez-Lazaro F., Sastre A., Torres T., Agullo-Lopez F., Zyss J. *J. Phys. Chem.* **1994**, *98*, 4495–4497.
16. de la Torre G., Martínez-Díaz M.V., Ashton P.R., Torres T. *J. Org. Chem.* **1998**, *63*, 8888-8893.
17. Rodríguez-Morgade M.S., Cabezón B., Esperanza S., Torres T. *Chem. Eur. J.* **2001**, *7*, 2407-2413.
18. Islyaikin M.K., Danilova E.A., Yagodarova L.D., Rodríguez-Morgade M.S., Torres T. *Org. Lett.* **2001**, *3*, 2153-2156.
19. Sessler J.L., Pantos G.D., Katayev E., Lynch V.M. *Org. Lett.* **2003**, *5*, 4141-4144.
20. Ghosh T., Maiya B.G., Wong M.W. *J. Phys. Chem. A* **2004**, *108*, 11249-11259.
21. Fernández-Lázaro F., de Mendoza J., Mó O., Rodríguez-Morgade S., Torres T., Yáñez M., Elguero J. *J. Chem. Soc. Perkin Trans. 2* **1989**, 797-803.

Received 12.06.2008
Accepted 13.06.2008

Synthesis, Characterization and Optical Limiting Properties of Novel Ball−type Four *tert*−Butylcalix[4]arene Bridged Double−decker Lutetium(III) and Indium(III) Phthalocyanines

Tanju Ceyhan,[a] Gül Yağlioğlu,[b] Hüseyin Ünver,[c] Bekir Salih,[d] Mehmet K. Erbil,[a] Ayhan Elmali,[b] and Özer Bekaroğlu[e,@]

[a] *Department of Biochemistry, Division of Organic Chemistry, Gülhane Medical Academy, (GATA), Ankara, Turkey*
[b] *Department of Engineering Physics, Faculty of Engineering, Ankara University, Ankara, Turkey.*
[c] *Department of Physics, Faculty of Sciences, Ankara University, Ankara, Turkey.*
[d] *Department of Chemistry, Hacettepe University, 06532 Ankara, Turkey.*
[e] *Department of Chemistry, Technical University of Istanbul, 80626, Maslak, Istanbul, Turkey.*
[@] *Corresponding author E-mail: obek@itu.edu.tr*

*Novel ball type four tert-butylcalix[4]arene bridged double-decker lutetium(III) phthalocyanine [$LuPc_2(tbca)_4$] **2** which exhibit nonlinear optical limiting behaviour and indium(III) phthalocyanine [$InPc_2(tbca)_4$] **3** were prepared by the reaction of 1,3-bis(3,4-dicyanophenoxy)-4-tert-butylcalix[4]arene **1** and the corresponding metal salts ($Lu(OAc)_3 \cdot 3H_2O$ and $InCl_3$) in the presence of lithium metal in 1-pentanol. Newly synthesized phthalocyanines were characterized by elemental analysis, UV-vis, IR, MALDI-TOF MS and ^1H NMR spectra.*

Introduction

Calix[4]arenes are versatile host molecules for supramolecular chemistry, which have been incorporated into numerous elaborate structures.[1] Double calix[4]-arenes[2] for example, have been constructed covalently through upper rim/upper rim linkage,[3] lower rim/lower rim linkage,[4] or upper rim/lower rim linkage[5] and also noncovalently through hydrogen bonding.[6] Thus a large number of calixarene derivatives with defined cavity and function have been designed and synthesized allowing efficient and selective complexation with various species.[7] More importantly, calixarenes provide building blocks for more complex architectures.[2,8] Assemblies of two calix[n]arenes via both upper rims, head-to-head using covalently bonded spacers such as aromatic chains[9] and porphyrins[10] have lead to molecular capsules with enforced cavity. The resulting molecular capsules were capable of encapsulating a number of aromatic molecules.[11] Based on the intrinsic cavity of calix[4]arene and its hydrophobic and CH-π interactions[12] with guest substrates we envisaged that oligomeric calix[4]arenes would provide novel and efficient receptors to complex larger and more complicated organic molecules such as phthalocyanines. This led us to undertake this investigation.

Phthalocyanines (Pcs) are one of the major types of tetra-pyrrole derivatives showing a practical applications in a wide range of high technology fields such as nonlinear optics, photosensitizers, gas sensors, catalysts, liquid crystals, optical data storage, sensitizers for photodynamic therapy of cancer, electrodes in fuel cell, photoelectric conversion materials in solar cells and laser service substances, among others.[13-15] A great number of remarkable applications of phthalocyanines arise from their unique 18π electron conjugated aromatic cloud which makes them present high thermal and chemical stability and remarkable photoelectric properties.[16] The exceptional chemical and physical properties of these compounds can be due to various substituents on the phenyl rings. Much research on this concept has been devoted to the synthesis of phthalocyanines that have been peripherally functionalized with appendages that can coordinate metal cations.

Diphthalocyaninates of rare-earth metals, especially the lutetium derivative, have become objects of intense investigations. The interest for compounds of this kind, first due to their electrochromic properties,[17-19] is actually increasing because of their unusual conductivity.[20-23] Substituents on the periphery of a macrocycle ring like a phthalocyanine are known to affect its physicochemical properties. Many relationships between the chemical structure and properties like photoconductivity,[24] electrocrystallization[25] and redox potentials[26] have been established. Chemical groups linked to the peripheral benzene rings not only modify the electronic properties of the phthalocyanines, but also those of the materials obtained from these molecular units.[27,28]

We have reported on the synthesis, characterization of novel *s*-triazines bearing three oxygen-linked metallo Pcs and lutetium bisphthalocyanine sandwich complexes.[29,30] Synthesis, characterization, conduction and gas sensing properties of novel multinuclear metallo Pcs with alkylthio substituents were also reported in the literature.[31] In our previous study, we achieved for the first time the synthesis of a novel ball-type four *tert*-butylcalix[4]arene bridged binuclear zinc(II) Pc. This novel compound exhibited mixed-valence behaviour and non-Arrhenius type dependence of conductivity.[32] We have reported recently on the synthesis, characterization, and electrochemical, electrical and gas sensing properties of a novel *tert*-butylcalix[4]arene bridged *bis* double-decker lutetium (III) phthalocyanine.[33]

Hereafter we report for the first time, the synthesis and characterization of a novel ball type four *tert*-butylcalix[4]-arene bridged double-decker lutetium(III) **2** and indium(III) **3** phthalocyanines (Scheme 1). We also present the results of nonlinear optical limiting measurements. On the other hand, the importance of this new type of phthalocyanine may be regarded as an important step in that it may be one of the candidates for optical limiting applications.

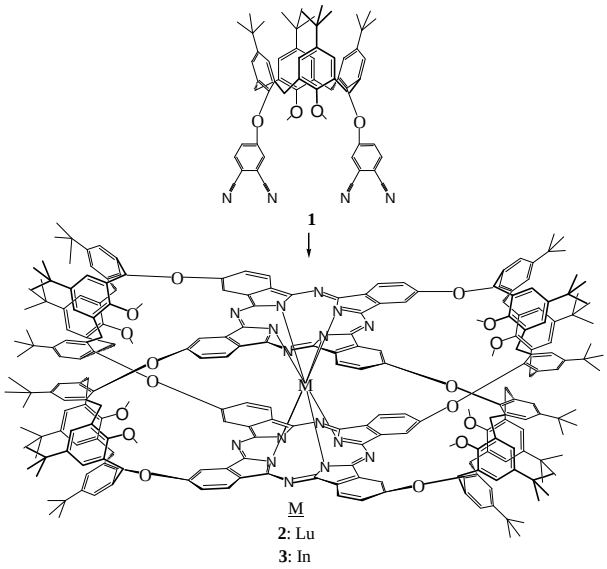

Scheme 1. Synthesis of compounds **2** and **3**.

Experimental

All reagents and solvents were of reagent-grade quality obtained from commercial suppliers. The solvents were stored over molecular sieves (4 Å). Compound **1** was prepared according the literature method.[32] Routine IR were recorded on a Shimadzu IR-470 Infrared spectrometer as KBr pellets, electronic spectra on a UNICAM UV 500 UV-vis spectrometer. Elemental analysis was performed by the LECO CHNS 932 in the Instrumental Analysis Laboratory of TUBITAK Ankara Research Center. ^{1}H NMR spectra were recorded on a Bruker Avance DPX-400 spectrometer. Mass spectra were acquired on a Voyager-DETM PRO MALDI-TOF mass spectrometer (Applied Biosystems, USA) equipped with a nitrogen UV-Laser operating at 337 nm. Spectra were recorded both in linear and reflection modes with average of 50 shots. 3-Indolylacrylic acid (IAA) MALDI matrix was used and prepared in chloroform at concentration of 20 mg/ml for Pcs **2** and **3** as the most efficient matrix. MALDI samples were prepared by mixing sample solutions (4 mg/ml, in acetic acid) with the matrix solution (1:10 v/v) in a 0.5 ml eppendorf® micro tube. Finally 1 µl of this mixture was deposited on the sample plate, dried at room temperature and then analyzed.

Syntheses

Reaction procedure for [$LuPc_2(tbca)_4$] (2). Clean lithium metal (50 mg, 7.355 mmol) was placed in a glass tube with 2 ml of 1-pentanol and the mixture was purged with nitrogen, sealed and refluxed until the complete reaction of lithium. Then, the glass tube was opened and compound **1** (200 mg, 0.215 mmol) was added and the tube was sealed again. The mixture was refluxed for another 1 h, then $Lu(OAc)_3{\cdot}3H_2O$ (75.6 mg, 0.215 mmol) was added, the tube was sealed again and the mixture refluxed for additional 15 h. After cooling to room temperature, 10 ml of ethanol was added to the dark green mixture to precipitate the product. The precipitate was suction filtered, multiply washed first with hot water and then with hot ethanol, hot methanol, chloroform, hot DMF, hot ethyl acetate and THF and then dried in vacuum to give the pure product. This compound is soluble in acetic acid and in the mixture of acetic acid-DMSO. Yield: 38 mg, 18 %. m.p. >300 °C. UV-vis (CH_3COOH, 106.08 µM): λ_{max}, nm (log ε) 335 (4.119), 673 (3.854), 708 (3.941). ^{1}H NMR (CD_3CO_2D): δ, ppm 7.83-6.91 (m, 56H, Ar-H), 3.87 (s, 24H, OCH_3), 3.76 (d, *J*=13.4 Hz, 16H, $ArCH_2Ar$), 3.28 (d, *J*=13.4 Hz, 16H, $ArCH_2Ar$), 1.49 (s, 72H, *t*-Bu), 0.98 (s, 72H, *t*-Bu). IR (KBr): ν, cm^{-1} 3054 (CH Ar), 2922-2836 (CH aliph.), 2328, 1727, 1654, 1612 (C=C Ar), 1470, 1358, 1290 (Ar-O-Ar), 1192, 1116, 945, 872, 758, 672, 619. MS (MALDI-TOF): *m/z* 3888 $[M+H]^+$. Anal calc. for $C_{248}H_{256}N_{16}O_{16}Lu$ (3887): C 76.56, H 6.58, N 5.76; found: C 76.12, H 6.21, N 5.84.

Reaction procedure for [$InPc_2(tbca)_4$] (3). Clean lithium metal (50 mg, 7.355 mmol) was placed in a glass tube with 2 ml of 1-pentanol and the mixture was purged with nitrogen, sealed and refluxed until the complete dissolution of lithium. Then, the glass tube was opened and compound **1** (200 mg, 0.215 mmol) was added and the tube was sealed again and the mixture was refluxed for another 1 h. Then $InCl_3$ (47.7 mg, 0.215 mmol) was added, the tube was sealed again and the mixture was refluxed for a further 15 h. After cooling to room temperature, 10 ml of ethanol was added to the dark green mixture to precipitate the product. The same purification process was carried out as described for compound **2**. This compound is soluble in acetic acid and in the mixture of acetic acid-DMSO. Yield: 117 mg, 57 %. m.p. >300 ºC. UV-vis (CH_3COOH, 92.62 µM): λ_{max}, nm (log ε) 346 (4.475), 634 (3.976), 702 (4.461). ^{1}H NMR (CD_3CO_2D): δ, ppm 7.92-7.02 (m, 56H, Ar-H), 3.72 (s, 24H, OCH_3), 3.37 (d, *J*=13.4 Hz, 16H, $ArCH_2Ar$), 3.28 (d, *J*=13.4 Hz, 16H, $ArCH_2Ar$), 1.49 (s, 72H, *t*-Bu), 0.98 (s, 72H, *t*-Bu). IR (KBr): ν, cm^{-1} 3042 (CH Ar), 2936-2872 (CH aliph.), 2326, 1730, 1655, 1615 (C=C Ar), 1470, 1357, 1292 (Ar-O-Ar), 1190, 1116, 945, 870, 761, 670, 620. MS (MALDI-TOF): *m/z* 3828 $[M+H]^+$. Anal calc. for $C_{248}H_{256}N_{16}O_{16}In$ (3827): C 77.76, H 6.68, N 5.85; found: C 77.22, H 6.70, N 6.02.

Results and Discussions

Syntheses and Characterization

The unsubstituted $LuPc_2$ derivatives are usually prepared by cyclic tetramerization of phthalonitrile in the presence of lanthanide salts.[34] The symmetrically substituted diphthalocyanines has also been obtained by this way.[35] The compounds prepared by following this synthetic route are always obtained in very poor yields, a few percents; moreover the purification is a major problem. Some operations like sublimation,[36] or column chromatography[37] have been used to increase the purity of the complex. Both these methods are quite unsatisfactory for a complete separation from the impurities since the unreacted phthalonitrile aggregates to the rare-earth metal diphthalocyaninates and both are eluted simultaneously during column chromatography. In another synthetic method,[38] the same reactants are heated in a solvent in the presence of DBU (1,8-diazabicyclo[5.4.0]undec-7-ene), a catalyst which favours the macrocycle formation. In this latter case, the yield of the desired phthalocyanine is also low and often inferior to 2%, the major product being the monophthalocyanine derivative of LuPc(OAc). However, a series of homoleptic sandwich complexes of

2,3,9,10,16,17,23,24-octakis(octyloxy)phthalocyanine with rare earth metals {M[Pc(OC_8H_{17})$_8$]$_2$ (M = La, Pr, Nd, Sm, Eu, Gd, Tb, Dy, Y, Ho, Er, Tm) and HCe[Pc(OC_8H_{17})$_8$]$_2$} has been prepared by the cyclic tetramerization of 4,5-di(octyloxy)phthalonitrile on the template of M(acac)$_3$·*n*H_2O in the presence of DBU in better yields.[39]

Dilithium phthalocyanines [Li_2Pc] are interesting materials for the preparation of substituted diphthalocyanines obtained by condensation of substituted macrocycle units. Thus, in the first step of our synthetic process, dilithium phthalocyanine was prepared by condensation of phthalodinitrile **1** in lithium pentane-1-olate in 1-pentanol which readily took place at reflux temperature. Treatment of the reaction mixture *in situ* with lutetium acetate and indium chloride gave novel ball type four *tert*-butylcalix[4]arene bridged double decker lutetium(III) phthalocyanine **2** and indium(III) phthalocyanine **3**, respectively (Scheme 1).

Characterization of the new products involved a combination of methods including elemental analysis, IR, UV-vis, MALDI-TOF MS and ^{1}H NMR spectroscopic techniques. The spectroscopic data of the new compounds were in accordance with the structures. IR spectroscopy has been proved useful in characterisation of the nature of the phthalocyanine ligand in tetrapyrrole sandwich complexes. The IR spectra of Lu^{III} complex **2** and In^{III} complex **3** closely resembles those of the reduced double-deckers of tervalent rare earth metals [$M^{III}(Pc^{-2})_2]^-$,[40] which also demonstrate the dianionic nature of the phthalocyanine rings in both compounds. The marker IR band for the phthalocyanine monoanion radical, $Pc^{\cdot-}$ appearing at 1310-1320 cm^{-1} in the IR spectra was not seen for both compounds **2** and **3.** This indicates that both phthalocyanine rings exist as dianions in H[$M^{III}(Pc^{-2})_2$] (M=Lu, In). The IR spectra taken in KBr pellets showed CH aliphatic peaks at 2922-2836 cm^{-1} and 2936-2872 cm^{-1}, while aromatic C=C peak at 1612 and 1615 cm^{-1} and aromatic CH peaks at 3054 and 3042 cm^{-1} for **2** and **3**, respectively. Comparison of the IR spectral data of compound **1** with compounds **2** and **3** clearly confirmed the formation of desired compounds by the disappearance of sharp absorption band attributable to C≡N group at 2229 cm^{-1}[32] for **1** . The absorptions at 1290 and 1292 cm^{-1} indicated the presence of Ar-O-Ar groups in the structure for **2** and **3**, respectively.

Only a few NMR data concerning bis(phthalocyaninates) of rare earth elements are available from the literature,[41,42] most of them dealing with the reduced forms.[43,44] Reduced form of both compounds enabled us to record satisfactory ^{1}H NMR data. The ^{1}H NMR spectra for both compounds indicate that the two phthalocyanine rings exist as dianions. Compounds **2** and **3** gave the ^{1}H NMR spectra which are very similar to each other as they have similar structure. In the ^{1}H NMR spectra which were taken in CD_3CO_2D, the aromatic protons appeared at 7.83-6.91 and 7.92-7.02 ppm as multiplets for compounds **2** and **3**, respectively. Observations of singlet peaks at 3.87 and 3.72 ppm indicated the presence of methoxy protons in the structures of compounds **2** and **3**, respectively. Compounds **2** and **3** adopted a cone conformation, which was evidenced by the AB system of the methylene protons within calix[4]arene units with a pair of AB type doublets observed for the methylene ($ArCH_2Ar$) protons at 3.76 and 3.28 ppm in **2** and 3.37 and 3.28 ppm in **3**, with a coupling constant of 13.4 Hz. The non-equivalance of terminal calix[4]arenes with the middle one(s) was further demonstrated by the observation of two singlets of *tert*-butyl groups at 1.49 and 0.98 ppm with proton ratio of 72:72 for both compounds **2** and **3**.

Positive ion MALDI-MS spectra of **2** and **3** are given in Figure 1 and Figure 2, respectively. Many different MALDI matrixes were tried to find intense molecular ion peak and low fragmentation under the MALDI-MS conditions for these compounds. Only 3-indolylacrylic acid yielded good MALDI-MS spectra as seen in Figures 1 and 2.

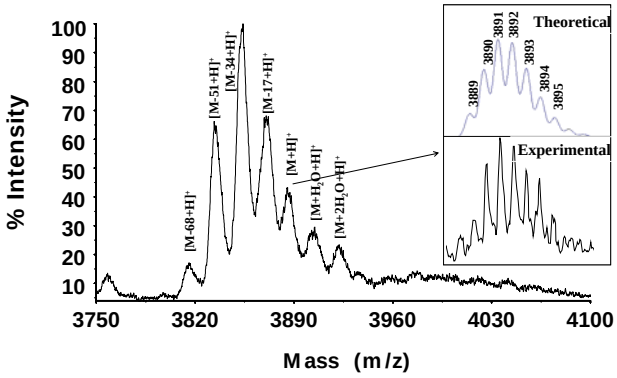

Figure 1. MALDI-MS spectrum of compound **2**.

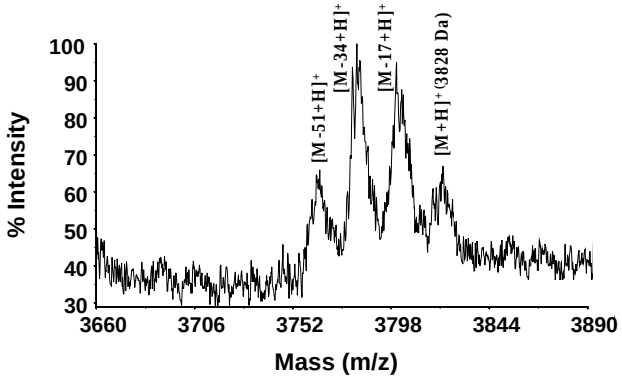

Figure 2. MALDI-MS spectrum of compound **3**.

Protonated molecular ion peak of **2** was observed at 3889, having isotopic distribution between 3889 and 3896 Da masses, with two adduct peaks and four fragment ion peaks together (Figure 1). Two adduct peaks are resulted from the one and two moles of water adducts to the protonated molecular ion peak of **2** showing the easy water coordination.

Protonated etheric oxygen ($^{H}_{+}$R-O-CH_3) on the side aromatic ring could be rearranged and the -OH group leaves from the protonated molecule with CH_3 migration to the side aromatic chains. In this way, -OH leaving from the main protonated molecule could be followed. So, the mass difference between the fragment ion peaks corresponding 17 Da results from the -OH group elimination on the ligand at the side etheric groups. The inset in Figure 1 shows the theoretical and the experimental isotopic distribution of compound **2**. It is clearly shown that isotopic mass

distribution of compound **2** is exactly overlapped with the experimental isotopic mass distribution of **2** obtained in the positive ion reflection mode. When the UV-vis spectrum of compound **2** in acetic acid was investigated, some pecularities were observed. UV-vis spectrum of **2** resembles the spectrum of metal free phthalocyanines. In order to control whether the Lu^{III} complex **2** undergoes demetallation in acetic acid, it was dissolved completely in of acetic acid (10 mg in 1 ml) and about 1 ml of diionized water was then added into the solution drop by drop. After the addition of water, precipitation was occurred. Supernatant over the precipitate was removed and precipitate was dried in vacuum oven at 35 ^{o}C for 5h at 17 mTorr pressure. Dried precipitate was redissolved again in 0.5 ml acetic acid and positive ion and linear mode MALDI-MS spectrum of this redissolved species was recorded with average of 50 laser shots using the IAA matrix. Both MALDI-MS spectra obtained in acetic acid initially and after reprecipitation were found to be identical. No metal free form of that complex after dissolving in acetic acid and reprecipitation with water addition was observed in MALDI-MS. This shows high stability of the Lu^{III} complex **2** in acetic acid.

Positive ion and linear mode MALDI mass spectrum of **3** is given in Figure 2. In the case of **3**, no water adduct peak(s) was observed but only three fragment ion peaks appeared in the MALDI-MS spectrum of **3** beside the intense protonated molecular ion peak at 3828 Da mass. Absence of the water adduct(s) peaks show that their stability in the case of **3** is less when compared to that of **2**. The mass difference between the protonated molecular ion peak and the following fragments of **3** again is 17 Da due to elimination of the –OH group from the side etheric moieties on the ligand. All of the results show that compounds **2** and **3** were synthesized perfectly.

Figure 3 presents the UV-vis spectra of the compounds **2** and **3** in acetic acid. In the visible region, the absorption spectra for both compounds in acetic acid shows distinct characteristic bands by 670-710 nm corresponding to the *Q* absorption bands with vibration overtones at shorter wavelength. The characteristic *Q*-bands attributed to the $\pi\rightarrow\pi^*$ transitions from the highest occupied molecular orbital (HOMO) to the lowest unoccupied molecular orbital (LUMO) of the Pc ring are responsible for the colour of the compound.[48] For the compound **2**, similar to the literature data,[39,49] the *Q*-band appears at 708 nm as a strong absorption with a vibration overtone of comparable intensity at 673 nm. For compound **3**, the most intensive band is the *Q* band at 702 nm with a vibronic band at 634 nm. The spectral features are different from those of phthalocyanine analogues in the neutral form $M^{III}(Pc^{-2})(Pc^{\cdot-})$, but resembles those of the anionic $[M^{III}(Pc)_2]^-$ and $HM^{III}(Pc)_2$ due to their similar electronic structure.[45-47] This is supported by the fact that the UV-vis absorption of the band around 450-510 nm characteristic for π-radicals was not observed for both compounds.

Additionally, compounds **2** and **3** show a typical Soret band (*B*-band) absorption arising from the deeper π→LUMO transitions in UV region at 335 and 346 nm, respectively. The position of all bands is metal dependent, indicating the existence of the π-π interaction between the phthalocyanine ligands. The decrease in the ionic radius of metal leads to the blue shift of the *Q*-bands in the spectra.[50]

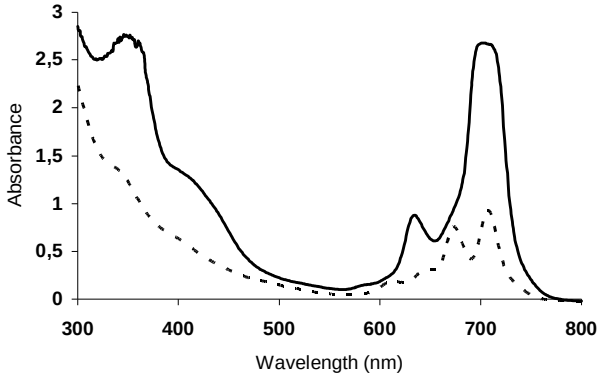

Figure 3. UV-vis spectra for compounds **2** (dashed line) and **3** (solid line) in acetic acid. Concentration ≈ $1\cdot10^{-4}$ M.

The energies and relative intensities and broadening of the bands observed are in accordance with the pattern that would be anticipated on the basis of excitation coupling theory for the phthalocyanines.[51]

Nonlinear Absorption and Optical Limiting Measurements

Since the nonlinear optical response of compound **3** is neglectable, we only present nonlinear optical properties of compound **2**. Nonlinear optical responses were measured by *z*-scan experiment,[52,53] with a frequency-doubled (532 nm) Q-switched, mode-locked Nd:YAG laser (Quantel Brillant) at about 4 ns pulse duration. A single nearly Gaussian beam was tightly focused with a 30 cm focal length lens. The transmittance of a sample was measured at far field with 2 mm diameter aperture (close aperture) and without aperture (open aperture) simultaneously as the sample moves along the propagation direction (*z*) of the focused beam. From the open aperture *z*-scan experiments at various input fluences it was found that this compound shows considerably large nonlinear absorption. Therefore, the optical limiting experiment was performed with the open aperture mode of the *z*-scan setup by fixing sample position at about the focus and changing the input fluence. The fluence at the sample was adjusted by a combination of neutral-density filters. The sample was prepared in acetic acid and DMSO solution (1:1) at $2.9\cdot10^{-3}$ M concentration which yields 82% linear transmittance. The absorption coefficient is 0.9 cm^{-1} at 532 nm.

The open-aperture *z*-scan performed in this study showed intensity dependent absorption (*i.e.* nonlinear absorption) of the incident light. It is assumed to be due to reverse saturable excited state absorption (RSA) in phthalocyanines.[54] Effective absorption coefficients are calculated using theory reported previously.[53,55] All open aperture *z*-scan data were fitted using nonlinear regression method with the following equation. In the equation, the normalized transmittance is given as a function of position *z*:

$$T_{Norm}(z) = \left[\frac{\log_e \left[1 + \frac{q_{000}}{1+(z/z_0)^2} \right]}{\frac{q_{000}}{1+(z/z_0)^2}} \right]$$

In this equation z_0 is the diffraction length of the beam and $q_{000} = \beta_{eff} I_0 L_{eff}$, where $L_{eff} = \frac{1-e^{-(\alpha L)}}{\alpha}$ and β_{eff} is the effective intensity dependent nonlinear absorption coefficient and I_0 is the intensity of the light at focus. L_{eff} is known as the effective length of the sample, α is the absorption coefficient, L is the sample thickness. In the equation, the normalized transmittance is given as a function of position z.

The beam waist radius w_0 and the nonlinear absorption coefficient β_{eff} were used as free parameters in the fit. The waist radius w_0 was found to be almost constant for various input intensities (I_0). The averaged value of w_0 was found to be 34.2 μm.

A sample of typical open aperture z-scan data is given in Figure 4.

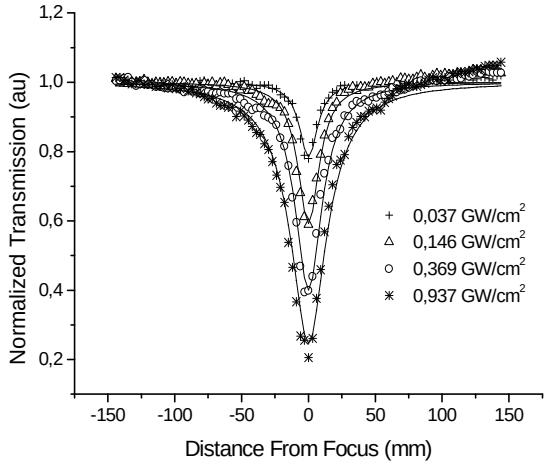

Figure 4. Typical open aperture z-scan spectra of compound **2** with normalized transmission plotted as a function of sample position z; concentration = $2.9 \cdot 10^{-3}$ M.

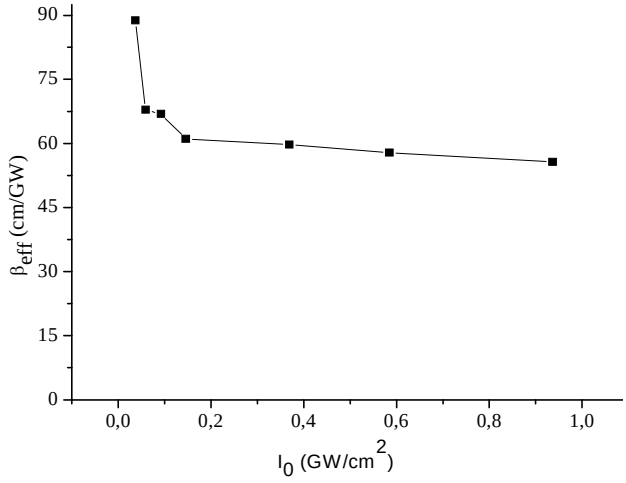

Figure 5. Plot of effective nonlinear absorption coefficient β_{eff} against the on-focus beam intensity I_0 for the compound **2**.

The effective nonlinear absorption coefficients β_{eff} versus on focus intensities were plotted in Figure 5. It is found that the effective nonlinear optical coefficient β_{eff} decreases slightly with increasing beam intensity in Pcs.[56,57] However, as seen from Figure 5, in our case, although there is a sharp decrease of β_{eff} at lower intensities, it becomes almost stable at higher intensities. For optical limiting applications it is desirable to have stable β_{eff} at high intensities.

Due to the high nonlinear absorption of the sample, we performed optical limiting experiments. The sample was placed at the focus where beam radius is 34.2 μm. Input fluences versus output fluences were plotted in Figure 6.

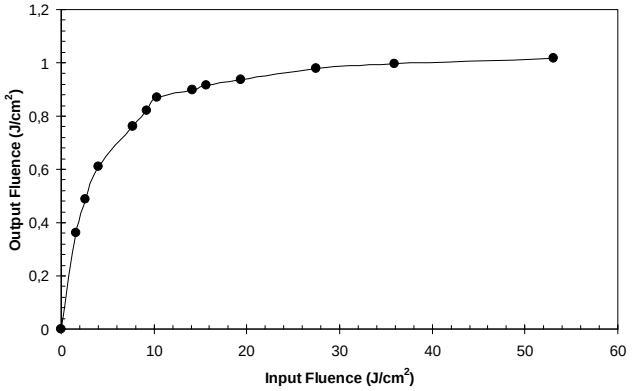

Figure 6. Optical limiting response of the compound **2** at 532 nm; concentration = $2.9 \cdot 10^{-3}$ M.

It is clearly seen that although input fluences increase up to 60 J/cm^2, output fluences remain almost constant at about 1 J/cm^2. This indicates that investigated sample shows good optical limiting behaviour.

Conclusions

We have presented the synthesis and characterization of novel ball type double-decker lutetium(III) [$LuPc_2(tbca)_4$] **2** and indium(III) phthalocyanine [$InPc_2(tbca)_4$] **3**, bridged with four *tert*-butylcalix[4]arene groups. The phthalocyanines were prepared using a phthalodinitrile derivative of 1,3-dimethoxy-4-*tert*-butylcalix[4]arene **1** and proper materials. The preparations of the new products are supported by elemental analysis, IR, UV-vis, ^{1}H NMR and by MALDI-TOF MS spectra.

Nonlinear absorption and optical limiting experiments were performed with the double-decker Lu^{III} phthalocyanine [$LuPc_2(tbca)_4$] **2**. From the open aperture z-scan experiments at various input fluences we found that this compound shows considerably large intensity dependent absorption (*i.e.* nonlinear absorption) of the incident light and although there is a sharp decrease of β_{eff} at lower intensities, it becomes almost stable at higher intensities. The optical limiting experiments performed with compound **2**, clearly shows that although input fluences increase up to 60 J/cm^2, output fluences remain almost constant at about 1 J/cm^2 indicating that investigated sample shows good optical limiting behaviour.

Acknowledgements. Financial assistance from the Research Fund of Gülhane Medical Academy of Ankara and in part from Turkish Academy of Sciences (TUBA), from the Research Fund of Marmara University (Project No. Science-107/020603), from Scientific and Technical Research Council of Turkey (TUBİTAK, No. 105T708), from the Research Funds of Ankara University and Turkish State of Planning Organization (DPT) under grant number 2003K120190 are gratefully acknowledged. We also thank Dr. Ömür Çelikbıçak, research assistant, Hacettepe University, Department of Chemistry, Ankara for the assistance with some spectral data.

References

1. Gutsche C.D. *Calixarenes revisited*. Monographs in *Supramolecular Chemistry*. London, RSC Publishing, **1998**.
2. Higler I., Timmerman P., Verboom W., Reinhoudt D.N. *Eur. J. Org. Chem*. **1998**, 2689-2702.
3. Liu J.-M., Zheng Y.-S., Zheng Q.-Y., Xie J., Wang M.–X., Huang Z.-T. *Tetrahedron* **2002**, *58*, 3729-3736.
4. Al-Saraierh H., Miller D.O., Georghiou P.E. *J. Org. Chem*. **2005**, *70*, 8273-8280.
5. Szemes F., Drew M.G.B., Beer P.D. *Chem. Commun*. **2002**, 1228-1229.
6. Rincon A.M., Prados P., de Mendoza J. *J. Am. Chem. Soc*. **2001**, *123*, 3493-3498.
7. Diamond D., McKervey M. A. *Chem. Soc. Rev*. **1996**, *25*, 15.
8. Asfari Z., Weiss J., Vicens J. *Synlett*. **1993**, 719.
9. Siepen A., Zett A., Vögtle F. *Liebigs Ann*., **1996**, 757.
10. Rudkevich D.M., Verboom W., Reinhoudt D.N. *J. Org. Chem*. **1995**, *60*, 6585.
11. Rebek J.Jr. *Chem. Commun*. **2000**, 637.
12. For a review of CH-π interactions, see: Nishio M., Hirota M. *Tetrahedron* **1989**, 45, 7201.
13. Maya E.M., Garcio-Frutos E.M., Vazquez P., Torres T. *J. Phys. Chem. A* **2003**, *107*, 2110.
14. *Phthalocyanines: Properties and Applications* (Leznoff C.C., Lever A.B.P., Edrs) Vols. 1-4, New York, VCH-Wiley, **1989-1996**.
15. McKeown N.B. *Phthalocyanine: Materials Synthesis, Structure and Function*, Cambridge, Cambridge University Press, **1998**.
16. Du X., Ma C., Hou X., Wang G., Li W., Du G. *Heterocycles* **2003**, *60*, 2535.
17. Moskalev P.N., Kirin I.S. *Russ. J. Inorg. Chem*. **1971**, *16*, 57-60; *ibid* **1972**, *46*, 1019.
18. Nicholson M.M., Pizarello F.A. *J. Electrochem. Soc*., **1979**, *126*, 1490.
19. Corker G.A., Grant B., Clecak N.J. *J. Electrochem. Soc*. **1979**, *126*, 1339.
20. Simon J., Andre J.J. *Molecular Semi-Conductors*, Berlin, Springer **1985**. Ch. 3.
21. Andre J. J., Holczer K., Petit P., Riou M. T., Clarisse C., Even R., Fourmigue M., Simon J. *Chem. Phys. Lett*. **1985**, *115*, 463-466.
22. Turek P., Petit J.J., Andre J.J., Simon J., Even R., Boudjema B., Guillaud G., Maitrot M. *J. Am. Chem. Soc*. **1987**, *109*, 5119.
23. Maitrot M., Guillaud G., Boudjema B., Andre J.J., Strzelecka H., Simon J., Even R. *Chem. Phys. Lett*. **1987**, *133*, 59-62.
24 Meier H., Albrecht W., Wöhrle D., Jahn A. *J. Phys. Chem*. **1986**, *90*, 6349-6353.
25. Orimashi Y., Ohno H., Tsuchida E., Matsuda H., Nakanishi H., Kato M. *Mol. Cryst. Liq. Cryst.* **1988**, *160*, 139-149.
26. Louati A., El Meray M., Andre J. J., Simon J., Kadish K.M., Gross M., Giraudeau A. *Inorg. Chem*. **1985**, *24*, 1175-1179 and references given therein.
27. Ohta K., Jacquemin L., Sirlin C., Bosio L., Simon J. *New J. Chem*. **1988**, *12*, 751.
28. Simon J., Andre J.J., Skoulios A. *Nouv. J. Chim*. **1986**, *10*, 295-311.
29. Ceyhan T., Korkmaz M., Kutluay T., Bekaroğlu Ö. *J. Porphyrins Phthalocyanines* **2004**, *8*, 1383.
30. Ceyhan T., Korkmaz M., Erbil M.K., Bekaroğlu Ö. *J. Porphyrins Phthalocyanines* **2005**, *9*, 423-429.
31. Ceyhan T., Altındal A., Erbil M.K, Bekaroğlu Ö. *Polyhedron* **2006**, *25*, 737.
32. Ceyhan T., Altındal A., Özkaya A.R., Salih B., Bekaroğlu Ö. *Chem. Commun*. **2006**, 320-322.
33. Ceyhan T., Altındal A., Özkaya A.R., Erbil M.K., Bekaroğlu Ö. *Polyhedron* **2007**, *26*, 73-84.
34. Kirin I.S., Moskalev P.N., Makashev A. *Russ. J. Inorg. Chem*. **1965**, *10*, 1065.
35. Tomilova L.G., Chernykh E.V., Ioffe T.T., Luk'yanets E.A. *J. Gen. Chem. USSR* **1983**, *53*, 2339-2345.
36. Clarisse C., Riou M.T. *Inorg. Chim. Acta*. **1987**, *130*, 139-144.
37. Liu Y., Shigehara K., Yamada A. *Thin Solid Films* **1989**, 303-308.
38. De Cian A., Moussavi M., Fisher J., Weiss R. *Inorg. Chem*. **1985**, *24*, 3162-3167.
39. Liu W., Jiang J., Du D., Arnold D.P. *Aust. J. Chem*. **2000**, *53*, 131-135.
40. Jiang J., Kasuga K., Arnold D.P. In *Supramolecular Photosensitive and Electro-active Materials* (Nalwa H.S., Edr), New York, Academic Press, **2001**, 113-210.
41. Toupance T., Bassoul P., Mineau L., Simon J. *J. Phys. Chem*. **1996**, *100*, 11704.
42. Toupance T., Ahsen V., Simon J. *J. Am. Chem. Soc*. **1994**, *116*, 5352.
43. Pandoven A., Cozien Y., L'Her M. *New. J. Chem*. **1991**, *15*, 515.
44. Konami H., Hatano M., Tajiri A. *Chem. Phys. Lett*. **1989**, *160*, 163.
45. Battisti D., Tomilova L., Aroca R. *Chem. Mater*. **1992**, *4*, 1323
46. Ricciardi G., Belviso S., Leli F., Ristori S. *J. Porphyrins Phthalocyanines* **1998**, *2*, 177.
47. Tomilova L. G., Dyumaev K. M. *Mendeleev Commun*. **1995**, 109.
48. Sleven J., Görller-Walrand C., Binnemans K. *Mater. Sci. Eng. C* **2001**, *18*, 229-38.
49. Chen Y., Liu H.-G., Pan N., Jiang J. *Thin Solid Films* **2004**, *460*, 279-285.
50. Martynov A.G., Gorbunova Y.G. *Inorg. Chim. Acta* **2007**, *360*, 122-130.
51. Nevin W. A., Liu W., Hempstead M. R., Marcuccio S. M., Melnik M., Leznoff C.C, Lever A.B.P. *Inorg. Chem*. **1987**, *26*, 891.
52. Sheik-bahae M., Said A.A., Van Stryland E.W. *Opt. Lett*. **1989**, *14*, 955.
53. Sheik-bahae M., Said A.A., Wei T.H., David D.H., Van Stryland E.W. *IEEE J. Quantum Electron*. **1990**, *26*, 760.
54. Coulter D. R., Miskowski V.M., Perry J.W., Wei T.H., Van Stryland E.W., Hagan D.J. *SPIE Proc*. **1989**, 1105, *42*.
55. Kwak C.H., Lee Y.L., Kim S.G. *J. Opt. Soc. Am. B* **1999**, *16*, 600.
56. O'Flaherty S.M., Hold S.V., Cook M.J., Torres T., Chen Y., Hanack M., Blau W.J. *Adv. Mater*. **2003**, *15*, 19.
57. Slodek A., Wöhrle D., Doyle J.J., Blau W. *Macromol. Symp*., **2006**, *235*, 9.

Received 17.03.2008
Accepted 08.05.2008

Highly Sensitive Halide Ions Recognition with Diprotonated Porphyrin

M.M. Kruk,[a] Yu.B. Ivanova,[b] V.B. Sheinin,[b] A.S. Starukhin,[a] N.Zh. Mamardashvili,[b,@] and O.I. Koifman[b]

[a] *B.I. Stepanov Institute of Physics of National Academy of Sciences, Minsk, 220072, Belarus*
[b] *Institute of Solution Chemistry of Russian Academy of Sciences, Ivanovo, 153045, Russia*
[@] *Corresponding author E-mail: ngm@isc-ras.ru*

The titration of the diprotonated form of 3,7,13,17-tetramethyl-2,8,12,18-tetrabutylporphyrin with the series of halide ions has been done in the acetonitrile solution. It was shown that the stable complexes of 1:1 and 1:2 structures with halide ions have been formed. The influence of complexation with halide ions on the porphyrin fluorescent properties has been studied. The strong quenching of the porphyrin fluorescence has been found. It was established that both static quenching upon the nonfluorescent complex formation due to internal heavy atom effect and dynamic diffusion-controlled quenching took place. Based on the analysis of dependencies of fluorescence intensity and lifetime on the iodide ions concentration in solution, it was proposed to use the diprotonated form of the porphyrin as a basic compound for design of the fluorescent molecular receptor for the halide ions.

Introduction

The design of new efficient means for real-time detection of chemical and biochemical species through the use of sensors is among the most significant fields in modern science.[1] The nature of the molecular sensing agent used to generate the chemical diagnostic signal upon the recognition of the given substance is central to determining the overall performance of any chemical sensor. The way of transduction of this chemical signal into appropriate analytical signal is also of great importance since it determines the ease of production and exploitation of the sensing device. The optical transduction seems to be the most attractive for several reasons which include inherent safety, less noise pickup in signal transmission over long distances, and the possibility of obtaining much more comprehensive information from a single probe.

The representatives of the tetrapyrrolic compounds family can serve as good candidates for optical transduction. They are known to have rather strong luminescence (fluorescence and/or phosphorescence) that can be tuned in the appropriate spectral range by modification of the molecule. The sensitivity of the rate constant and quantum yield of porphyrin luminescence to the properties of molecular microenvironment provides the possibility to use tetrapyrrolic molecules not only as optical transducers but as sensing agents also. Design of the molecular sensor can be simplified in such a case, since the same molecule combines both functions.

Anions play a fundamental role in a wide range of chemical and biological processes, and numerous efforts have been devoted to the development of abiotic receptors for anion species,[2] but they are still very limited. The detection of different anions in the solution can be achieved with using of tetrapyrrolic compounds. The diprotonated forms of tetrapyrrolic compounds are able to form adducts with the organic and inorganic acid residues[3-5] and to form complexes with salt anions.[6,7] The large efforts has been made in the elucidation of the molecular conformation,[3,5,8-16] acid-base equilibria involved ([17-21] and Refs. therein), ground and excited states properties[4,15,20-24] of the diprotonated porphyrins. The essential progress has been achieved in this area. It was found, that upon protonation of the macrocycle core the nonplanar conformation is adopted.[3,5,8-16] The type and extent of macrocycle nonplanar distortions have been extensively discussed in terms of molecular flexibility,[5,10] pattern of the peripherical substitution,[5,8,10,15,16,22] strength of intermolecular interactions with acid residues.[3,5,11,12,15] The relationship between the molecular structure and macrocycle core acidity-basicity equilibrium has been studied,[18-21] and the intermediate monoprotonated form has been characterized for several tetrapyrrolic compounds.[20,21,25-27] The dramatic changes in the rates and channels of the excitation energy deactivation have been documented in going from the free base to diprotonated compounds,[4,20-23] and different mechanisms involved in these changes were proposed.[4,15,22-24]

One of the most interesting issues from point of view of possible practical applications is the interaction of diprotonated macrocycle with anions. The X-ray studies,[3,5] NMR, IR, Raman and UV-vis spectroscopies,[6,7,25,28] theoretical calculations[11,12,15,24] have been applied to study this problem. It was established that both in solid state and in liquid organic solutions the hydrogen bonding between the positively charged core protons and anions occurs,[3-5,15,16] and the properties of this bond has been extensively discussed. The most of these studies have focused mainly on the structural aspects[3,5,15] or the consequences of this hydrogen bond formation for the photophysical properties of diprotonated compounds.[3,22,24] The detailed studies of the complexation constants and the relationship between amount of the salt added and the spectral response of porphyrin have received much less attention.[7,30-32] In this

work we report the experimental results on the recognition of halide ion salts in solution with the diprotonated form of 3,7,13,17-tetramethyl-2,8,12,18-tetrabutylporphyrin (Figure 1). The fluorometric and spectropotentiometric titration experiments have been done. The mechanisms of the diprotonated porphyrin fluorescence quenching upon complexation with halide ions are studied. We discuss the possibility of using of diprotonated porphyrins as the basic compounds in the design of new efficient fluorescent molecular sensors for recognition of halide ions and measurements of halide ion salts concentration in the solutions.

Experimental

Materials and Methods

3,7,13,17-tetramethyl-2,8,12,18-tetrabutylporphyrin (Figure 1) was prepared using method described elsewhere.[33] The identity of the structure was checked by spectroscopic methods and was found to correspond to the literature data.[34] The halide salts and perchloric acid solutions were prepared with carefully dried acetonitrile. Acetonitrile was purified with dynamic drying on the column with neutral aluminium oxide and with following rectification.[35] Potassium iodide (KI) and sodium iodide (NaI) were dried under vacuum (1.33 Pa) at 393 K during 48 hours until the constancy of mass has been achieved. The perchloric acid as 8.75 M water solution was used for the preparation of the 0.01 M $HClO_4$ solution in dried acetonitrile (water content in dried acetonitrile was no more than 0.01 M). The total amount of water added to the solutions in the most acidic solution (pH = 4.5) was calculated to be about 0.011 M. The value was estimated by the method of Fischer titration. Tetraethylammonium bromide (Et_4NBr) was recrystallized twice from acetonitrile and dried in vacuum-desiccator over NaOH during 24 hours at 293 K. Tetraethylammonium chloride (Et_4NCl) was recrystallized twice from acetonitrile and dried under vacuum (1.33 Pa) during 24 hours at 293 K. The halide salts were chosen taking into account their dissociation degrees in acetonitrile.[36-39]

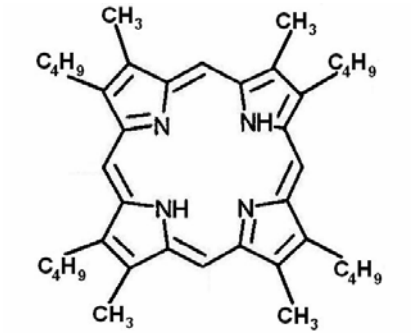

Figure 1. Structure of 3,7,13,17-tetramethyl-2,8,12,18-tetrabutylporphyrin.

The spectrophotometric titration of the diprotonated species H_4P^{2+} with halide ion salts was carried out at pH = 6.5, which has been maintained with microaddition of 0.05 N solution of perchloric acid in acetonitrile. At the each titration step the analytical concentrations of reagents were corrected for dilution according to the equation $A_T = A^0_T/(1 + \sum\Delta V/V_0)$, where V_0 is an initial solution volume, $\sum\Delta V$ is a sum of titrants, A_T is a current optical density value at the analytical wavelength taking into account the titrants added, A^0_T is a measured current optical density at the analytical wavelength.

For the fluorescent experiments the porphyrin powder were dissolved in the acetonitrile that contained the chloric acid in the amount required for the complete transformation of all the porphyrin molecules from free base form into diprotonated form (pH = 6.5).[31] Titration of the porphyrin samples with potassium iodide was done with addition of the small amounts of the concentrated potassium iodide solution that were prepared in the same acidificated acetonitrile as the porphyrin sample.

The concentration of diprotonated porphyrin in solutions was determined spectrophotometrically with known extinction coefficients (ε = 8710 $M^{-1}cm^{-1}$ at 585 nm, ε = 28180 $M^{-1}cm^{-1}$ at 543 nm, ε = 102330 $M^{-1}cm^{-1}$ at 403.7 nm[34]) and was ~$2\cdot10^{-6}$ and $1.5\cdot10^{-5}$ M in the fluorometric and spectropotentiometric titration experiments, respectively. The cell for the studies of the acid-base equilibria and the procedure of the spectropotentiometric titration in acetonitrile were described in details.[30] Electronic absorption spectra were measured with CARY 500 Scan (Varian).

The fluorescence measurements was done in the standard quartz rectangular cells (1×1 cm, Hellma) in the air equilibrated solutions at 293 ± 2 K. The deoxygenated solutions were used for the measurements of the fluorescence quantum yield Φ_{fl} of the diprotonated form of 3,7,13,17-tetramethyl-2,8,12,18-tetrabutylporphyrin (hereafter referred as H_4P^{2+}). Deoxygenation of the solutions has been performed with argon bubbling during 20 min just before measurements. The fluorescence spectra and fluorescence excitation spectra were measured using of spectrofluorometer SFL-1211 (Solar). The fluorescence decay kinetics was measured with the using of photon counting system (Edinburgh Instruments). The fluorescence quantum yield Φ_{fl} was determined using the standard sample method.[40] The free base 5,10,15,20-tetraphenylporphyrin (H_2TPP) was taken as a standard sample (Φ^0_{fl}=0.11[41]).

Results and Discussions

Acid-base Equilibria of Macrocycle

Prior the studies of porphyrin interactions with halide ions the acid-base equilibria of 3,7,13,17-tetramethyl-2,8,12,18-tetrabutylporphyrin have been studied with the use of the spectropotentiometric titration method. Titration was carried out in acetonitrile with 0.01 M perchloric acid solution. In this case the perchloric acid is completely dissociated and porphyrin protonation occurs by means of solvated proton (pK_a^{298}=2.8[42,43]). The corresponding titration curve reveals two steps (Figure 2).

This observation indicates that successive formation of the monoprotonated H_3P^+ and diprotonated species H_4P^{2+} takes place upon increase in the concentration of perchloric acid. The difference in the equilibrium constants for the formation of mono- and diprotonated species (K_{a1} and K_{a2}) is three orders of magnitude (K_{a1} = (1.66·±0.05)·10^{12} M^{-1} and K_{a2} = (1.66±0.05)·10^9 M^{-1}). Therefore for the given system "porphyrin – acetonitrile – perchloric acid" three pH ranges are available in which the studied molecules exist either exclusively in the free base H_2P (pH > 15) or diprotonated H_4P^{2+} forms (pH ≤ 7) or mainly in the monoprotonated H_3P^+ form (pH=9 - 11). The electronic absorption spectra in the Q band range for each of the free base H_2P, monoprotonated H_3P^+ and diprotonated H_4P^{2+} forms are shown in Figure 3.

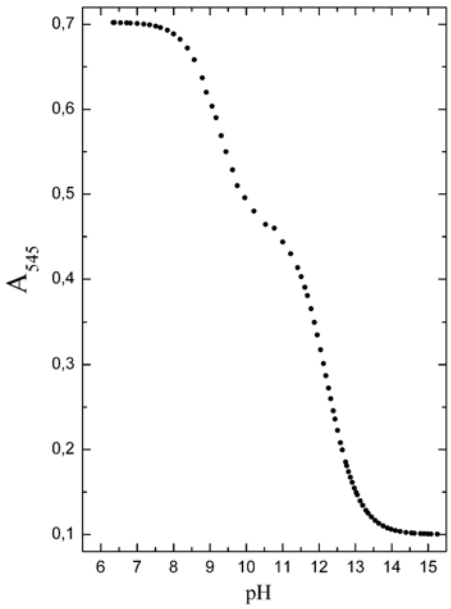

Figure 2. Absorption titration curve at λ = 545 nm for 3,7,13,17-tetramethyl-2,8,12,18-tetrabutylporphyrin in acetonitrile at 298 K.

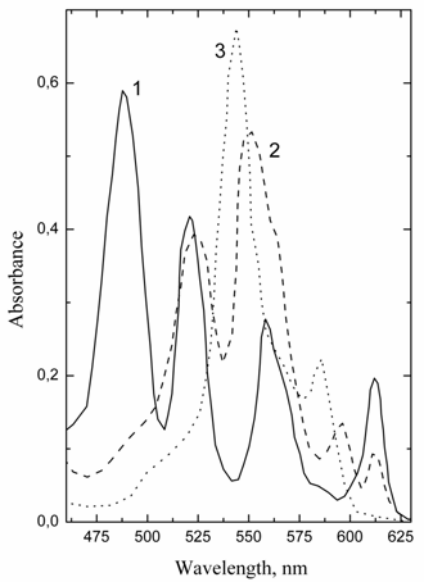

Figure 3. Electronic absorption spectra in the *Q*-band region: free base H_2P (1), monoprotonated H_3P^+ (2) and diprotonated H_4P^{2+} (3) forms. Porphyrin concentration is $1.5 \cdot 10^{-5}$ M.

Spectropotentiometric Titration with Halide Ions

The diprotonated form H_4P^{2+} was titrated with three halide ion salts. Electronic absorption spectra (Figure 4) indicate that increase of halide ion concentration [X^-] leads to the red shift of the porphyrin absorption bands indicating that the complexation takes place. The two sets of the isobestic points during the transformation of the absorption spectra were identified for each of the studied halide ions. These isobestic points are related to the equilibria (1) and (2) respectively:

$$H_4P^{2+} + X^- \xrightarrow{K_1} H_4P^{2+}\cdot X^- \quad (1)$$

$$H_4P^{2+}\cdot X^- + X^- \xrightarrow{K_2} H_4P^{2+}\cdot 2X^-, \quad (2)$$

where the constant K_1 is referred to the formation of porphyrin-halide ion complex with 1:1 ratio, and the constant K_2 is related to the complex with 1:2 ratio. The isobestic points for the equilibrium (1) have been measured as 526 and 553 nm, 548 and 590 nm, 549 and 590 nm in case of iodide, bromide and chloride ions, respectively. For equilibrium (2) the isobestic points are 528 and 555 nm, 550 and 592 nm, 552 and 593 nm, in case of iodide, bromide and chloride ions, respectively.

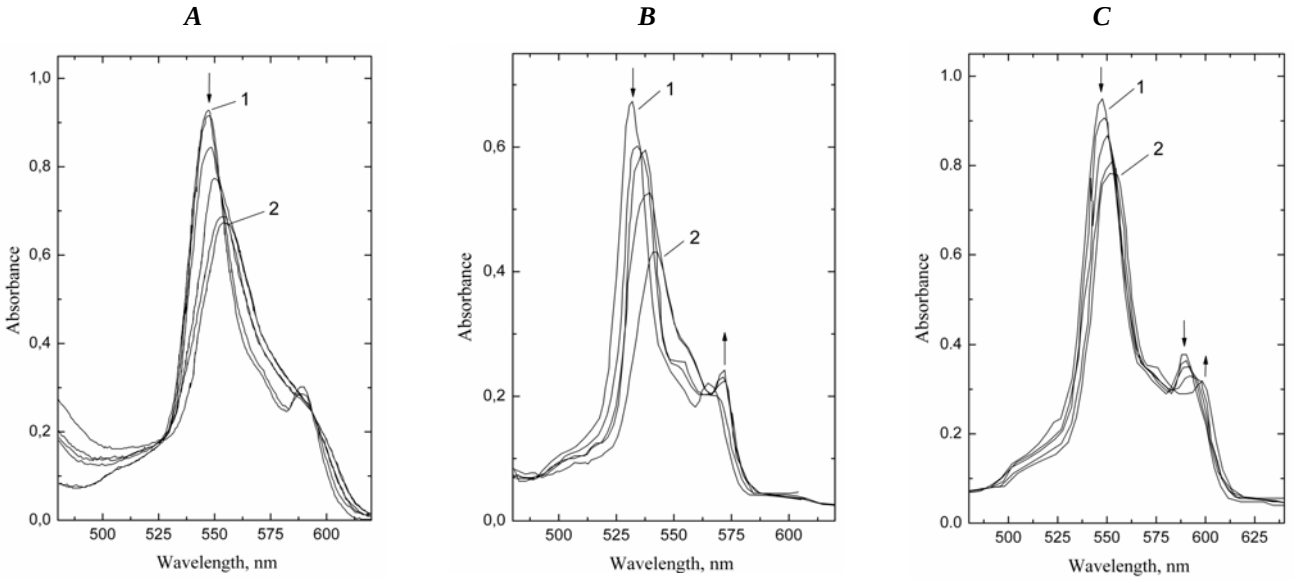

Figure 4. The transformation of the electronic absorption spectra of H_4P^{2+} upon the formation of complexes with halogenide ions in acetonitrile at p*H* = 6.5: *A* - titration with NaI, 1 - H_4P^{2+}, 2 - $H_4P^{2+}\cdot 2I^-$; *B* - titration with Et_4NBr, 1 - H_4P^{2+}, 2 - $H_4P^{2+}\cdot 2Br^-$; *C* - titration with Et_4NCl, 1 - H_4P^{2+}, 2 - $H_4P^{2+}\cdot 2Cl$-. Arrows indicate the direction of the absorbance changes upon formation of the complexes.

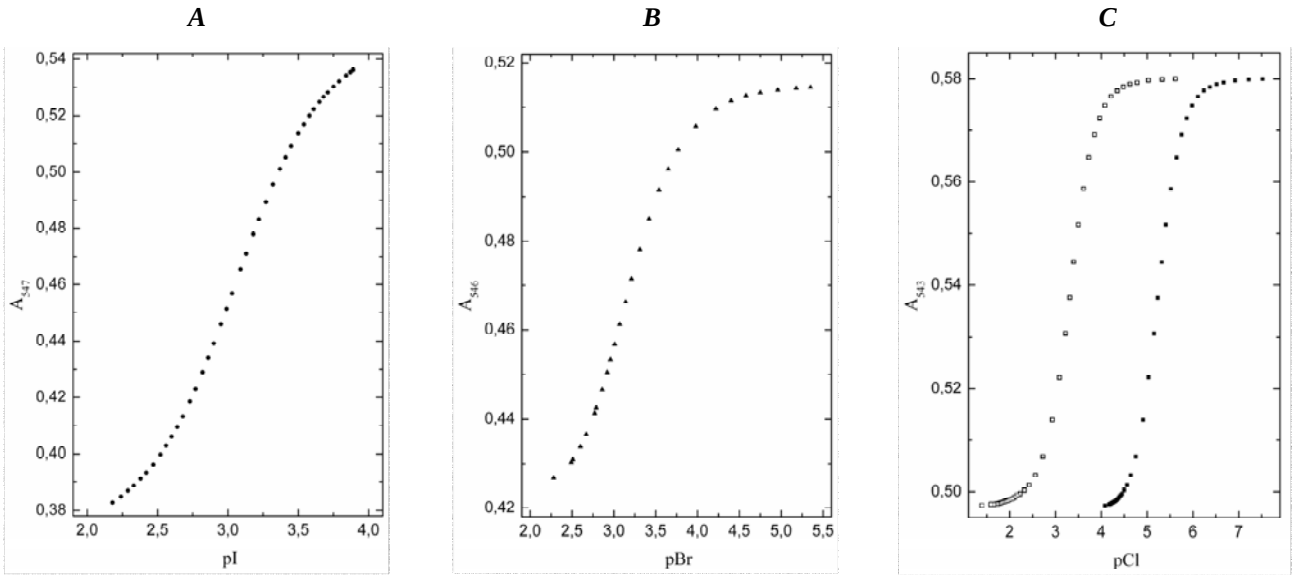

Figure 5. The dependence of the absorbance of the H_4P^{2+} on the concentration of the halide salts in acetonitrile at 298 K: *A* - NaI, *B* - Et_4NBr and *C* - Et_4NCl. Open and closed symbols in case of Et_4NCl denote the total concentration of salt and the concentration of nonaggregated solvated chloride ions, respectively.

The formation of complexes of diprotonated porphyrin with halide ions was analyzed with the titration curves (Figure 5). There are no two sharp well separated steps at the titration curves which correspond to the equilibria (1) and (2). Such behaviour is characteristic when the constants K_1 and K_2 of the conjugated equilibria differ less than two orders of magnitude.[44] However, the values of the

$$A = \frac{A_{H_4P^{2+}} + A_{H_4P^{2+}\cdot X^-}\cdot[X^-]\cdot K_1 + A_{H_4P^{2+}\cdot 2X^-}\cdot[X^-]^2\cdot K_1\cdot K_2}{1+[X^-]\cdot K_1+[X^-]^2\cdot K_1\cdot K_2} \quad (3)$$

equilibrium constants K_1 and K_2 have been calculated with the nonlinear least-square method for the equation (3) where $A_{H_4P^{2+}}$, $A_{H_4P^{2+}\cdot X^-}$, $A_{H_4P^{2+}\cdot 2X^-}$ are the optical densities measured for the solutions of uncomplexed diprotonated species H_4P^{2+}, monoligated $H_4P^{2+}\cdot X^-$ and diligated $H_4P^{2+}\cdot 2X^-$ complexes, respectively. During least-square fitting $A_{H_4P^{2+}}$ and $A_{H_4P^{2+}\cdot 2X^-}$ values were taken as they have been measured experimentally, and $A_{H_4P^{2+}\cdot X^-}$ value was the variable parameter. The obtained values for the equilibrium constants are presented in Table.

Table. The equilibrium constants K_1 and K_2 for the formation of the $H_4P^{2+}\cdot X$- and $H_4P^{2+}\cdot 2X^-$ complexes in acetonitrile at 298 K.

Halide ion	K_1, M^{-1} [a]	K_2, M^{-1} [a]
I^-	$1.20\cdot10^3$	$1.07\cdot10^3$
Br^-	$2.46\cdot10^3$	$1.23\cdot10^3$
Cl^-	$4.08\cdot10^3$	$1.27\cdot10^3$
	$2.51\cdot10^5$ [b]	$2.01\cdot10^5$ [b]

[a] The error in determination of the K_1 and K_2 values is 3-5%.
[b] The values are calculated taking into account the aggregation of chloride ions (see text).

As for the possible complexation of ClO_4^- with porphyrin, it can be excluded since the experiments evidence that the complexation constant is very low and the large excess of acid is required to achieve the complexation.[5] In our case the concentration of acid was very low and seems to be insufficient for complexation.

The measured equilibrium constant is strongly influenced by the state of the given ion in the solution. In the case of incomplete dissociation of salts or due to the aggregation phenomena (ion pair formation[45]) the measured equilibrium constants values may deviate strongly from the actual ones. The aggregation of the halide ions has been studied in the separate experiments using the specific ion electrodes Crutur 52-27, 35-27, 17-27. The results of this study indicate that in the acetonitrile solution at pH = 6.5 the formation of multiple H_nCl_m aggregates (namely, HCl, H_2Cl^+, HCl_2^- and HCl_3^{2-}) takes place. The special procedure has been used to evaluate the true chloride ion concentration.[31] In the Table both the apparent (uncorrected for the aggregation) and true equilibrium constants are given for the $H_4P^{2+}\cdot 2Cl^-$ complex.

The presented data indicate that the stability of both $H_4P^{2+}\cdot X^-$ and $H_4P^{2+}\cdot 2X^-$ complexes in acetonitrile increases when the halide ion radius decreases. The complexation constants for the chloride (Cl^-) complexes are about 100 times higher than those for bromide (Br^-) and iodide (I^-) complexes. Low complexation constants for two last halide ions are likely due to their larger ionic radii as compared with those for the former. These results are in line with the conclusions on the relationship between the size of halide ion and the contribution from orbital and electrostatic interactions energy into the hydrogen bond formation within $H_4P^{2+}\cdot 2X^-$ complexes.[15] With the relation to the application of the diprotonated form of porphyrin for the ions detection in the solution, the ions aggregation leads to decrease in the sensitivity of measurements. This is because of the porphyrin recognizes the free solvated ions only, and the ionic aggregates (mentioned above) are not bound by diprotonated porphyrin molecule.

It is significant to note that the monoprotonated H_3P^+ molecules do not form stable complexes with halide ions in the same conditions. We have observed the transformation of the H_3P^+ absorption spectrum into spectrum characteristic for $H_4P^{2+}\cdot 2X^-$ during titration of H_3P^+ with halide salts. The calculation of current concentrations of the H_2P, H_3P^+, H_4P^{2+}, $H_4P^{2+}\cdot X^-$ and $H_4P^{2+}\cdot 2X^-$ are in good agreement with the results of the H_3P^+ titration by halide salts. The anion-induced protonation of monoprotonated species[7] takes place first and the newly formed diprotonated species bind anions.

Structure of Complexes with Halide Ions

The molecular structure of $H_4P^{2+}\cdot 2X^-$ complexes with halide ions was the subject of numerous experimental and theoretical investigations.[3,5,8-16] It was shown[3] that Cl^- ions are symmetrically aligned exactly at the porphyrin macrocycle symmetry axis at two sides of the porphyrin plane. The similar results have been obtained later for the complexes of several porphyrins with perchlorate ions ClO_4^-.[5] The length of the hydrogen bond between the porphyrin core protons and Cl^- ions in the complexes $H_4TPP^{2+}\cdot 2Cl^-$ and $H_4TPyrP^{2+}\cdot 2Cl^-$ was found to be ~3 – 4 Å.[3] The length of the hydrogen bond between protons and oxygen of perchlorate ion in complexes $H_4TPP^{2+}\cdot 2ClO_4^-$ and $H_4OEP^{2+}\cdot 2ClO_4^-$ is about 2 Å.[5]

The difference in the hydrogen bond length reflects the different value of the complexation constant due to dissimilarity of the properties of both porphyrin molecules and ligating ions. For the porphyrin under investigation, the complexation constant with halide ions decreases in the order $Cl^- > Br^- > I^-$ (see Table). Relatively low complexation constant for $H_4P^{2+}\cdot 2I^-$ complex may lead to the fluctuations of the hydrogen bond H...I length in the solution as well the deviations from the symmetrical structure of the complex. The substantial broadening of the $H_4P^{2+}\cdot 2I^-$ complex absorption spectrum (Figure 4*A* and 7*B*) as compared with that of uncomplexed H_4P^{2+} molecule seems to be explained from that point of view. Thus, for the $H_4P^{2+}\cdot 2Br^-$ complex the broadening of the absorption spectrum is distinctly less (Figure 4*B*), and for the $H_4P^{2+}\cdot 2Cl^-$ complex it is vanishing (Figure 4*C*).

According to the X-ray data analysis for the diprotonated form H_2OEP with perchlorate ions ($H_4OEP^{2+}\cdot 2ClO_4^-$) the average value of dihedral angle θ between the planes of the pyrrolic rings and mean porphyrin plane is about 14°,[5] and the dihedral angle value depends on the interaction force between the ions in the complex.[3,5,15] Therefore, the long wavelength shift in the electronic absorption spectrum upon the formation of $H_4P^{2+}\cdot 2I^-$ complex seems to be due to the increase in the tilting angle θ, *i.e.* results from an increase of the degree of the tetrapyrrolic macrocycle distortion upon complexation. This suggestion is in line with the results of quantum-chemical calculations, reported recently.[12,15,16]

Steady State and Time-Resolved Fluorescence

As it was stated above, the formation of the $H_4P^{2+}\cdot 2I^-$ complexes upon increase of the KI concentration in the solution leads to the long wave-length shift of *Q*-bands in the electronic absorption spectra and the changes of their spectral profiles. The absorption spectrum of H_4P^{2+} has two distinct *Q*-bands with maxima at 548 and 592 nm. The $H_4P^{2+}\cdot 2I^-$ complexes at 0.01 M concentration of KI show the diffusive spectrum with band maximum at 559 nm with a weak shoulder at 605 - 606 nm. Complex formation also leads to the substantial decrease in the intensity of the Soret band and small long wavelength shift of the maximum (1 nm at 0.01 M concentration of KI).

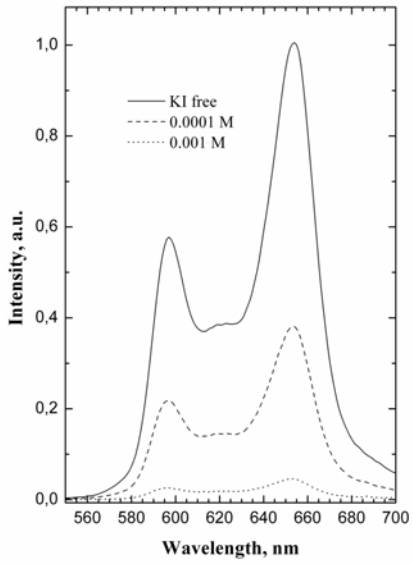

Figure 6. Fluorescence spectra of H_4P^{2+} as a function of KI concentration in acetonitrile; λ_{exc} = 400 nm.

The fluorescence spectrum of the diprotonated H_4P^{2+} form has two sharp bands with maxima at 597 and 654 nm (Figure 6). The fluorescence quantum yield Φ_{fl} of the diprotonated H_4P^{2+} form in the halide salts free solution is 0.11. The strong fluorescence intensity decrease is observed upon formation of the complexes $H_4P^{2+}\cdot 2I^-$ upon increase of KI concentration in the solution (Figure 6). At 0.01 M concentration of KI the integral fluorescence intensity is reduced for more than 300 times. Upon this fluorescence quenching the shape of the fluorescence spectrum remains the same.

The fluorescence excitation spectra have been measured in the *Q*-band region for the salts free sample and for the solutions with $3\cdot 10^{-4}$ and $1\cdot 10^{-3}$ M concentration of KI. All three spectra are identical (Figure 7*A*) and the maxima positions in the fluorescence excitation spectra were found at ~548 and ~592 nm, as it was found for the absorption spectrum of uncomplexed H_4P^{2+} molecules (Figure 7*B*).

This finding indicates that fluorescence belongs to the uncomplexed diprotonated H_4P^{2+} form, and the fluorescence of complexes $H_4P^{2+}\cdot 2I^-$ is not observed. In other words, the complexed porphyrin $H_4P^{2+}\cdot 2I^-$ is nonfluorescent. If we neglect the contribution into the emission from the minor concentration of uncomplexed diprotonated form H_4P^{2+} in 0.01 M KI solution,[31] the upper limit of the fluorescence quantum yield Φ_{fl} for $H_4P^{2+}\cdot 2I^-$ complex can be estimated as low as $3.6\cdot 10^{-4}$.

The fluorescence time decay (λ_{exc} = 410 nm,

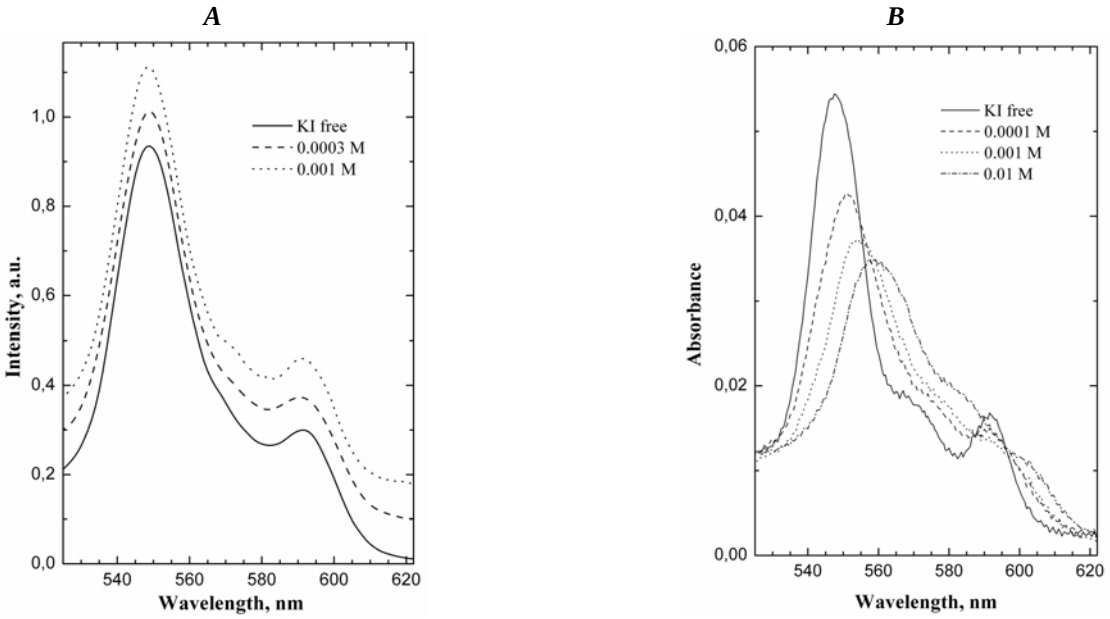

Figure 7. ***A*** **-** Excitation fluorescence spectra of H_4P^{2+} as a function of KI concentration in acetonitrile; λ_{obs} = 654 nm. The spectra are shifted up for 0.1 arbitrary units each for clarity sake; ***B*** **-** Electronic absorption spectra of H_4P^{2+} as a function of KI concentration in acetonitrile; porphyrin concentration is $1.9 \cdot 10^{-6}$ M.

λ_{em} = 595 nm) has monoexponential character for all the solutions studied. The fluorescence lifetime τ_{fl} progressively decreases in going from the salt free solution to solutions containing KI (Figure 8). For the initial solution of H_4P^{2+} (without KI) the fluorescence lifetime τ_{fl} is found to be 5.86 ± 0.05 ns, and τ_{fl} value is reduced down to 3.80 ± 0.05 ns at 0.002 M concentration of KI.

Static and Dynamic Fluorescence Quenching

As it was shown above, the fluorescence of diprotonated form is efficiently quenched by iodide ions. The Stern-Volmer plot (Figure 9) deviates from the "classical" linear dependence. The concavity of Stern-Volmer plot with regard to the ordinate axis is an indication that both static and dynamic diffusion-controlled quenching take place simultaneously.[46] Concaving up is because the quenching in such a case is the second order function of iodide ion concentration

$$I_0/I = 1 + (K^c_{SV} + K^d_{SV})[I^-] + K^c_{SV}K^d_{SV}[I^-]^2, \qquad (4)$$

where K^c_{SV} is the Stern-Volmer constant for the static fluorescence quenching, K^d_{SV} is the Stern-Volmer constant for the dynamic fluorescence quenching and $[I^-]$ is concentration iodide ion. The calculated Stern-Volmer constant K^c_{SV} of the static fluorescence quenching due to

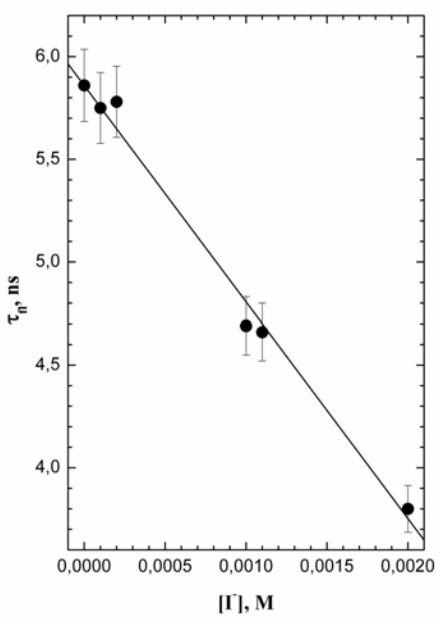

Figure 8. Fluorescence lifetime τ_{fl} as a function of KI concentration in acetonitrile; λ_{exc} = 410 nm, λ_{obs} = 595 nm.

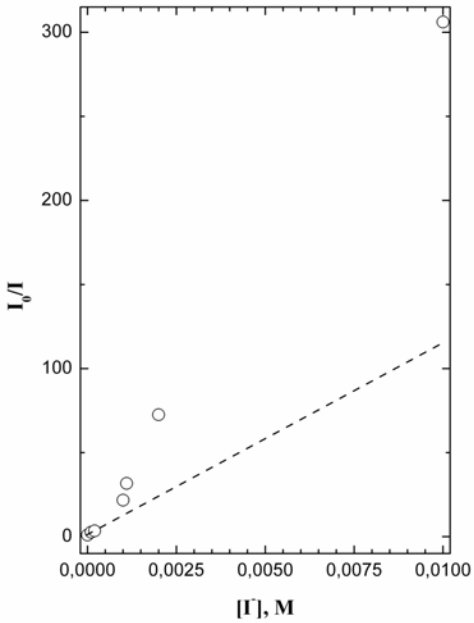

Figure 9. The Stern-Volmer plot for the fluorescence quenching of H_4P^{2+} with iodide ions in acetonitrile.

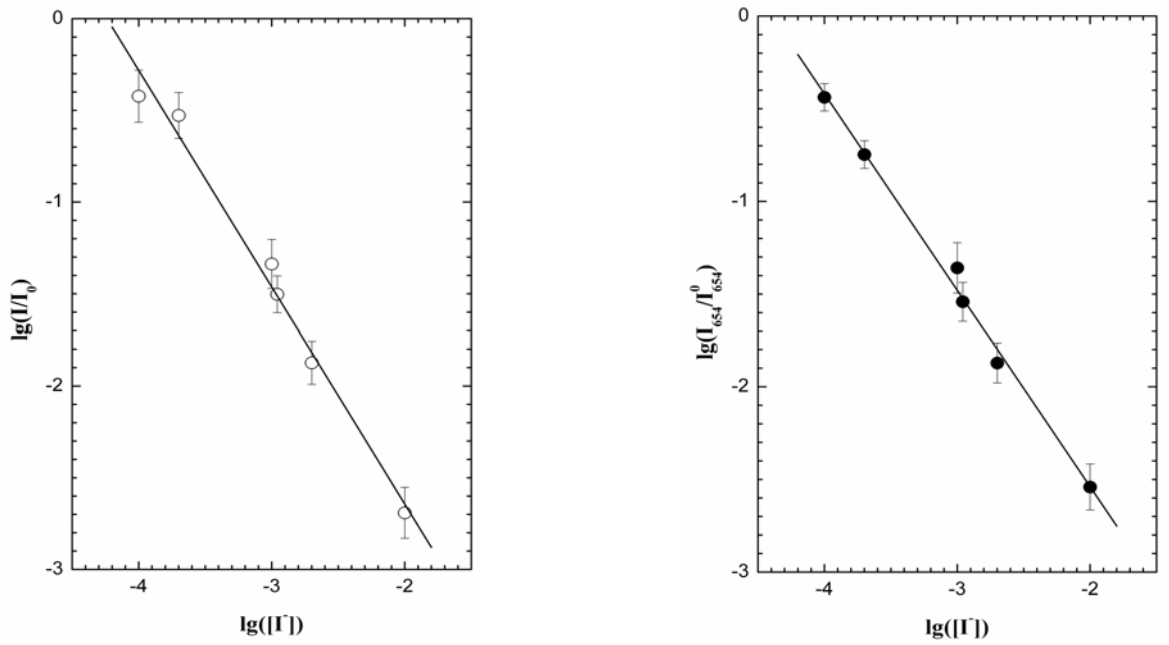

Figure 10. Double logarithmic plot for: *A* - the integral fluorescence intensity ratio I/I_0, *B* - the peak intensity ratio I_{654}/I^0_{654} as a function of KI concentration.

complex formation with iodide-ions is 7860 M^{-1}. Fluorescence of diprotonated form of porphyrin in the complex with iodide-ions is quenched by mechanism of the internal heavy atom effect.[4] The above data on the electronic absorption spectra and fluorescence intensity as the functions of the concentration of iodide ions in the solution indicate that the fluorescence quenching is practically parallel to the formation of the nonfluorescent $H_4P^{2+}\cdot 2I^-$ complexes, *i.e.* static quenching due to the complexation with halide ions is a dominating channel of the fluorescence quenching of the H_4P^{2+} molecule.

At the same time the shortening of the fluorescence lifetime of "halide ion free" diprotonated H_4P^{2+} form cannot be explained with the static quenching due to internal heavy atom effect. The dependence of the fluorescence lifetime on the concentration of iodide ions I^- in the solution is linear one (Figure 8). This fact indicates that the quenching can be described with Stern-Volmer approach.[46] Therefore, one can state that the dynamic diffusion-controlled fluorescence quenching due to external heavy atom effect coexists with the static quenching due to complex formation. The Stern-Volmer constant K^d_{SV} of the dynamic fluorescence quenching by iodide-ions 277 M^{-1} has been calculated with an equation

$$\tau^0_{fl}/\tau_{fl} = 1 + K^d_{SV}[I^-], \quad (5)$$

where τ^0_{fl} and τ_{fl} are the fluorescence lifetimes measured in the absence of quencher and with halide salts added in the solution, respectively. The calculated K^d_{SV} value for the dynamic quenching is almost 30 times smaller than that for the static quenching. This finding proves once more that the formation of the nonfluorescent complexes with halide ions is the dominating channel of the H_4P^{2+} porphyrin fluorescence quenching by halide ions.

Determination of the Iodide Ion Concentration

The concentration dependencies of both the integral fluorescence intensity and peak fluorescence intensity at λ = 654 nm are shown in Figure 10. The double logarithmic plot is an analogue of the Scatchard plot, which is used widely in the fluorometric analysis of the ligand binding at the different hosts.[47,48] The both plots demonstrate the linear character and can be proposed as the calibration for the iodide ion concentration measurements in the solution.[32,49] In order to measure the iodide ions concentration the integral fluorescence intensity I_0 for the reference sample and intensity I for the studied sample with unknown iodide ion concentration should be measured first. Then the I_0/I ratio is calculated. The iodide ion concentration (in M) is available from the calibration formula (6)

$$[I^-] = 10^{(0.84\lg(I_0/I)-4.24)} \quad (6)$$

In a similar manner, the halide ion concentration can be determined with the ratio I^0_{654}/I_{654} of the peak fluorescence intensities at 654 nm for the studied and reference samples. With this approach the iodide ion concentration (in M) in the solution is given from the calibration formula (7)

$$[I^-] = 10^{(0.94\lg(I^0_{654}/I_{654})-4.40)} \quad (7)$$

Moreover, the iodide ion concentration can also be determined with the measured concentration dependence of porphyrin fluorescence lifetime τ_{fl} (see Figure 8). The measurements of the fluorescence time decay can be achieved at any given wavelength in the range from 560 to 720 nm. The concentration of iodide ions (in M) is given as

$$[I^-] = 0.0055 - 0.00095\tau_{fl}, \quad (8)$$

where τ_{fl} is the fluorescence lifetime in nanoseconds.

Conclusions

The philosophy of measurements described above underlies the submitted Russian Federation patent pending.[49] The proposed methods allow the determination of the iodide ions in the concentration range from

$3.0 \cdot 10^{-2}$ M to $3.0 \cdot 10^{-5}$ M. As far as we know, the luminescent methods for the iodide ion concentration measurements described to date provide the sensitivity not higher than $1.5 \cdot 10^{-4}$ M.[50] Therefore, the developed approach seems to be promising way to increase the sensitivity of the luminescent methods of the halide ion determination in the solutions.

The additional advantage of the proposed method is the possibility to carry out the measurements in the air-equilibrated solutions. The upper limit of the Stern-Volmer constant K_{SV} for the fluorescence quenching by molecular oxygen do not exceed 100 M^{-1} ($K_{SV} = \tau^0_{fl} k_q$, where k_q is a bimolecular rate constant of the fluorescence quenching by molecular oxygen). This value is almost two orders of magnitude smaller than Stern-Volmer constant K^d_{SV} dominating in the fluorescence quenching by iodide ions. Therefore, the interfering influence of fluorescence quenching by molecular oxygen can be neglected.

The presented results demonstrate that diprotonated form of 3,7,13,17-tetramethyl-2,8,12,18-tetrabutylporphyrin can be used as a basic compound for the design of the luminescent molecular sensor for the measurements of the halogenide ion concentration in the solution. The diprotonated porphyrin binds the halide ions with equilibrium constant of order 10^3-10^5 M^{-1}. The fluorescence of porphyrin molecule was shown is quenched by halide ions due to both external and internal heavy atom effect. The methods for measurements of the iodide ion concentration using the fluorescence quenching of diprotonated porphyrin by halide ions have been proposed. These methods allow the ions to be detected in the air-equilibrated solutions at room temperatures in the wide concentration range.

Acknowledgments. This work was supported by Russian Academy of Sciences (program №7 «Chemistry and physical chemistry of supramolecular systems and atomic clusters», Russian Foundation for Basic Research (grants №№ 08-03-00009 and 08-03-90000-Bel.) and Foundation for Fundamental Research of the Republic of Belarus (project Ch08R-033).

References

1. Koifman O.I., Mamardashvili N.Zh, Antipin I.S. *Synthetic Receptors on Basis of Porphyrin-calix-[4]-arene Conjugates.* Moscow, Science, **2006**. 249.
2. Bianchi E., Bowman-James K., Garcia-Espana E. *Supramolecular Chemistry of Anions.* New-York, Wiley-VCH, **1997**. 461.
3. Stone A., Fleischer E.B. *J. Am. Chem. Soc.* **1968**, *90*, 2735-2748.
4. Gradushko A.T., Knuykshto V.N., Solovyov K.N., Tsvirko M.P. *J. Applied Spectroscopy* **1975**, *23*, 444-452.
5. Cheng B., Munro O.Q., Marques H.M., Scheidt W.R. *J. Am. Chem. Soc.* **1997**, *119*, 10732-10742.
6. Chida Y., Wararai H. *Bull. Chem. Soc. Jpn.* **1996**, *69*, 341-347.
7. Zhang Y., Li M.X., Lii Y., Yang R.H., Liu F., Li K.A. *J. Phys. Chem. A* **2005**, *109*, 7442-7448.
8. Senge M.O. *J. Photochem. Photobiol. B: Biol.* **1992**, *16*, 3-36.
9. Milgrom L.R. *The Colours of Life: Introduction to the Chemistry of Porphyrins and Related Compounds.* Oxford: Oxford University Press, **1997**. 249 p.
10. Shelnutt J.A., Song X.-Z., Ma J.-G., Jia S.-L., Jentzen W., Medforth C.J. *Chem. Soc. Rev.* **1998**, *27*, 31-41.
11. Gael V.I., Kuzmitsky V.A., Solovyov K.N. *J. Applied Spectroscopy* **1999**, *66*, 559-562.
12. Gael V.I., Kuzmitsky V.A., Solovyov K.N. *J. Applied Spectroscopy* **2000**, *67*, 696-702.
13. Ma S.Y. *Chem. Phys. Lett.* **2000**, *332*, 603-610.
14. Chen D.-M., Liu X., He T.-J., Liu F.-C. *Chem. Phys.* **2003**, *289*, 397-407.
15. Rosa A., Ricciardi G., Baerends E.J., Romeo A., Scolaro L.M. *J. Phys. Chem. A* **2003**, *107*, 11468-11482.
16. Rosa A., Riccardi G., Baerends E.J. *J. Phys. Chem. A* **2006**, *110*, 5180-5190.
17. Phillips J.N. Physico-Chemical Properties of Porphyrins, in *Comprehensive Biochemistry* Vol. 9 (Florkin M., Stotz E., Eds.) Amsterdam, Elsevier, **1963**. 34-73.
18. Fleischer E.B., Webb L.E. *J. Phys. Chem.* **1963**, *67*, 1131-1133.
19. Hambright P., Fleischer E.B. *Inorg. Chem.* **1970**, *9*, 1757-1761.
20. Gensch T., Viappiani C., Braslavsky S. *J. Am. Chem. Soc.* **1999**, *121*, 10573-10582.
21. Kruk M.M., Braslavsky S.E. *J. Phys. Chem. A* **2006**, *110*, 3414-3425.
22. Knyukshto V.N., Solovyov K.N., Egorova G.D. *Biospectroscopy* **1998**, *4*, 121-133.
23. Chirvony V.S., van Hoek A., Galievsky V.A., Sazanovich I.V., Schaafsma T.J., Holten D. *J. Phys. Chem. B* **2000**, *104*, 9909-9917.
24. Avilov I.V., Panarin A.Yu., Chirvony V.S. *Chem. Phys. Lett.* **2004**, *389*, 352-358.
25. Ogoshi H., Watanabe E., Yoshida Z. *Tetrahedron* **1973**, *29*, 3241-3245.
26. Tsvirko M.P., Solovyov K.N., Knuykshto V.N., Gradushko A.T. *J. Applied Spectroscopy* **1975**, *23*, 643-647.
27. De Luca G., Romeo A., Scolaro L.M., Ricciardi G., Rosa A. *Inorg. Chem.* **2007**, *46*, 5979-5988.
28. Saini G.S.S., Sharma S., Kaur S., Tripathi S.K., Mahajan C.G. *Spectrochimica Acta Part A* **2004**, *61*, 3070-3076.
29. Saini G.S.S. Medhi O.K., Verma A.L. *Chem. Phys. Lett.* **2000**, *322*, 293-299.
30. Ivanova Yu.B., Sheinin V.B., Berezin B.D. *Russ. J. Anal. Chem.* **1993**, *48*, 1205-1209.
31. Ivanova Yu.B., Sheinin V.B., Mamardashvili N.Zh. *Russ. J. Gen. Chem.*, **2007**, 77, 1561-1568.
32. Kruk M.M., Starukhin A.S., Mamardashvili N.Zh., Sheinin V.B., Ivanova Yu.B. *J. Applied Spectr*oscopy **2007**, *74*, 750-755.
33. Mamardashvili N.Zh, Zdanovich S.A., Golubchikov O.A. *Russ. J. Org. Chem.* **1996**, *32*, 788-792.
34. Falk J.E. *Porphyrins and Metalloporphyrins*. Amsterdam, Elsevier, **1964**, 231.
35. Reichardt C. *Solvents and Solvent Effects in Organic Chemistry*, 2nd ed. Weinheim, VCH Publishers, **1988**. 736.
36. Viynik I.N., Golnovach A.M., Shkodin A.M. *Russ. J. Phys. Chem.* **1977**, *51*, 485-487.
37. Safonova L.P., Patsatsiyia B.K., Kolker A.M. *Russ. J. Phys. Chem.* **1992**, *66*, 2201-2208.
38. Janz G., Tomkins P. *Nonaqueous Electrolytes Handbook*, Vols. 1-2. London, The Chemical Society, Burlington House, **1972**, 192.
39. Evans D., Zawoyski C., Kay R. *J. Phys. Chem.* **1965**, *69*, 3878-3885.
40. Demas J.N., Crosby G.A. *J. Phys. Chem.* **1971**, *75*, 991-1024.
41. Seybold P., Gouterman M. *J. Mol. Spectroscopy.* **1969**, *31*, 1-11.
42. Kolthoff I.M., Chantooni M.K. *J. Am .Chem. Soc.* **1965**, *87*, 4428-4436.

43. Kolthoff I.M., Chantooni M.K. *J. Anal. Chem.* **1967**, *39*, 1627-1634.
44. Bernstein I.I., Kaminskiy Yu.L. *Spectrophotometric Analysis in Organic Chemistry*. Leningrad, Khimia, **1986**, 199. (in Russ.).
45. Kolthoff I.M., Bruckenstein S., Chantooni M.K. *J. Am. Chem. Soc.* **1961**, *83*, 3927-3935.
46. Lakowicz J.R. *Principles of Fluorescent Spectroscopy*. New York, Plenum Press, **1983**. 496.
47. Aveline B.M., Hasan T., Redmond R.W. *J. Photochem. Photobiol. B: Biol.* **1995**, *30*, 161-169.
48. Cohen S., Margolit R. *Biochem. J.* **1990**, *270*, 325-330.
49. Kruk M.M., Starukhin A.S., Mamardashvili N.Zh., Sheinin V.B., Ivanova Yu.B. *Russian Federation patent pending*, № 2007122152 from 13.06.2007.
50. Eggins B. *Chemical Sensors and Biosensors*. Chichester, John Wiley & Sons, **2002**, 335.

Received 23.03.2008
Accepted 15.05.2008

Laser Confocal and Spatially−Resolved Fluorescence Spectroscopy of Porphyrin Distribution on Plasma Deposited Polymer Films

Eduard I. Zenkevich,[a,@] Joerg Martin,[b] Christian von Borczyskowski,[b] Tatjana A. Ageeva,[c] Valery A. Titov,[c] and Valery N. Knyukshto[d]

[a] *National Technical University of Belarus, Minsk, 220013, Belarus*
[b] *Chemnitz University of Technology, Chemnitz, 09107, Germany*
[c] *Ivanovo State University of Chemistry and Technology, Ivanovo, 153000, Russia*
[d] *B.I. Stepanov Institute of Physics of National Academy of Sciences, Minsk, 220072, Belarus*
[@] *Corresponding author E-mail: zenkev@tut.by*

Laser confocal microscopy and spatially-resolved fluorescence spectroscopy have been used for the study of the interaction of di(p-aminophenyl)etioporphyrin (DAPEP) and tetra(p-aminophenyl)porphyrin (TAPP) molecules with the surface of thin (7-15 μm) polypropylene films treated by 0.5 M KCl solution and activated by air non-equilibrium plasma at the normal atmospheric pressure. Confocal microscopy data (using laser scanning microscope LSM 510, Carl Zeiss) show that after treatment the polymer surface becomes inhomogeneous, and porphyrin moieties are randomly distributed on both film surfaces with a penetration depth of ~1 μm. On the basis of spatially resolved fluorescence measurements (using a home-built confocal microscope with a time resolution up to 100 ms/frame and high spatial resolution) it has been found that fluorescence spectra of individual spots correspond to monomeric species. It means that spatially closed few porphyrin molecules in the spot are not aggregated and do not interact significantly.

Introduction

At present, synthetic porphyrins and phthalocyanines being fixed on synthetic polymer carries by various methods[1-8] or being polymers themselves[9-12] are the subject of interest both as model compounds of natural polymer-bonded tetrapyrroles (chlorophyll, hemoglobin, cytochrome),[13-19] new biological and catalytically active materials[2-5] as well as modified membranes and sensors.[20-24] The fixation of porphyrins on polymer carrier allows to realize some advantages which are absent when using non-bonded porphyrins. Some of them are as follows:[25] cooperative interactions in polymeric chains, the separation of active centres, the possibility of the specific binding of various substrates on active centres, the increase of tetrapyrrole macrocycle stability, the lowering of the porphyrin toxicity relative to biological environment. In this respect, the evaluation of these combined new porphyrin-polymer properties seems to be perspective both from fundamental and application aspects (biotechnology, biology, pharmacology, medicine and catalysis).

Polymers are a class of materials widely used for a broad field of applications. The covalent and non-covalent attachment of bioactive compounds to functionalized polymer surfaces includes relevant techniques in polymer surface modification such as wet chemical, organo-silanization, ionized gas treatments, and UV irradiation.[26] Ion irradiation ranging from several eVs to GeVs is a quite efficient tool to modify the properties of polymers like wettability, optical properties, adhesion between organic substrates and polymer surfaces. Ion irradiation is a promising method to generate structures with a modified index of refraction, which is necessary for the guidance of light with different wavelengths in optical devices.[27] Recently reported applications in the areas such as biomedicine, biosensors, enzyme reactors, and textiles, all of which utilize a common set of surface bioconjugation techniques to address these diverse needs, are also discussed in the literature.[26,28]

Typically, in order to elucidate the fundamental mechanisms occurring in a revolutionary plasma deposition process, atmospheric pressure plasma deposition as well as to analyze biofunctionalized polymer surfaces, spectral methods (X-ray photoelectron spectroscopy, Fourier transform infrared spectroscopy, atomic force microscopy, quadrupole mass spectrometry and others) as well as non-spectral methods (contact angle, 90° peel tests, dye assays, biological assays, and zeta potential) are being used.[26,28-30]

In this report, we present the results showing the possibilities of the modern experimental methods such as laser confocal microscopy and spatial-resolved fluorescence spectroscopy for the study of the interaction of biologically active molecules, di(*p*-aminophenyl)etioporphyrin (DAPEP) and tetra(*p*-aminophenyl)porphyrin (TAPP), with the surface of thin (7.2-15 μ) polypropylene films treated by 0.5 M KCl solution and activated by air non-equilibrium plasma at normal atmospheric pressure. Specifically, these methods open the possibility to control the distribution of active organic component on the film surface as well as to discriminate the nature (monomeric or aggregated forms) of adsorbed molecular species. The choice of polypropylene films is governed by the fact that this material is one of the most inert polymers with a low surface energy and low sorbtion properties and thus is widely used in medico-biological applications.[26, 31] At last, it should be mentioned that the fixation of porphyrins (in monomeric form

presumably) on polymer film may be considered for possible applications in photodynamic therapy and blood cleaning as well as for the thermostabilization of polymers and the development of optical limiters (using metalloporphyrins and metallophthalocyanines).[25]

Experimental

Sampling

The synthesis, purification and identification (by absorption, IR and NMR data) of di(*p*-aminophenyl)etioporphyrin *II* (DAPEP) molecules were carried out according to,[32] the corresponding procedure for tetra-(*p*-aminophenyl)porphyrin (TAPP) molecules is described in.[33] The structures of the corresponding compounds used for the anchoring to the treated polypropylene films are shown in Figure 1. It was supposedly believed that side active amino groups may be responsible for the non-covalent attachment of porphyrin macrocycles to the polypropylene film surface.

Samples of commercial isotactic polypropylene (PP) films with the thickness of 7-15 μm were cleaned by ethanol and distilled water and dried under vacuum before plasma treatment.

The analysis of ATR-FTIR spectra of untreated but cleaned PP films has shown that the strong own absorption bands are accompanied by the existence of bands belonging to oxygen containing functional groups: i) bands in the range of 3000-3600 cm^{-1} are characteristic for hydroxyl groups; ii) bands in the region of 1660-1750 cm^{-1} may be attributed to aldehyde and carboxyl groups; iii) bands at 890 cm^{-1} (double bonds of vinylidene type) and 1377 cm^{-1} (branch methyl groups) were also observed. The basic simplified scheme of experimental setup for excitation of the atmospheric pressure glow discharge (APGD) with liquid electrolyte cathode is shown in Figure 2.

The discharge cell was open to ambient air. DC power supply with the 30 kΩ ballast resistor was used for the discharge excitation. High voltage (up to 4 kV) was applied between liquid electrolyte cathode and copper anode placed at the position of 1 – 5 mm above the solution surface. The electrolyte solution was connected to the negative pole of the power supply through a Cu electrode. A discharge current was varied from 10 to 70 mA. A distance between the polymer surface and electrolyte-gas interface was 2 mm, thus both polymer film sides were immersed in the liquid. Typically, samples were of 70 mm and in length 10 mm in width. The liquid solution volume was capped of about 70 ml. Distilled water and aqueous KCl solutions of 0.01, 0.05, 0.1, and 0.5 M were utilized as a liquid cathode.

Treatment of polymer samples in low-pressure O_2 plasma or in afterglow of the O_2 plasma was used for surface activation too. The experimental setup for polymer treatment in low-pressure plasma and treatment conditions were described in details earlier.[35]

After the treatment, polymer film samples were washed with distilled water and dried under the vacuum at the pressure of 1 Pa. Basically, the main results will be discussed for PP films with attached 10,20-di(*p*-aminophenyl)ethioporphyrin II (DAPEP) and tetra(*p*-aminophenyl)porphyrin (TAPP): (1A) is a control sample, non-treated film, (2A) is the film treated by O_2-plasma + DAPEP, (3A) is the film treated by afterglow of O_2-plasma + DAPEP, (1B) is the film treated by O_2-plasma, (2B) is the film treated by afterglow of O_2-plasma, (3B) is the film treated in plasma-solution system, (4B) is the non-treated film + TAPP, (5B) is the non-treated film + DAPEP, (6B) is the film treated by afterglow of O_2-plasma + DAPP.

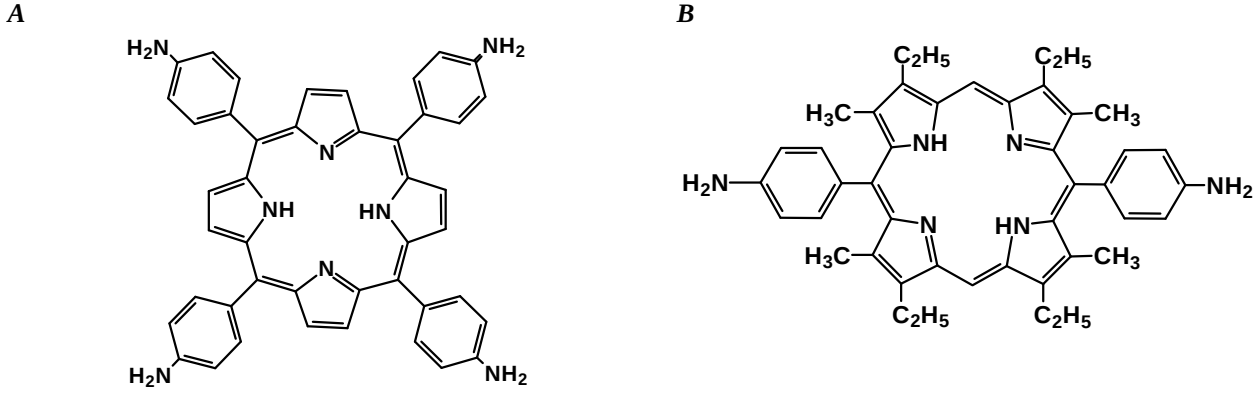

Figure 1. Structures of tetra(*p*-aminophenyl)porphyrin (*A*) and 10,20-di(*p*-aminophenyl)etioporphyrin II (*B*).

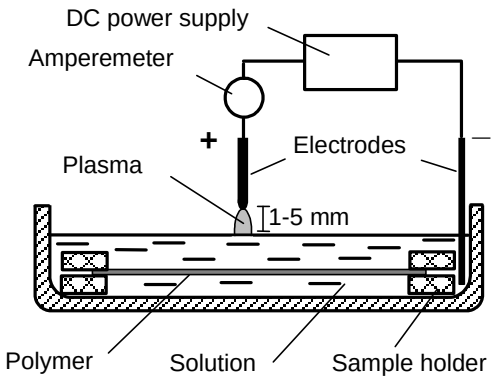

Figure 2. Schematic diagram of the experimental setup for APGD with liquid electrolyte cathode.

Optical and Fluorescence Measurements

The commercial laser scanning microscope LSM 510 (Release 2.8, Carl Zeiss, Germany, Figure 3) was used in order to measure the thickness of PP films as well to analyze the porphyrin distribution from both sides of the films under study. Technical data of the scanning microscope are as follows: Z drive scanning stage by DC motor with the optoelectronic coding and the smallest step size of 50 nm; motorized XY scanning stage with the smallest step of 250 nm; the fine focusing stage HRZ 200 with total range of 200 μm and the smallest step size < 10 nm; one pinhole per confocal channel; VIS laser modules: Ar^+ laser 458, 477, 488, 514 nm, 30 mW and HeNe laser 633 nm, 5 mW. The spatial resolution of the microscope is not high enough in order to obtain structural changes below 200 nm. In order to measure the thickness of the films, some *x*-*z*-cuts through the films were recorded in reflection mode, because the resolution is much better than in fluorescence

regime recording. For each film samples cut images have been obtained with different magnification.

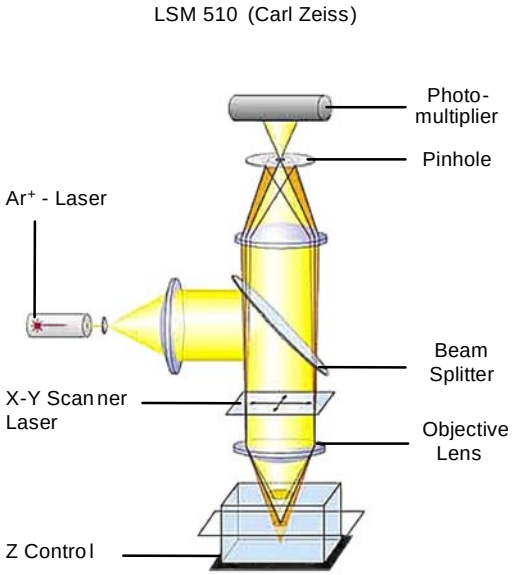

Figure 3. Principal optical scheme of commercial laser scanning microscope LSM 510 (Release 2.8, Carl Zeiss).

Spatially-resolved fluorescence measurements have been carried out by means of a home-built confocal microscope which is shown schematically in Figure 4.[34] The samples were mounted on a closed-loop *xyz*-piezo translation stage (Piezosystems, Karl Zeiss , Jena, Germany) with a maximum scan range of 80 μ. The 482 nm line of a Krypton$^+$ ion laser or the 514.5 nm line of an Argon$^+$ ion laser were used for the fluorescence excitation of the samples. The light was coupled into the set-up via an optical fiber and focused onto the PP film surface by an objective characterized by 100x magnification and numerical aperture of 0.9 (Carl Zeiss, Jena, Germany). Sample fluorescence was collected by the same objective and imaged onto an avalanche photodiode (APD, EG&G SPCMAQR-13) by an achromatic lens. By this way spectral images have been visualised on a PC screen. In order to register spatially-resolved fluorescence spectra the second dichroic 50/50-beamsplitter in the detection light path was used for the collecting and imaging the part of the fluorescence emission onto the entrance slit of a grating monochromator (Acton SP-300i) with an attached liquid-nitrogen-cooled CCD (Princeton Instruments, USA). This part of the confocal fluorescence microscope is not shown in Figure 4 and presented in details earlier.[34] Longpass Notch filters (Omega Optical, USA) were placed in front of the APD and the spectrometer (530 nm and 505 nm cut-off wavelengths) to separate the fluorescence signal from the excitation flow. Finally, a home-built confocal microscope is characterized by the following parameters:[34] i) a time resolution up to 100 ms/frame, ii) a lateral resolution of 235 nm and a vertical resolution of 970 nm, iii) a detection efficiency of 10 % for the whole confocal set-up (without the second 50/50-beamsplitter).

Commercial spectrophotometers Shimadzu UV 3101PC (Japan) and Carry 500 (USA) were used for absorption measurements, whereas spectrofluorimeter Shimadzu RF5101PC (Japan) and a high sensitive home-made recording complex both calibrated for the spectral response of the detection channel were used for usual steady-state fluorescence measurements. The details of experimental technique have been reported earlier.[36,37]

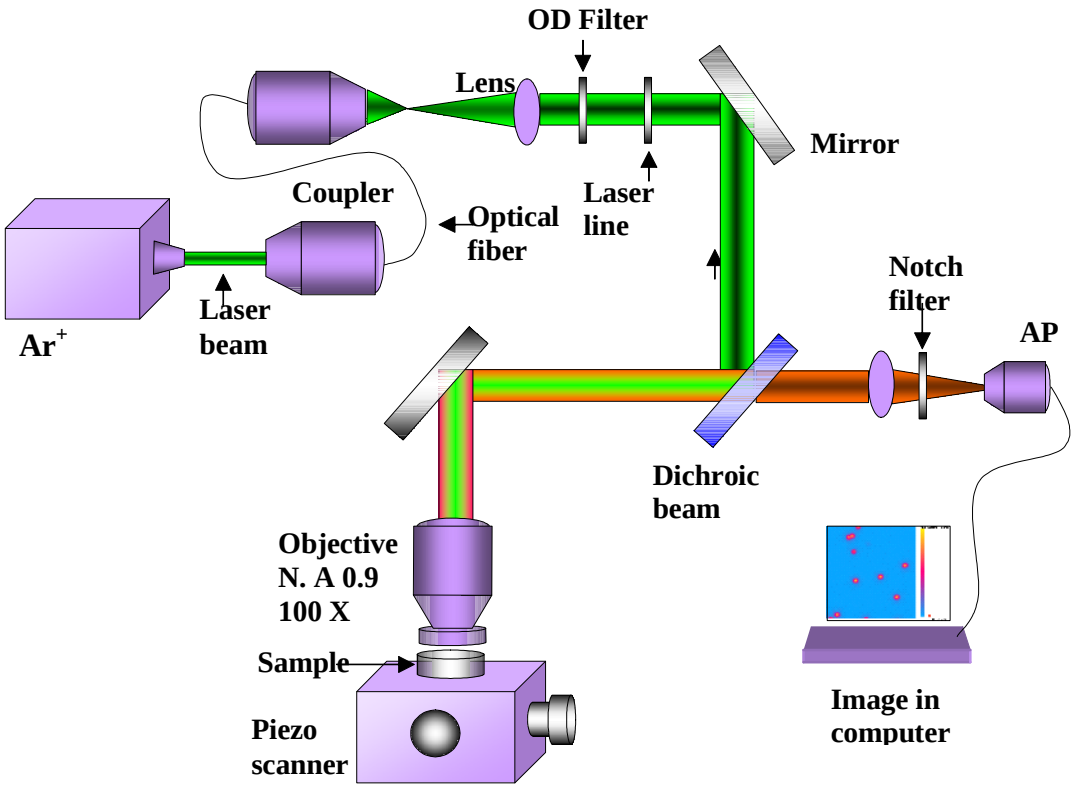

Figure 4. Principal optical scheme of home-built confocal microscope for fluorescence imaging and spectra detection.

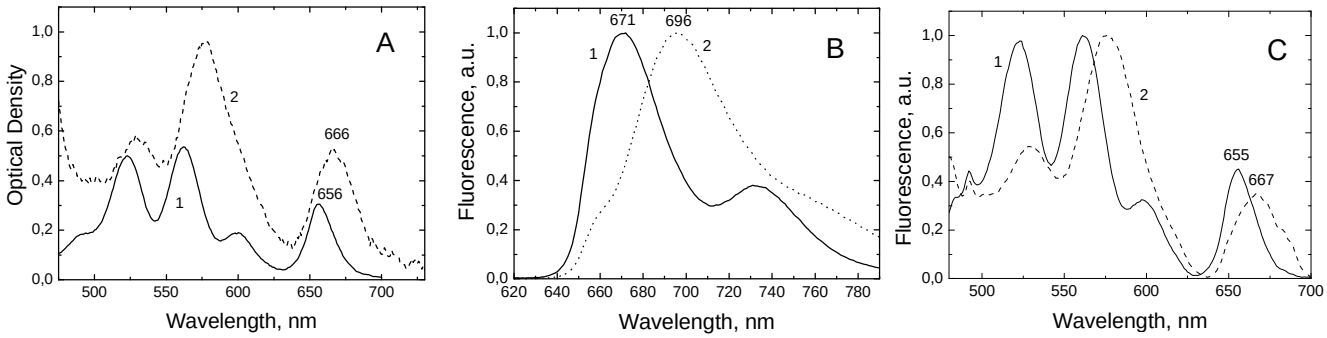

Figure 5. Absorption (A), fluorescence (B, λ_{exc}=420 nm) and fluorescence excitation (C, λ_{reg}=720 nm) spectra of tetra(*p*-aminophenyl)porphyrin (TAPP) in toluene (1) and pyridine (2) at 295 K.

Results and Discussions

Usual Steady-State Fluorescence Spectra

It should be mentioned that spectral properties of DAPEP and TAPP molecules in solutions depend significantly on the solvent properties. As it is presented in Figure 5 for TAPP, when transition from non-polar toluene to pyridine the noticeable transformation of absorption spectra is observed in the visible region: a significant broadening of all bands accompanied by the shift to the red region by ~12 nm, the four-band spectrum transforms to the three-band one. Fluorescence spectra in pyridine are also broadened by ~2 times with respect to those registered in toluene. Stokes shift between *Q*(0,0)-bands in absorption and fluorescence is essentially higher in pyridine and amounts to 600 cm^{-1} in comparison with that of 360 cm^{-1} in toluene. Nevertheless, fluorescence excitation spectra coincide to absorption spectra both in toluene and pyridine thus confirming monomeric state of TAPP molecules in both solvents.

The observed experimental spectral findings may be connected with two reasons at least: the reorganisation of solvate shell and the conformational dynamics of tetrapyrrole macrocycle for DAPEP and TAPP molecules in the excited S_1-state due to the interaction of *meso*-phenyl rings with bulky side β-substituents in pyrrole rings (especially in the case of DAPEP[38,39]).

Figure 6 shows standard fluorescence and fluorescence excitation spectra registered for PP film 6 B, treated by O_2-plasma in after-emission zone and then activated by TAPP (it was difficult to record appropriate absorption spectra because of a small content of porphyrin molecules on the PP film, interference effects and scattering). Evidently, both spectra belong to TAPP molecules. Noteworthy, for TAPP on the PP film, the position of *Q*(0,0)-band in fluorescence excitation spectrum is the practically same as that being observed in toluene, while the fluorescence maximum is measured to be at 660 nm, that is relatively shorter in comparison with λ_{max}= 671 nm in non-polar toluene. The decrease of stokes shift down to ~ 70 cm^{-1} in comparison with 360 cm^{-1} or 600 cm^{-1} in solutions may be caused by a more rigid fixation of TAPP (and DAPEP) molecules on the PP film surface. At last, the fluorescence of a control sample 1A (non-treated film without porphyrins) is very low and characterized by admixture of luminescent dirt.

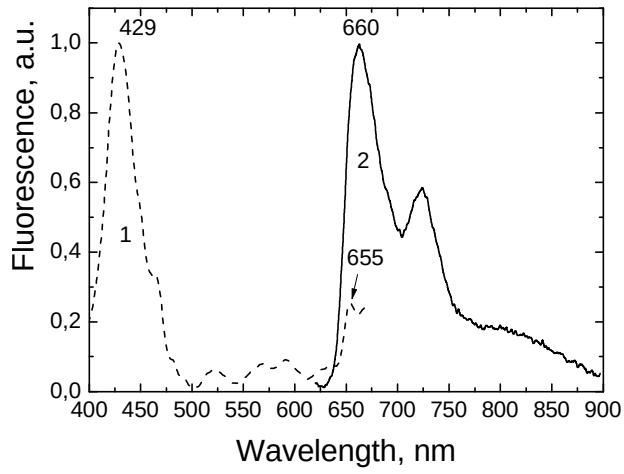

Figure 6. Fluorescence excitation (1, λ_{reg} = 720 nm) and fluorescence (2, λ_{exc} = 420 nm) spectra of tetra(*p*-amino-phenyl)porphyrin (TAPP) attached to polypropylene film 6B, treated in afterglow of O_2-plasma (295 K).

Confocal Microscopy of Polypropylene Films Without and with Porphyrins

The basic results obtained by confocal microscopy for PP films were obtained for more than 70 images. Here, we present some statistical results characterizing the possibilities of this method for the analysis of the film thickness and porphyrin distribution on both sides of the film. In order to measure the thickness of the films, *x*-*z*-cuts through the films were recorded in reflection mode (excitation by 514.5 nm line of the argon ion laser), because the resolution is much better than in fluorescence regime recording.

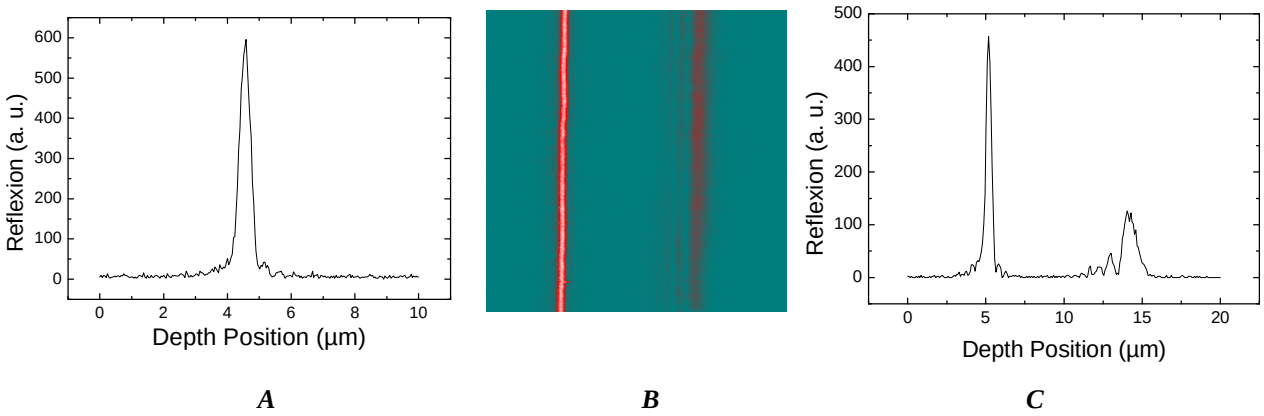

Figure 7. Depth profile (A), cut of the reflection image with a size of 20×20 μm^2 (B) and depth profile (C) through the film A (without porphyrin).

For each film samples cut images were obtained with different magnification. Figure 7A shows the depth resolution which was recorded with a mirror and is estimated by ~700 nm. The analysis of the film images (*x*-*z*-cut, Figure 7) shows two peaks: the left peak originates from the upper side of the film, the right corresponds to the lower one. The oscillations in the peak intensities are due to interference in the film. From these kinds of images film thicknesses were extracted using the fitting procedure by two Gaussian components and displayed in Table 1.

Table 1. Film thicknesses obtained in reflection mode.

Films	1A	1B	2A	2B	3A	3B	4B	5B	6B
Thick-ness [μm]	9.03	8.75	9.00	8.76	9.18	8.82	9.02	8.96	9.03

Description of the films with and without porphyrins is presented in the Experimental part.

It should be mentioned that even though the depth resolution of the setup is only 700 nm, the position of the peaks can be quantified with a much higher accuracy. This is only depends on the signal-to-noise ratio, in our case the experimental depth resolution is estimated to be ~50 nm. The corresponding profiles obtained in the fluorescence mode (especially for the lower side of the film) are wider thus giving less accuracy in the film thickness measurements. At last, from it follows the above measurements that the detected deviations in the film thicknesses are due to the manufacturing process presumably.

After recording cut images lateral images (in reflection and fluorescence modes) of PP film surfaces were measured and visualized. For all the films, the obtained pictures look quite similar, that means one could not detect pronounced effects of the plasma treatment (Figure 8). In some respect, the reason of that may be connected with a relatively low resolution of the microscope which is not high enough in order to analyze structural changes below 200 nm. Dark areas in the upper left and lower right corners of the reflection image are due to the high depth resolution and the ripples of the film. So, the more informative part of the film is a small bright central area. So, if one could manage to put the films uniformly on a substrate the better images may be obtained. Additionally there is much dirt (black spots) on the films remaining after the manufacturing process, which reduces the quality of the images.

Now we would like to come to the fluorescence part of the work which seems to be more interesting.

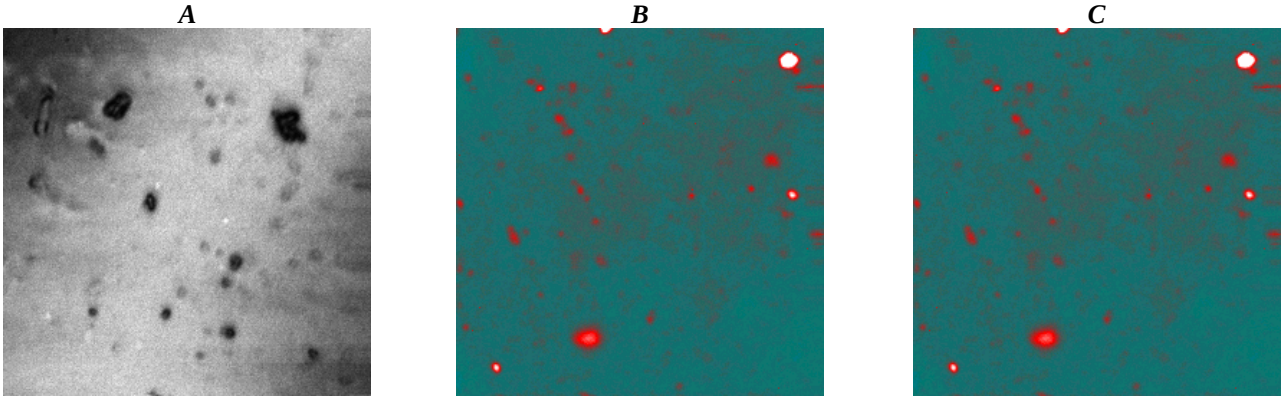

Figure 8. Reflexion lateral image of a control non-treated PP film 1A (A) as well as fluorescence lateral images of films 2A (B, film treated by O_2-plasma in zone of positive range of charge + di(*p*-aminophenyl)etioporphyrin II, DAPEP) and 6B (C, film treated in afterglow of O_2-plasma + tetra(*p*-aminophenyl)porphyrin, TAPP). All images have a size of 20 x 20μm^2, λ_{exc} = 514.5 nm by Ar^+ laser, λ_{det} > 530 nm at fluorescence mode.

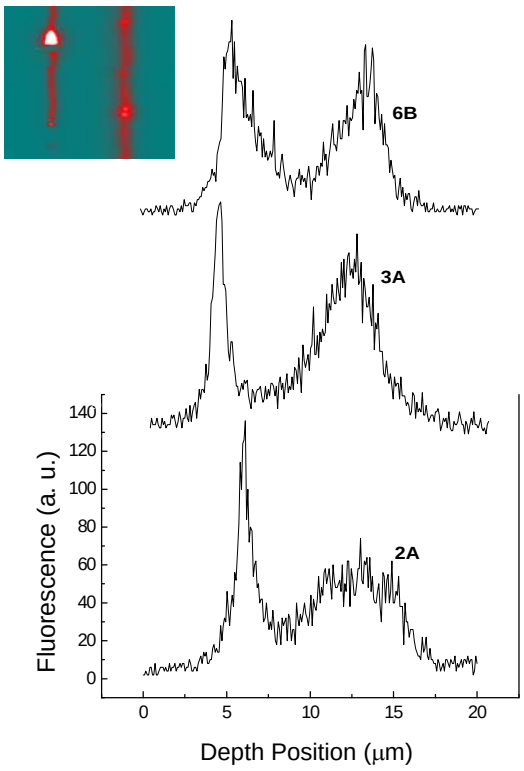

Figure 9. Depth profiles of the fluorescence image cuts with a PP films size of 20 x 20 μm^2: 2A - film treated by O_2-plasma in zone of positive range of charge + di(*p*-aminophenyl)etioporphyrin II, DAPEP); 3A - is the film treated by O_2-plasma in after-emission zone + DAPEP and 6B - film treated in afterglow of O_2-plasma one + tetra(*p*-aminophenyl)porphyrin, TAPP. λ_{exc} = 514.5 nm by Ar^+ laser, λ_{det} > 530 nm at fluorescence mode. The inset shows the cut of the fluorescence image with a size of 20 x 20 μm^2 for PP film 3A.

The necessary measurements were carried out in the same way as for the reflexion mode. The excitation conditions (λ_{exc} = 514.5 nm by Ar^+ laser) were suitable for the direct excitation of porphyrin molecules thus providing enough signal for *x*-*z*-cuts recording. Some of the results are shown in Figure 9. Like in reflexion mode, the left peak corresponds to the upper side (which is also the reaction side in case of plasma treatment), the right one corresponds to the lower side. The analysis of fluorescence profiles of cut images shows rather strong differences in the distributions of the porphyrins on film surfaces treated by various ways. From these findings it may be concluded that after plasma treatment the polymer surface becomes non-homogeneous, and porphyrin moieties are seen to be randomly distributed on both film surfaces with a penetration depth of ~1 μm.

Spatially-Resolved Fluorescence Spectroscopy of Polypropylene Films with and without Porphyrins

One primary motivation for the studying the spatially-resolved emission of individual objects (more clearly, individual organic molecules,[40] porphyrins,[41,42] spins[43] or semiconductor quantum dots[44]) in solids, liquids, proteins or on interfaces and surfaces is due to the possibilities to elucidate both the local environment influence (heterogeneous by nature) and the individual object state and properties, so that the behaviour of individuals may not be fully represented by the standard (large number N) ensemble average. At present, conventional confocal microscope technique (home-built presumably) permits to carry out steady-state and kinetic fluorescent measurements in a wide temperature range including liquid helium temperatures. The development of high-spatial-resolution optical microscopy has fostered a considerable progress in this field. Briefly, this method has now broad interdisciplinary impact, ranging from physical and analytical chemistry to biophysics, medicine, material science and nanotechnology.

Our use of the spatially-resolved fluorescence spectroscopy for polypropylene films activated by porphyrins is to gather information about the spatial arrangement of these molecules adsorbed on film surfaces as well as to clearly recognize the state of the molecules on the PP surface (monomeric or aggregated, at least). As it is shown in Figure 5, fluorescence spectra of TAPP molecules in both toluene and pyridine are relatively wide being ensemble averaged due to inhomogeneous broadening. For TAPP on the PP film, the fluorescence band (detected from the square of 0.5 cm^2) is noticeably narrower with respect to toluene solution and its maximum is measured to be at 660 nm, that is relatively shorter in comparison with λ_{max} = 671 nm in non-polar toluene (Figure 6). The decrease of stokes shift down to ~70 cm^{-1} in comparison with 360 cm^{-1} or 600 cm^{-1} in solutions is proposed to be caused by a more rigid fixation of TAPP molecules on the PP film surface. In this case, the standard steady-state registration gives us TAPP emission which is also ensemble averaged due to inhomogeneous broadening caused by the specific interaction of every TAPP molecule with PP film surface.

In the first step of data evaluation, the fluorescence images of PP films without and with porphyrin molecules have been analyzed (Figure 10, left side A, B, C). Figure 10 A shows that even for pure film without porphyrin there are some fluorescing admixtures visualized (in fluorescence mode) like relatively bright spots remaining after the industry manufacturing process and non-eliminated by the solvent treatment.

It is seen from Figure 10 B that for the film treated by plasma and then activated by TAPP, the number of fluorescing spots becomes relatively larger. We attribute it to the appearance of porphyrin molecules on PP film surface. In order to verify such a possibility we have excited these bright spots by the narrow laser beam and detected the spectral distribution of this emission using home-built confocal microscope. In Figure 10 B one examined spot is shown by a white arrow. For the comparison, the other arrow in Figure 10 B shows the empty place on PP film surface, emission from which was used for the background emission detection at the same experimental conditions. We want to emphasize that spatially-resolved fluorescence measurements need a relatively high laser power densities thus leading to a noticeable photobleaching of organic molecules. Really, Figure 10 C shows that after spectral detection the brightness of the investigated spot became smaller.

On the right side of Figure 10 the background emission of the film (D), total fluorescence spectrum (E) and the spectrum with subtracted film emission (F) are presented being obtained for the empty film place and the

spot shown by arrows on left images. The comparison of fluorescence profiles and the maximum position obtained for the spots (Figure 10 F) with those detected in ensemble measurements (Figure 6) shows a good coincidence.

Thus, for bright spots the emission originates from TAPP molecules, and our assumption about the nature of the majority of bright spots seems to be justified. The same results were obtained in numerous experiments with both TAPP and DAPEP molecules absorbed on PP films treated in various plasma conditions.

At last, it should be mentioned that the lateral resolution of the confocal setup does not exceed $\Delta l \approx 235$ nm and a vertical resolution is of 970 nm. This means that spots may contain few or even more porphyrin molecules disposed closely to each other. Correspondingly, the possibility of porphyrin aggregation effects should be taken into account. A set of experimental data which we have at the moment leads to the following conclusions. From one hand, as it was mentioned above, it was difficult to record appropriate absorption spectra of the samples because of a small content of porphyrin molecules on the PP film, interference effects and scattering. From the other hand, a spontaneous aggregation of porphyrins in solutions does not manifest significantly in absorption spectra (small spectral shift and bands broadening, the more sensitive is Soret band, see a review chapter[12]). For TAPP molecules on PP film surfaces, ensemble average fluorescence excitation spectra in UV-vis region (relative intensities of the bands, Figure 6) coincide with the same distribution measured for monomeric TAPP molecules in toluene (insert in Figure 6). Noteworthy also is the full coincidence in the positions of Soret bands (429 nm) in both spectra. It is seen also that the intensities ratio of vibronic $I(1,0)$ to pure electronic $I(0,0)$ bands in fluorescence spectra of TAPP is

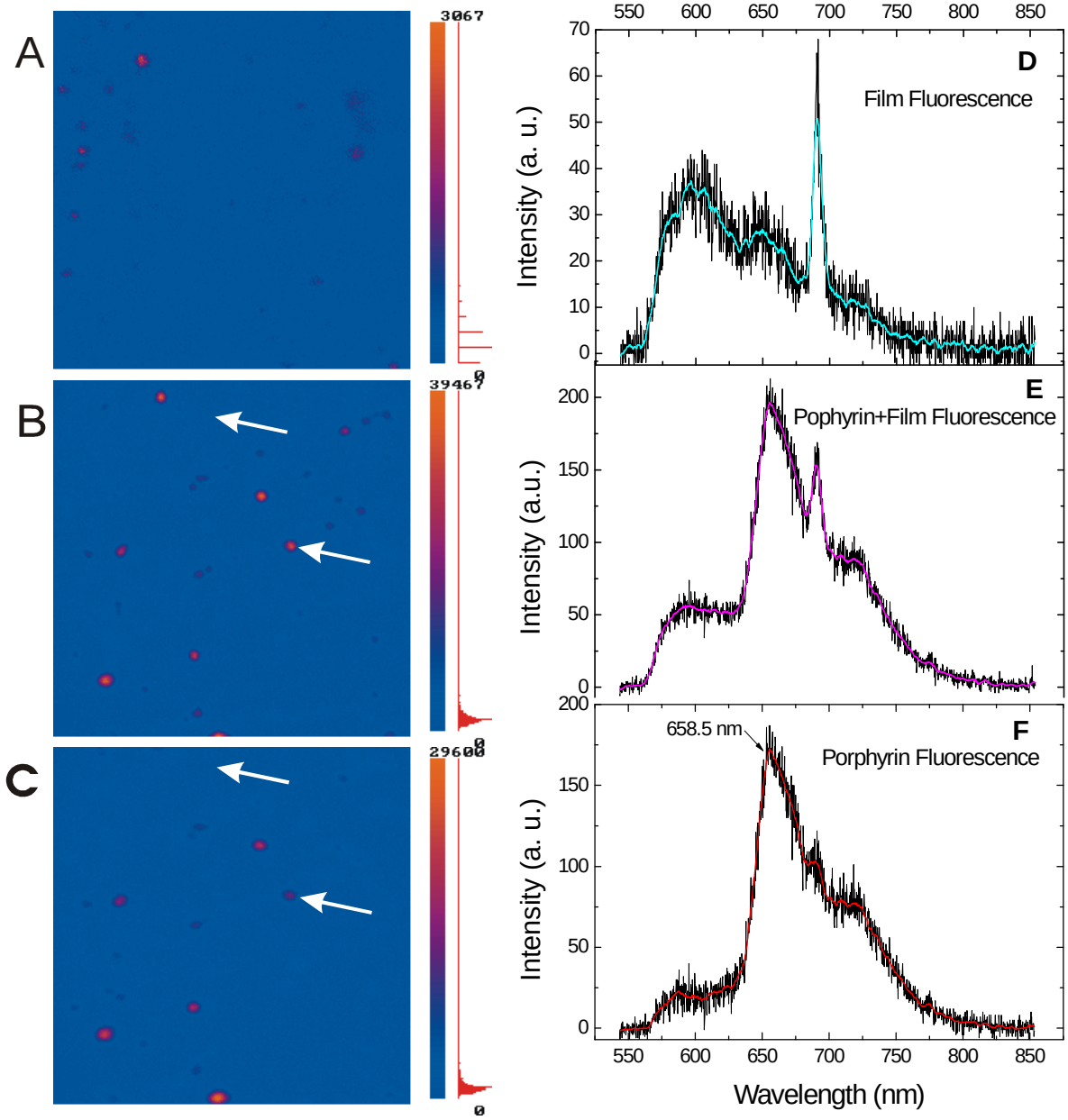

Figure 10. Fluorescence images of pure PP film with a size of 20×20 μm^2, upper side (A) and film treated in afterglow of O_2-plasma + tetra(*p*-aminophenyl)porphyrin, TAPP, before (B) and after (C) laser spectral measurements. Fluorescence spectra of the PP film spot without porphyrin (D) and with porphyrin (E); the spectrum shown in part (F) represents fluorescence of the attached porphyrin molecules with subtracted admixture of the PP film emission. λ_{exc} = 407 nm, power density N = 25 μW /μm^2, 295 K.

practically the same for toluene solutions of monomeric porphyrin (Figure 5, spectrum 1), ensemble average fluorescence of PP surface (Figure 6, spectrum 2) and fluorescence spectrum of the PP film spot with porphyrin (Figure 10 F), and is equal to $I(1,0)/I(0,0) \approx 0.4 \div 0.5$. The decrease of stokes shift down to ~ 70 cm^{-1} in comparison with 360 cm^{-1} in toluene solution may be caused by a more rigid fixation of TAPP molecules on the PP film surface. Correspondingly, in the spot the fluorescing species of TAPP molecules as monomeric ones may be taken as proved.

In this respect, some additional arguments should be taken into account. Typically, spontaneous porphyrin aggregates and oligomeric/polymeric porphyrins are characterized by low fluorescence efficiencies.[10-12] Accordingly, TAPP spontaneous aggregates are hardly detected by emission with respect to monomers in one spot. But in the case of the considerable existence of aggregated TAPP species together with monomeric form in one spot at relatively small distances, the non-radiative resonant energy transfer "monomer→aggregate" should take place thus leading to the strong quenching of the monomer fluorescence (fluorescence efficiency decrease and decay shortening). Nevertheless, our preliminary time-correlated single photon counting measurements have shown that fluorescence decay of TAPP in spots (three have been analysed) is of 8.7÷9.3 ns. These values are typical for monomeric porphyrins of various types in liquid solvents in the presence of dissolved oxygen.[12,13,36,38] This situation may be explained by two ways: i) TAPP molecules are in monomeric form presumably in the spot; ii) there is a distribution of monomers and aggregates in the spot, but intercenter monomer–aggregate distances are relatively large and the effective energy transfer "monomer→aggregate" does not realise. The statistical analysis of time-correlated single photon counting measurements being obtained for various spots and concentrations of TAPP and DAPEP molecules on PP surface is under the way.

Conclusions

We have studied the interaction of di(*p*-aminophenyl)-etioporphyrin (DAPEP) and tetra(*p*-aminophenyl)porphyrin (TAPP) molecules with the surface of thin (7-15 μm) polypropylene films using laser confocal microscopy and spatially-resolved fluorescence measurements. On the basis of these contemporary spectroscopic methods in the combination with ensemble averaged measurements it has been elucidated that fluorescence spectra of individual bright spots on film surfaces correspond to porphyrin monomeric species. Thus it seems to be concluded that spatially closed few porphyrin molecules in the spot do not form aggregates. Polypropylene films with low surface energy and low sorbtion properties being surfacely activated by porphyrins (in monomeric form known as affective sensitizers of singlet oxygen $^1\Delta_g$ [45,46]) may be used in photodynamic therapy and blood cleaning. Porphyrins fixed on polymer surfaces are considered for possible applications and thermostabilization of polymers (especially metallo-porphyrins).[25] Samples "porphyrin-polymer", like tetrapyrrole compounds forming strongly absorbing excited states in solutions,[47,48] may be used as optical limiters, which can protect sensors or human eyes from optical damage. Concerning our interests, two practical questions (blood cleaning and optical limiters) based on these systems will be the subject of further thorough investigations.

Acknowledgements. This work was supported by BRFFR Grant No Ф07МС–022 (Belarus, Germany) and GKPNI «KMS-17» (Belarus). Authors thank also Prof. A. Semeikin and Dr. S. Syrbu for the synthesis and purification of DAPEP and TAPP molecules.

References

1. Shtilman M.I. *Immobilization on polymers*. Utrecht, Tokio, VSP, **1991**.
2. Pomogailo D.A. Uflyand I.E. *Macromolecular Metallochelates* Moscow, Khimiya **1991**. 304.
3. *Polymeric Reagents and Catalysts* (Ford U.E., Ed.) Moscow, Khimiya **1991**. 256 p.
4. Solov'eva A.B., Timashev S.F. *Uspekhi Khimii* **2003**, *72*, 1081-1097.
5. Lisichkin G.F., Yuffa A.Ya. *Heterogeneous Metalocomplex Catalysts*. Moscow, Khimiya **1981,** 160
6. Valkova L., Borovkov N., Koifman O., Kutepov A., Berzina T., Fontana M., Rella R., Valli L. *Biosensors and Bioelectronics* **2004**, *20*, 1177-1182.
7. Wöhrle D. In *Phthalocyanines: Properties and Applications.* Vol. 1. (Leznoff C.C., Lever A.B.P., Eds.) N.Y, VCH, **1989**, 55-87.
8. Ulbricht M. *Polymer* **2006**, *47*, 2217-2262.
9. Kosal M.T., Suslick K.S. *J. Solid State Chem.* **2000**, *152*, 87-98.
10. Nakai K., Kurotobi K., Osuka A., Uchiyama M., Kobayashi N. *J. Inorg. Biochem.* **2008**, *102*, 466-471.
11. Yang J., Park M., Yoon Z., Hori T., Peng X., Aratani N., Dedecker P., Hotta J., Uji-I H., Sliwa M., Hofkens J., Osuka A., Kim D. *J. Am. Chem. Soc.* **2008**, *130*, 1879-1884.
12. Zenkevich E.I., von Borczyskowski C. In *Handbook of Polyelectrolytes and Their Applications* Vol. 2 (Tripathy S.K., Kumar J., Nalwa H.S., Eds.) USA: American Scientific Publishers, **2000**, Ch. 11, 301-348.
13. Zenkevich E.I., von Borczyskowski C., Shulga A.M., Bachilo S.M., Rempel U., Willert A. *Chemical Physics* **2002**, *275*, 185-209.
14. Chambron J.-C., Heitz V., Sauvage J.-P. In *The Porphyrin Handbook* Vol. 6 (Kadish K.M., Smith K.M., Guilard R., Eds) New York, Academic Press, **2000**, Ch.40, 1-35.
15. Sessler J.L., Wang B., Springs S.L., Brown C.T. In *Comprehensive Supramolecular Chemistry* Vol. 4 *(*Marakami Y., Ed.) Oxford, **1996**, 311.
16. Ogoshi H., Mizutani T., Hayashi T., Kuroda Y. In *The Porphyrin Handbook* Vol. 7 (Kadish K.M., Smith K.M., Guilard R., Eds) New York, Academic Press, **2000**, Ch. 46, 279.
17. Gust D., Moore T.A. In *The Porphyrin Handbook* Vol. 8 (Kadish K.M., Smith K.M., Guilard R., Eds) New York, Academic Press, **2000**, Ch. 57, 57.
18. Fukuzumi S. *In The Porphyrin Handbook* Vol. 8 (Kadish K.M., Smith K.M., Guilard R., Eds) New York, Academic Press, **2000**, 115.
19. Hayes R.T., Walsh C.J., Wasielewski M.R. *J. Phys. Chem. A.* **2004**, *108*, 2375-2383.
20. DiMarco G., Lanza M. *Sensors and Actuators* B. **2000**, *63*, *42*.
21. Amao Y., Tabuchi Y., Yamashita Y., Kimura K. *Eur. Polymer J.* **2002**, *38*, 675.
22. Nakagawa K., Kumon K., Tsutsumi C., Tabuchi K., Kitagawa T., Sadaoka Y. *Sensors and Actuators* B, **2000**, *65*, 138.

23. Tsivadze A.Yu. *Uspekhi Khimii* **2004**, *73*, 6.
24. Tsivadze A.Yu. Crown-compounds as „ion traps“, in *Encyclopedia «State-of-the-art natural science»* Vol. 6 Moscow, Magistr-Press, **2000**, 247.
25. Koifman O.I., Ageeva T.A. *Porphyrinopolymers* Moscow: Phys.-Math. Lit. Press, **2006** 194
26. Goddard J.M., Hotchkiss J.H. *Progress in Polymer Science* **2007**, *32*, 698-725.
27. Rück D.M. *Nuclear Instruments and Methods in Physics Research Section B: Beam Interactions with Materials and Atoms* **2000**, *166-167*, 602-609.
28. Zaporojtchenko V., Zekonyte J., Faupel F. *Nuclear Instruments and Methods in Physics Research Section B: Beam Interactions with Materials and Atoms* **2007**, *265*, 139-145.
29. Nasef M.M., Saidi H., Dahlan K.Z.M. *Polymer Degradation and Stability* **2002**, *75*, 85-92.
30. Rietveld I.B., Kobayashi K., Yamada H., Matsushige K. *Journal of Colloid and Interface Science* **2006**, *298*, 639-651.
31. Golubchikov O.A., Ageeva T.A., Titov V.A., Vershinina I.A., Shikova T.G., Semeikin A.S., Maksimov A.I., Zenkevich E.I. *Method of the surface modification for propylene material*. The Patent of Russian Federation № 2223982, Invention Bulletin №5 (20.02.2004).
32. Syrbu S.A., Glazunov A.V., Semeikin A.S. *Izv. Vysch. Uchebn. Zaved. Khim. Teknol.* **2006**, *49*, 122-123.
33. Semeikin A.S., Koifman O.I., Berezin B.D. *Izv. VUZov Khim. Teknol.* **1985**, *28*, 47-51.
34. Cichos F., Martin J., von Borczyskowski *C. Phys. Rev. B* **2004**, *70*, 115314.
35. Choi H.S., Rybkin V.V, Titov V.A., Shikova T.G., Ageeva T.A. *Surface and Coatings Technology* **2006**, 4479-4488.
36. Zenkevich E., Sagun E, Knyukshto V., Shulga A., Mironov A., Efremova O., Bonnett R., Pinda Songca S., Kassem M. *J. Phochem. Photobiol. B: Biol.* **1996**, *33*, 171-180.
37. Zenkevich E., Cichos F., Shulga A., Petrov E., Blaudeck T., von Borczyskowski C. *J. Phys. Chem. B.* **2005**, *109*, 8679-8692.
38. Knyukshto V., Zenkevich E., Sagun E., Shulga A., Bachilo S. *Chem. Phys. Lett.* **1999**, *304*, 97-108.
39. Avilov I.V., Zenkevich E.I., Sagun E.I., Filatov I.V. *J. Phys. Chem. A.* **2004**, *108*, 5684-5691.
40. Hinze G., Haase M., Nolde F., Muellen K., Basche Th. *J. Phys. Chem. A.* **2005**, *109*, 6725-6729.
41. Starukhin A., Shulga A., Sepiol J., Kolos R., Renn A., Wild U.P. *Single Molecules* **2001**, *2*, 203 – 206.
42. Bricas R.P., Troxler T., Hochstrasser R.M., Vinogradov S.A. *J. Am. Chem. Soc.* **2005**, *127*, 11851-11862.
43. von Borczyskowski C., Koehler J., Moerner W.E., Orrit M., Wrachtrup *J. Appl. Magn. Reson.* **2007**, *31*, 665-676.
44. Shimizu K.T., Woo W.K., Fisher B.R., Eisler H.J., Bawendi M.G. *Phys. Rev. Lett.* **2002**, *89*, 117401.
45. Dougherty T.J., Gomer C.J., Henderson B.W., Jori G., Kessel D., Kovbelik M., Moan J., Peng Q. *J. Natl. Cancer Inst.* **1998**, *90*, 889-905.
46. Grin, M.A., Lonin I.S., Fediounin S.V., Tsiprovskiy A.G., Strizhakov A.A., Tsygankov A.A., Krasnovsky A.A., Mironov A.F. *Mendeleev Commun.* **2007**, *17*, 209-211.
47. Perry J.W., Mansour K., Lee I.-Y.S., Wu X.-L., Bedworth P.V., Chen C.-T., Ng D., Marder S.R., Miles P., Wada T., Tian M., Sasabe H. *Science* **1996**, *273*, 1533 – 1536.
48. Kuznetsova R., Kopylova T., Mayer G., Svetlichnyi V., Samsonova L., Tel'minov E., Sergeev A. *Proc. SPIE Int. Soc. Opt. Eng.* **1997**, *3403*, 186-191.

Received 24.04.2008
Accepted 02.06.2008